Polymer Solutions: An Introduction to Physical Properties. Iwao Teraoka

ISBNs: 0-471-38929-3 (Hardback); 0-471-22451-0 (Electronic)

3

Dynamics of Dilute Polymer Solutions

3.1 DYNAMICS OF POLYMER SOLUTIONS

In the first two chapters, we learned about thermodynamics (free energy, osmotic pressure, chemical potential, phase diagram) of polymer solutions at equilibrium and static properties (radius of gyration, static structure factor, density correlation function) of dissolved polymer chains. This chapter is about dynamics of polymer solutions. Polymer solutions are not a dead world. Solvent molecules and polymer chains are constantly and vigorously moving to change their positions and shapes. Thermal energy causes these motions in a microscopic world.

Solution dynamics deals with the motion of molecules dissolved in a solvent. A typical mode of motion is center-of-mass diffusion. A nonuniform concentration distribution is leveled to a uniform distribution as the solution approaches the equilibrium state. Viscosity of the solution is another form of dynamics. Slowly moving solute molecules increase the viscosity more than fast moving molecules.

Center-of-mass diffusion and viscosity are universally observed in all fluids including pure solvents. What makes the polymer solution dynamics distinctly different from the dynamics of other solutions is the numerous degrees of freedom for the internal motion of each solute molecule. As we learned in Chapter 1, polymer chains can take many different conformations. They are incessantly switching from one to another, thereby changing the shape of the polymer chain. In small molecules, the internal motions such as vibration (changes in the bond lengths, bond angles, and dihedral angles) and rotation are observed at frequencies typically between 1 GHz and 100 THz. The motions are resonant. In contrast, the change in the conformation of the polymer chains occurs at much lower frequencies (radio, audio, and lower frequencies) in addition to the resonant vibrational motions at the high frequencies.

Solvent viscosity makes the motion overdamped and therefore relaxational. Different modes of motion are observed over an extended range at the low frequencies.

A small change in the thermodynamic properties of the solution, as represented by A_2, leads to a shift in the dynamics, typically the time scale of motion and dependence on the concentration and the molecular weight. It often happens that the shift in the dynamic properties is more pronounced compared with the shift in the static properties. Thus, how the time scale depends on the polymer concentration, the molecular weight, and the temperature gives us an important piece of information on the state of the polymer molecules, especially their interactions with the solvent molecules.

In Chapter 3, we will learn about the dynamics of an isolated polymer chain in the dilute solution limit and the first-order change in the dynamics with polymer concentration. We will also learn typical experimental methods to investigate the dynamics—dynamic light scattering and viscosity. The dynamics of polymer solutions above the overlap concentration will be discussed in Chapter 4, along with their thermodynamics.

3.2 DYNAMIC LIGHT SCATTERING AND DIFFUSION OF POLYMERS

3.2.1 Measurement System and Autocorrelation Function

3.2.1.1 Measurement System Motions of polymer molecules in solution can be conveniently studied by using **dynamic light scattering** (**DLS**). It is also called **quasi-elastic light scattering** (**QELS**) and **photon correlation spectroscopy** (**PCS**). Measurement at a single scattering angle gives information on the dimension of the polymer molecule in the solution with reasonable accuracy. Unlike its static version, DLS does not rely on the excess scattering. There is no need to calculate a small difference in the scattering intensity between the pure solvent and a dilute solution. The signal from the slowly moving polymer is unambiguously separated from the signal that originates from the rest of the solution. The principle of DLS has been utilized in some commercial particle-sizing systems for many years. The measurement and data analysis are automated. Users need only to prepare clean solutions by filtration. In recent years, DLS has been also used as an on-line detector in size exclusion chromatography (SEC). In this section, we will learn how the signal obtained in DLS is related to the dimension and motions of solute molecules and other dynamic modes.

As shown in Figure 3.1, a DLS system requires an **autocorrelator** on top of a regular SLS system. The light-scattering intensity from the polymer solution is not a constant. Figure 3.2a illustrates how the intensity (I) varies with time (t). $I(t)$ fluctuates around its mean $\langle I \rangle$. It may appear completely random (white noise) and therefore meaningless, but it is not. Motions of the polymer molecules and the solvent molecules contribute to a change of $I(t)$ with time. The noisy signal then

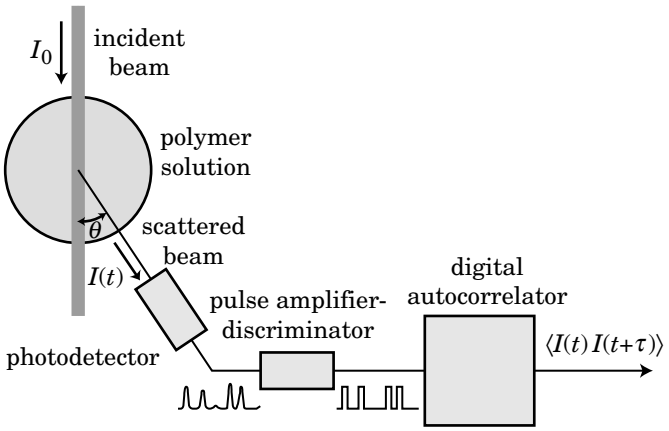

Figure 3.1. Dynamic light scattering measurement system. The pulse-amplifier discriminator converts the analog signal of the photodetector, $I(t)$, into a digital signal, which is further converted by the autocorrelator into the autocorrelation function of the signal.

carries the information on the motions and other fluctuations. The autocorrelator uncovers the embedded information.

3.2.1.2 Autocorrelation Function The autocorrelator calculates the average of the product of two scattering intensities $I(t)$ and $I(t + \tau)$ measured at the two times separated by τ. Here τ is called the **delay time**. The average $\langle I(t)I(t + \tau)\rangle$ is a function of τ and is called the **autocorrelation function** of $I(t)$ or the intensity-intensity autocorrelation function. The autocorrelator converts $I(t)$ into $\langle I(t)I(t + \tau)\rangle$.

What the autocorrelator calculates is the average of $I(t)I(t + \tau)$ with respect to t over a long period T_A. We assume that the long-time average is equal to the ensemble average—the average with respect to the configuration of the system or, simply put, the average over all possible positions and shapes of the molecules in the solution:

$$\langle I(t)I(t + \tau)\rangle = \lim_{T_A\to\infty} \frac{1}{T_A}\int_0^{T_A} I(t)I(t + \tau)\,\mathrm{d}t \tag{3.1}$$

This assumption, in general, is called **ergodicity**. It is one of the few hypotheses in statistical mechanics. We cannot prove it but believe it is correct. Note that, if the system is at equilibrium, the ensemble average does not change with time and therefore $\langle I(t)I(t + \tau)\rangle = \langle I(0)I(\tau)\rangle$.

The autocorrelation function of $I(t)$ in panel a of Figure 3.2 is shown in panel b. When $\tau = 0$, $\langle I(t)I(t + \tau)\rangle = \langle I^2\rangle$. With an increasing τ, $I(t + \tau)$ becomes more irrelevant to $I(t)$, and $\langle I(t)I(t + \tau)\rangle$ decays to an asymptotic level called a **baseline**. The baseline level is $\langle I\rangle^2$; when $I(t + \tau)$ and $I(t)$ are irrelevant, $\langle I(t)I(t + \tau)\rangle = \langle I(t)\rangle\langle I(t + \tau)\rangle = \langle I\rangle^2$.

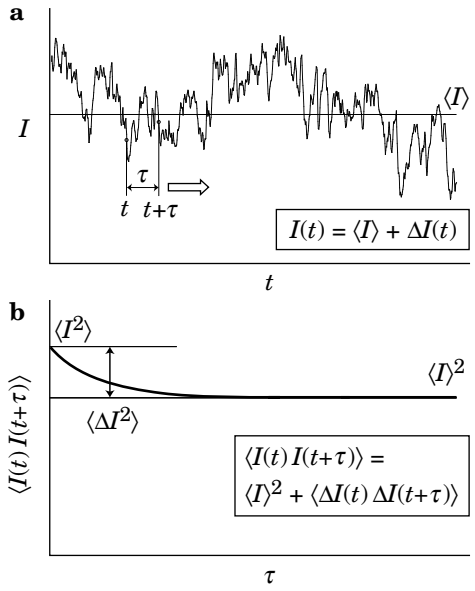

Figure 3.2. a: Light scattering intensity $I(t)$ fluctuates around its mean $\langle I \rangle$. b: Autocorrelation function $\langle I(t)I(t+\tau)\rangle$ is obtained as the long-time average of $I(t)I(t+\tau)$ with respect to t for various delay times τ. The autocorrelation function decays from $\langle I^2\rangle$ to $\langle I\rangle^2$ over time. The amplitude of the decaying component is $\langle \Delta I^2\rangle$.

3.2.1.3 Photon Counting The scattering intensity $I(t)$ can be measured as an analog quantity I that varies continuously with time t. More often than not, $I(t)$ is measured as pulses. Each pulse corresponds to a photon that reaches the photodetector. For this purpose, a photomultiplier or an avalanche photodiode is used in a photon-counting mode. A pulse amplifier–discriminator eliminates ghost pulses of a low height and converts each proper pulse into a pulse of a fixed height and width to be led to the autocorrelator (see Fig. 3.1). With the use of pinholes of different openings, the number of photons reaching the detector can be adjusted so that there are not too many photons entering the photodetector in each time window ($\sim$1 μs). The intensity is now expressed as the number of pulses in each time window. It is a nonnegative integer.

3.2.2 Autocorrelation Function

3.2.2.1 Baseline Subtraction and Normalization Because the scattering intensity $I(t)$ fluctuates around its mean $\langle I \rangle$, it is convenient to separate its fluctuating component $\Delta I(t)$ as

$$I(t) = \langle I \rangle + \Delta I(t) \tag{3.2}$$

By definition, $\langle \Delta I(t) \rangle = 0$. Then, the autocorrelation function is rewritten to

$$\langle I(t)\, I(t + \tau) \rangle = \langle I \rangle^2 + \langle \Delta I(t) \Delta I(t + \tau) \rangle \tag{3.3}$$

The autocorrelation of $\Delta I(t)$ is lost to zero with an increasing τ. When $\tau \rightarrow \infty$, $\langle \Delta I(t) \Delta I(t + \tau) \rangle = \langle \Delta I(t) \rangle \langle \Delta I(t + \tau) \rangle = 0$. The decaying component in $\langle I(t) I(t + \tau) \rangle$ is $\langle \Delta I(t) \Delta I(t + \tau) \rangle$. The initial height of the decaying component is $\langle \Delta I^2 \rangle = \langle I^2 \rangle - \langle I \rangle^2$ (see Fig. 3.2).

Division of $\langle I(t) I(t + \tau) \rangle$ by $\langle I \rangle^2$ leads to

$$\begin{aligned} \langle I(t) I(t + \tau) \rangle / \langle I \rangle^2 &= 1 + \langle \Delta I(t) \Delta I(t + \tau) \rangle / \langle I \rangle^2 \\ &= 1 + f_c g_2(\tau) \end{aligned} \quad \text{intensity autocorrelation function} \tag{3.4}$$

where f_c is called the **coherence factor**, defined as

$$f_c \equiv \langle \Delta I^2 \rangle / \langle I \rangle^2 \tag{3.5}$$

and the second factor is the baseline-subtracted, normalized intensity autocorrelation function:

$$g_2(\tau) \equiv \langle \Delta I(t) \Delta I(t + \tau) \rangle / \langle \Delta I^2 \rangle \tag{3.6}$$

The coherence factor depends, as the name suggests, on the coherence of the light falling on the photodetector. The beam has a finite cross section, and different parts of the beam may not have the same phase. If they have the same phase, the number of photons will be distributed with a Poisson distribution. The variance of I is then equal to the square of the mean, i.e., $f_c = 1$. In general, $0 < f_c < 1$. Use of a smaller pinhole increases f_c at the expense of a weakening intensity. As shown in Figure 3.3a, $g_2(\tau)$ is 1 at $\tau = 0$ and decays to zero as $\tau \rightarrow \infty$.

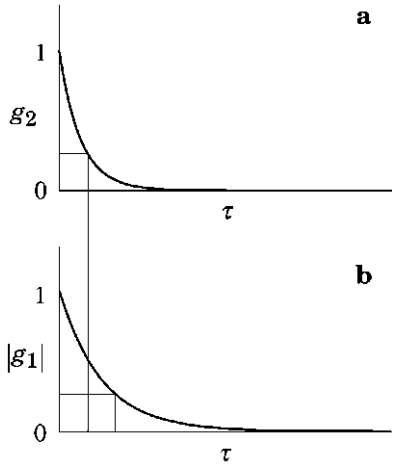

Figure 3.3. Baseline-subtracted, normalized intensity autocorrelation function $g_2(t)$ (a) and the absolute value of the baseline-subtracted, normalized electric-field autocorrelation function, $|g_1(t)|$ (b).

3.2.2.2 Electric-Field Autocorrelation Function We consider the autocorrelation function of the electric field $\mathbf{E}_s(t)$ of the light scattered by solutes. As we have seen in Section 2.4, $\mathbf{E}_s(t)$ is a complex quantity. We introduce another normalized autocorrelation function $g_1(\tau)$, which is defined as

$$g_1(\tau) \equiv \frac{\langle \mathbf{E}_s^*(t) \cdot \mathbf{E}_s(t+\tau) \rangle}{\langle \mathbf{E}_s^*(t) \cdot \mathbf{E}_s(t) \rangle} \tag{3.7}$$

It is known that $g_2(\tau)$ is related to $g_1(\tau)$ by[21]

$$\boxed{g_2(\tau) = |g_1(\tau)|^2} \tag{3.8}$$

Figure 3.3 compares $g_2(\tau)$ and $|g_1(\tau)|$. It takes twice as long for $|g_1(\tau)|$ to decay to a given level as it takes for $g_2(\tau)$.

Sometimes, $g_2(\tau)$ is defined as $g_2(\tau) \equiv \langle I(t)I(t+\tau)\rangle / \langle I \rangle^2$. This g_2 decays to 1 as $\tau \longrightarrow \infty$. Then, $|g_1(\tau)|^2 = [g_2(\tau) - 1]/[g_2(0) - 1]$.

3.2.3 Dynamic Structure Factor of Suspended Particles

3.2.3.1 Autocorrelation of Scattered Field We assume that the scattering volume contains n_P identical small particles and consider the autocorrelation function of $\mathbf{E}_s(t)$ for the scattering by the volume. Examples include a suspension of colloidal particles. The autocorrelation of the scattering by a polymer solution will be discussed in Section 3.2.6.

In Section 2.4, we considered light scattering by a chain of beads. Equation 2.53, along with Eq. 2.52, was obtained without assuming that the beads were connected to form a chain molecule. The same equation can therefore be used for a system of n_P particles, each consisting of a single bead. A photon detected at $\mathbf{r}$ and t was scattered some time ago by one of the particles at $\mathbf{r}'_m (m = 1, 2, \ldots, n_P)$ at t_0. The electric field $\mathbf{E}_s$ of the photon propagating in the direction of $\mathbf{k}_s$ is given as

$$\begin{aligned} \mathbf{E}_s(\mathbf{r}, t) &= \mathbf{E}_{sm} \exp[i(\mathbf{k}_s \cdot (\mathbf{r} - \mathbf{r}'_1) - \omega(t - t_0))] \sum_{m=1}^{n_P} \exp[i\mathbf{k} \cdot (\mathbf{r}'_1 - \mathbf{r}'_m)] \\ &= \mathbf{E}_{sm} \exp[i(\mathbf{k}_s \cdot \mathbf{r} - \mathbf{k}_i \cdot \mathbf{r}'_1) - i\omega(t - t_0)] \sum_{m=1}^{n_P} \exp(-i\mathbf{k} \cdot \mathbf{r}'_m) \end{aligned} \tag{3.9}$$

where the scattering event by particle 1 at $\mathbf{r}'_1$ and t_0 was selected as a reference point in space and time (Fig. 3.4). We take $(\mathbf{r}, t)$ to be the position and time of detection.

Another photon detected at $\mathbf{r}$ and $t + \tau$ is scattered by the particles at $\mathbf{r}_n$ ($n = 1, 2, \ldots, n_P$) at $t_0 + \tau$. Motion of the particles makes $\mathbf{r}'_m$ and $\mathbf{r}_n$ in general different. The reference point has moved to $\mathbf{r}_1$ as well, and the scattering occurs at $t_0 + \tau$. The incident light has changed its phase, since it hit particle 1 at $\mathbf{r}'_1$ and t_0. We take into account the phase shift due to the change in the scattering by the reference. We find

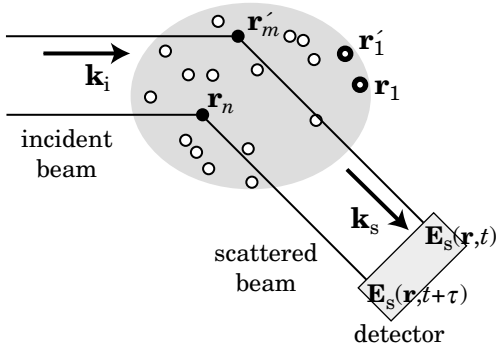

Figure 3.4. Scattering by the mth particle at t and by the nth particle at $t + \tau$ can be correlated. The two photons reach the detector at different times separated by τ.

the electric field of this second scattering is given as

$$\begin{aligned}\mathbf{E}_s(\mathbf{r},t+\tau) &= \mathbf{E}_{sm}\exp[i(\mathbf{k}_i\cdot(\mathbf{r}_1-\mathbf{r}'_1)-i\omega\tau)]\exp[i(\mathbf{k}_s\cdot\mathbf{r}-\mathbf{k}_i\cdot\mathbf{r}_1)\\ &\quad -i\omega(t-t_0-\tau)]\sum_{n=1}^{n_p}\exp(-i\mathbf{k}\cdot\mathbf{r}_n)\\ &= \mathbf{E}_{sm}\exp[i(\mathbf{k}_s\cdot\mathbf{r}-\mathbf{k}_i\cdot\mathbf{r}'_1)-i\omega(t-t_0)]\sum_{n=1}^{n_p}\exp(-i\mathbf{k}\cdot\mathbf{r}_n)\end{aligned} \tag{3.10}$$

Then, the autocorrelation function of $\mathbf{E}_s(\mathbf{r},t)$ is

$$\mathbf{E}_s^*(\mathbf{r},t)\cdot\mathbf{E}_s(\mathbf{r},t+\tau) = |\mathbf{E}_{sm}|^2\sum_{m,n=1}^{n_p}\exp[i\mathbf{k}\cdot(\mathbf{r}_m(t)-\mathbf{r}_n(t+\tau))] \tag{3.11}$$

where $\mathbf{r}'_m$ was rewritten to $\mathbf{r}_m(t)$ and $\mathbf{r}_n$ to $\mathbf{r}_n(t+\tau)$. Strictly speaking, $\mathbf{r}'_m = \mathbf{r}_m(t_0)$ and $\mathbf{r}_n = \mathbf{r}_n(t_0+\tau)$, but we can replace t_0 by t because the time difference between the scattering and the detection, $t - t_0$, is much smaller compared with τ. The statistical average of Eq. 3.11 is

$$\begin{aligned}\langle\mathbf{E}_s^*(\mathbf{r},t)\cdot\mathbf{E}_s(\mathbf{r},t+\tau)\rangle &= |\mathbf{E}_{sm}|^2\left\langle\sum_{m,n=1}^{n_p}\exp[i\mathbf{k}\cdot(\mathbf{r}_m(t)-\mathbf{r}_n(t+\tau))]\right\rangle\\ &= |\mathbf{E}_{sm}|^2\left\langle\sum_{m,n=1}^{n_p}\exp[i\mathbf{k}\cdot(\mathbf{r}_m(0)-\mathbf{r}_n(\tau))]\right\rangle\end{aligned} \tag{3.12}$$

The last transformation is allowed because the system is stationary. The autocorrelation function for $\tau = 0$ is

$$\langle\mathbf{E}_s^*(\mathbf{r},t)\cdot\mathbf{E}_s(\mathbf{r},t)\rangle = |\mathbf{E}_{sm}|^2\left\langle\sum_{m,n=1}^{n_p}\exp[i\mathbf{k}\cdot(\mathbf{r}_m(0)-\mathbf{r}_n(0))]\right\rangle \tag{3.13}$$

3.2.3.2 Dynamic Structure Factor From Eq. 3.7, division of Eq. 3.12 by Eq. 3.13 gives

$$|g_1(\tau)| = \frac{\left\langle \sum_{m,n=1}^{n_\mathrm{P}} \exp[\mathrm{i}\mathbf{k}\cdot(\mathbf{r}_m(0) - \mathbf{r}_n(\tau))] \right\rangle}{\left\langle \sum_{m,n=1}^{n_\mathrm{P}} \exp[\mathrm{i}\mathbf{k}\cdot(\mathbf{r}_m(0) - \mathbf{r}_n(0))] \right\rangle}. \tag{3.14}$$

It is convenient to introduce **dynamic structure factor** $S(\mathbf{k}, \tau)$, defined as

$$\boxed{S(\mathbf{k},\tau) = \left\langle \frac{1}{n_\mathrm{P}} \sum_{m,n=1}^{n_\mathrm{P}} \exp[\mathrm{i}\mathbf{k}\cdot(\mathbf{r}_m(0) - \mathbf{r}_n(\tau))] \right\rangle \quad \begin{array}{l}\text{dynamic structure factor}\\ \text{suspension of particles}\end{array}} \tag{3.15}$$

Then,

$$\boxed{|g_1(\tau)| = S(\mathbf{k},\tau)/S(\mathbf{k},0) \quad \begin{array}{l}\text{normalized electric-field}\\ \text{autocorrelation function}\end{array}} \tag{3.16}$$

As we have separated the static structure factor $S(\mathbf{k})$ into $S_1(\mathbf{k})$ and the rest (see Eq. 2.60), we can separate $S(\mathbf{k}, \tau)$ into two parts:

$$S(\mathbf{k},\tau) = S_1(\mathbf{k},\tau) + \langle (n_\mathrm{P} - 1)\exp[\mathrm{i}\mathbf{k}\cdot(\mathbf{r}_1(0) - \mathbf{r}_2(\tau))]\rangle \tag{3.17}$$

with the single-particle dynamic structure factor defined as

$$\boxed{S_1(\mathbf{k},\tau) = \langle \exp[\mathrm{i}\mathbf{k}\cdot(\mathbf{r}_1(0) - \mathbf{r}_1(\tau))]\rangle \quad \begin{array}{l}\text{single-particle}\\ \text{dynamic structure factor}\end{array}} \tag{3.18}$$

It is apparent that the dynamic structure factor for $\tau = 0$ is identical to the static structure factor:

$$S(\mathbf{k},0) = S(\mathbf{k}), \qquad S_1(\mathbf{k},0) = 1 \tag{3.19}$$

for a system of particles suspended in a liquid.

3.2.3.3 Transition Probability The ensemble average in Eq. 3.15 is taken with respect to the positions of the particles at $t = 0$ and $t = \tau$. Rewriting $\mathbf{r}_m(0)$ to $\mathbf{r}'_m$ and $\mathbf{r}_n(\tau)$ to $\mathbf{r}_n$, it is expressed as

$$\begin{aligned} S(\mathbf{k},\tau) = \frac{1}{{n_\mathrm{P}}^2} \prod_{m=1}^{n_\mathrm{P}} \int_V \mathrm{d}\mathbf{r}'_m \prod_{n=1}^{n_\mathrm{P}} \int_V \mathrm{d}\mathbf{r}_n \sum_{i,j=1}^{n_\mathrm{P}} \exp[\mathrm{i}\mathbf{k}\cdot(\mathbf{r}'_i - \mathbf{r}_j)] \\ \times P(\mathbf{r}_1,\ldots,\mathbf{r}_{n_\mathrm{P}};\mathbf{r}'_1,\ldots,\mathbf{r}'_{n_\mathrm{P}};\ \tau)\,\rho(\mathbf{r}'_1,\ldots,\mathbf{r}'_{n_\mathrm{P}};0) \end{aligned} \tag{3.20}$$

where $\rho(\mathbf{r}'_1,\ldots,\mathbf{r}'_{n_\mathrm{P}};0)$ is the joint density distribution for the n_P particles at time 0, and $P(\mathbf{r}_1,\ldots,\mathbf{r}_{n_\mathrm{P}};\mathbf{r}'_1,\ldots,\mathbf{r}'_{n_\mathrm{P}};\tau)\,\mathrm{d}\mathbf{r}_1\ldots\mathrm{d}\mathbf{r}_{n_\mathrm{P}}$ is the joint probability for the particles to

move from $\mathbf{r}'_1, \ldots, \mathbf{r}'_{n_\mathrm{P}}$ into a (n_P-dimensional) volume $\mathrm{d}\mathbf{r}_1 \ldots \mathrm{d}\mathbf{r}_{n_\mathrm{P}}$ at $\mathbf{r}_1, \ldots, \mathbf{r}_{n_\mathrm{P}}$ in time τ. The **transition probability** $P(\mathbf{r}_1, \ldots, \mathbf{r}_{n_\mathrm{P}}; \mathbf{r}'_1, \ldots, \mathbf{r}'_{n_\mathrm{P}}; \tau)$ satisfies the normalization condition:

$$\prod_{n=1}^{n_\mathrm{P}} \int_V \mathrm{d}\mathbf{r}_n \, P(\mathbf{r}_1, \ldots, \mathbf{r}_{n_\mathrm{P}}; \mathbf{r}'_1, \ldots, \mathbf{r}'_{n_\mathrm{P}}; \tau) = 1 \tag{3.21}$$

Integration of $\rho(\mathbf{r}'_1, \ldots, \mathbf{r}'_{n_\mathrm{P}}; 0)$ gives the number of particles in volume V:

$$\prod_{m=1}^{n_\mathrm{P}} \int_V \mathrm{d}\mathbf{r}'_m \, \rho(\mathbf{r}'_1, \ldots, \mathbf{r}'_{n_\mathrm{P}}; 0) = n_\mathrm{P} \tag{3.22}$$

In a homogeneous solution, the particles are uniformly distributed in V at $t = 0$, i.e., $\rho(\mathbf{r}'_1, \ldots, \mathbf{r}'_{n_\mathrm{P}}; 0) = n_\mathrm{P}/V^{n_\mathrm{P}}$. The transition probability depends only on the displacement ($\mathbf{r}_1 - \mathbf{r}'_1$, etc) and is an even function of the displacement. Then,

$$S(\mathbf{k}, \tau) = \frac{1}{n_\mathrm{P}} \prod_{n=1}^{n_\mathrm{P}} \int_V \mathrm{d}(\mathbf{r}_n - \mathbf{r}'_n) \sum_{i,j=1}^{n_\mathrm{P}} \exp[\mathrm{i}\mathbf{k} \cdot (\mathbf{r}_j - \mathbf{r}'_i)] \, P(\mathbf{r}_1 - \mathbf{r}'_1, \ldots, \mathbf{r}_{n_\mathrm{P}} - \mathbf{r}'_{n_\mathrm{P}}; \tau) \tag{3.23}$$

where the sign in the exponential function has been changed. The even function $P(\mathbf{r}_1 - \mathbf{r}'_1, \ldots, \mathbf{r}_{n_\mathrm{P}} - \mathbf{r}'_{n_\mathrm{P}}; \tau)$ makes $S(\mathbf{k}, \tau)$ a real function.

If each particle moves independently, the second term in Eq. 3.17 disappears:

$$S(\mathbf{k}, \tau) = S_1(\mathbf{k}, \tau) \tag{3.24}$$

Independent motions are typically observed at low concentrations. The single-particle ($n_\mathrm{P} = 1$) version of Eq. 3.20 is

$$S_1(\mathbf{k}, \tau) = \int_V \mathrm{d}\mathbf{r}' \int_V \mathrm{d}\mathbf{r} \exp[\mathrm{i}\mathbf{k} \cdot (\mathbf{r} - \mathbf{r}')] \, P(\mathbf{r}, \mathbf{r}'; \tau) \rho(\mathbf{r}'; 0) \tag{3.25}$$

where $P(\mathbf{r}, \mathbf{r}'; \tau)$ is the single-particle transition probability. If the solution is homogeneous at time 0, i.e., $\rho(\mathbf{r}'; 0) = 1/V$, then

$$\boxed{S_1(\mathbf{k}, \tau) = \int_V \mathrm{d}\mathbf{r} \exp[\mathrm{i}\mathbf{k} \cdot (\mathbf{r} - \mathbf{r}')] \, P(\mathbf{r}, \mathbf{r}'; \tau) \quad \begin{array}{l}\text{single-particle} \\ \text{dynamic structure factor}\end{array}} \tag{3.26}$$

which is the single-particle version of Eq. 3.23. Equation 3.26 means that $|g_1(\tau)| = S_1(\mathbf{k}, \tau)/S_1(\mathbf{k}, 0) = S_1(\mathbf{k}, \tau)$ is the Fourier-transform of the transition probability $P(\mathbf{r}, \mathbf{r}'; \tau)$.

Motion of the particles can be caused by an external flow and diffusion. In the flow, solvent molecules move together with the particles. Diffusion occurs regardless

of the presence of the external flow. We look closely at the diffusion phenomena of particles in a quiescent solution in the following subsection.

3.2.4 Diffusion of Particles

3.2.4.1 Brownian Motion When we place a blot of ink in still water, the colored region expands with time but the color fades, eventually filling the entire water in the container. The final state is a uniform concentration of the ink. Spreading of a substance throughout accessible volume is called **diffusion**. The phenomena is made possible by microscopic movement of water molecules.

Particles suspended in a liquid change their positions in the container by diffusion. If a particle is much larger compared with the solvent molecules, we can regard that particle to be suspended in a continuous medium of solvent. Figure 3.5 illustrates how the particle has traveled, starting at $\mathbf{r}'$ at time $t = 0$, to reach $\mathbf{r}$ at time t. The trajectory is random. The random motion of the particle is called a **Brownian motion**. It was discovered by Scottish botanist R. Brown when he was looking into an optical microscope to observe pollen on water. What he had thought was a motionless, dead world turned out to be filled with vigorous and perpetual movements. Later, it was found that a similar type of motion exists for suspensions in a liquid. Solvent molecules collide randomly with particles all the time to change the velocity of the particle, resulting in a random motion. The motions of the solvent molecules are activated by thermal energy; $k_B T$ is sufficient to cause the Brownian motion.

The Brownian motion is stochastic. There is no knowing in advance where the particle will reach in a given time. What we can know is the transition probability $P(\mathbf{r}, \mathbf{r}'; t)$ for the particle to move from $\mathbf{r}'$ at $t = 0$ to reach $\mathbf{r}$ at time t.

Polymer molecules in solution also display Brownian motion. Because the polymer molecule is not a simple sphere, each polymer conformation has its own diffusion characteristics. For rigid molecules, the shape of the molecule, spherical or rodlike, for instance, makes a difference. For a linear flexible molecule, connectivity

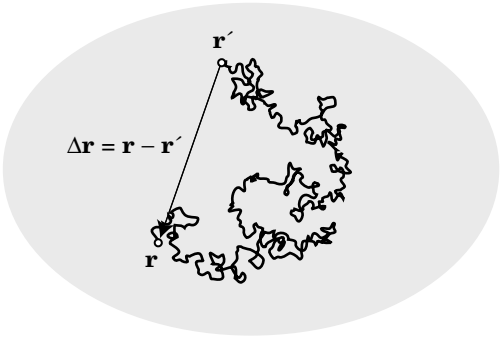

Figure 3.5. Trajectory of a Brownian particle. Starting at $\mathbf{r}'$ at time zero, it moves to $\mathbf{r}$ in time t. We cannot predict the displacement $\Delta\mathbf{r} = \mathbf{r} - \mathbf{r}'$.

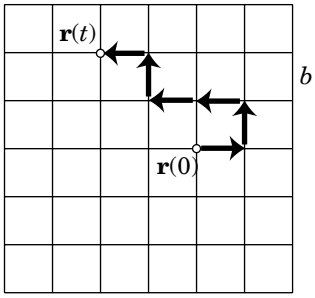

Figure 3.6. Random walk on a cubic lattice (two-dimensional rendering). In each step, the walker moves a distance of b randomly. Starting at $\mathbf{r}(0)$, the walker moves to $\mathbf{r}(t)$ in N steps.

of monomers generates a specific pattern in its Brownian motion. Before we elaborate on the motion of the polymer molecule (Section 3.4), we look at the Brownian motion of a simple particle suspended in a continuous medium and obtain the transition probability.

3.2.4.2 Diffusion Coefficient We learned about random walks in Section 1.2 to describe an ideal chain. The random walk on the cubic lattice (Fig. 3.6) shares stochastic nature of the whereabouts with the Brownian motion of the particle in solution. We can apply the results obtained for the ideal chains to the motion of the random walker.

Let t_1 be the time of each step and b the displacement. The **mean square displacement** of N steps in time $t = Nt_1$,

$$\langle [\mathbf{r}(t) - \mathbf{r}(0)]^2 \rangle = Nb^2 \quad \text{mean square displacement} \tag{3.27}$$

is proportional to the total time t. The ratio of the mean square displacement to the time, divided by 6 for the three dimensions, gives, in general, the **diffusion coefficient** D:

$$\boxed{D = \frac{\langle [\mathbf{r}(t) - \mathbf{r}(0)]^2 \rangle}{6t} \quad \text{diffusion coefficient}} \tag{3.28}$$

For the random walker on the cubic lattice,

$$\boxed{D = \frac{Nb^2}{6Nt_1} = \frac{b^2}{6t_1} \quad \text{random walk, 3D}} \tag{3.29}$$

The last equality proves that the ratio is the same for the whole motion of N steps and for the single-step motion. To estimate D, we can use either an N-step motion or a single-step motion. The results should be identical as long as the step motions are mutually independent (Markoffian).

3.2.4.3 Gaussian Transition Probability We learned in Section 1.2 that the transition probability becomes Gaussian in the limit of small b and large N. The Gaussian probability given by Eq. 1.18 gives the transition probability $P(\mathbf{r}, \mathbf{r}'; t)$ for the Brownian motion by replacing $(2/3)Nb^2$ by $4Dt$:

$$\boxed{P(\mathbf{r}, \mathbf{r}'; t) = (4\pi Dt)^{-3/2} \exp\left(-\frac{(\mathbf{r} - \mathbf{r}')^2}{4Dt}\right) \quad \text{Gaussian transition probability}} \tag{3.30}$$

The motion of the particle whose transition probability is given by this equation is called diffusion or a Wiener process.

The probability is independent for each of x, y, and z directions in the isotropic solution. In the x direction, for instance,

$$P_x(x, x'; t) = (4\pi Dt)^{-1/2} \exp\left(-\frac{(x - x')^2}{4Dt}\right) \tag{3.31}$$

and $P(\mathbf{r}, \mathbf{r}'; t) = P_x(x, x'; t)P_y(y, y'; t)P_z(z, z'; t)$.

The transition probability $P_x(x, x'; t)$ is essentially a normal distribution of a random variable $x - x'$ with a zero mean and a variance of $2Dt$. Therefore,

$$\boxed{\langle x - x' \rangle = 0, \quad \langle (x - x')^2 \rangle = 2\mathrm{D}t \quad \text{1D diffusion}} \tag{3.32}$$

These equations apply also to a particle that diffuses along a one-dimensional path. The mean square displacement $\langle (x - x')^2 \rangle$ is proportional to t. Figure 3.7 shows how P_x broadens with time. The plots are given as a function of $(x - x')/b$ for $4Dt/b^2 = 0.1$, 1, and 10, where b is a unit length. Initially ($t \to 0$), the particle is at x', i.e., $P(x, x'; 0) = \delta(x - x')$.

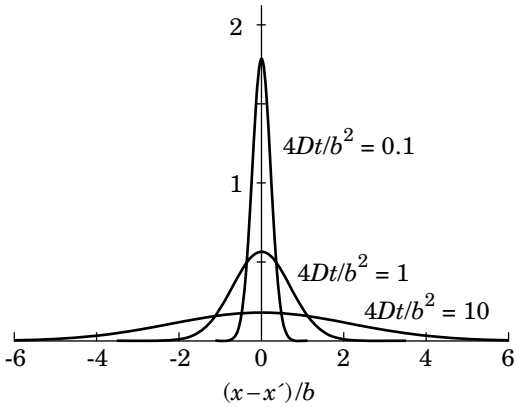

Figure 3.7. Broadening of the distribution with time for the position of a one-dimensional Brownian particle. Plots are for $4Dt/b^2 = 0.1$, 1, and 10.

For the three-dimensional diffusion, the displacement $\mathbf{r} - \mathbf{r}'$ satisfies

$$\boxed{\langle \mathbf{r} - \mathbf{r}' \rangle = 0, \quad \langle (\mathbf{r} - \mathbf{r}')^2 \rangle = 6Dt \quad \text{3D diffusion}} \tag{3.33}$$

because $\langle (\mathbf{r} - \mathbf{r}')^2 \rangle = \langle (x - x')^2 \rangle + \langle (y - y')^2 \rangle + \langle (z - z')^2 \rangle = 3 \times 2Dt$.

3.2.4.4 Diffusion Equation It is easy to find that $P_x(x, x'; t)$ given by Eq. 3.31 satisfies the one-dimensional **diffusion equation**:

$$\boxed{\frac{\partial P_x}{\partial t} = D\frac{\partial^2 P_x}{\partial x^2} \quad \text{1D diffusion equation}} \tag{3.34}$$

The initial condition is $P_x(x, x'; 0) = \delta(x - x')$. Likewise, $P(\mathbf{r}, \mathbf{r}'; t)$ given by Eq. 3.30 satisfies the three-dimensional diffusion equation:

$$\boxed{\frac{\partial P}{\partial t} = D\nabla^2 P \quad \text{3D diffusion equation}} \tag{3.35}$$

where $\nabla^2 = \partial^2/\partial x^2 + \partial^2/\partial y^2 + \partial^2/\partial z^2$ is the Laplacian. It is also written as $\partial^2/\partial \mathbf{r}^2$. The initial condition is $P(\mathbf{r}, \mathbf{r}'; 0) = \delta(\mathbf{r} - \mathbf{r}')$.

3.2.4.5 Concentration The meaning of the transition probability $P(\mathbf{r}, \mathbf{r}'; t)$ will be clearer when we look at the local concentration profile of the particles, $c(\mathbf{r}, t)$, at position $\mathbf{r}$ and time t. It is the mass of the particles in a small volume around $\mathbf{r}$, divided by the volume. The volume contains sufficiently many particles. With $P(\mathbf{r}, \mathbf{r}'; t)$, we can write

$$c(\mathbf{r}, t) = \int P(\mathbf{r}, \mathbf{r}'; t)\, c(\mathbf{r}', 0)\, \mathrm{d}\mathbf{r}' \tag{3.36}$$

The particles we find at $\mathbf{r}$ and t have come from all different positions in the system. At time zero, the particles were at $\mathbf{r}'$ with concentration profile $c(\mathbf{r}',0)$ (Fig. 3.8). They have migrated to $\mathbf{r}$ with the probability of $P(\mathbf{r}, \mathbf{r}'; t)$. Integration of

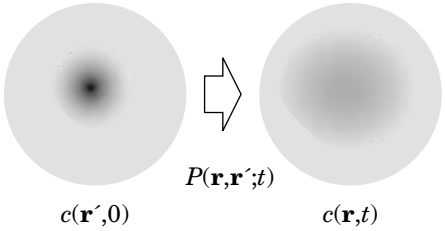

Figure 3.8. Transition probability $P(\mathbf{r}, \mathbf{r}'; t)$ accounts for a change from the initial concentration profile $c(\mathbf{r}', 0)$ to the final concentration profile $c(\mathbf{r}, t)$. The concentration is indicated by the gray level.

$c(\mathbf{r}', 0)P(\mathbf{r}, \mathbf{r}'; t)$ with respect to $\mathbf{r}'$ gives the concentration profile $c(\mathbf{r}, t)$ at time t. It is easy to show that $c(\mathbf{r}, t)$ satisfies the same diffusion equation as Eq. 3.35:

$$\frac{\partial c}{\partial t} = D\nabla^2 c \tag{3.37}$$

The initial concentration profile is $c(\mathbf{r}, 0)$.

3.2.4.6 Long-Time Diffusion Coefficient In various experiments and computer simulations, the mean square displacement $\langle(\mathbf{r} - \mathbf{r}')^2\rangle$ is often measured or calculated as a function of time t. If the double logarithmic plot of $\langle(\mathbf{r} - \mathbf{r}')^2\rangle$ versus t has a slope of 1, we can say that the relevant motion is diffusional. It often happens that the proportionality is reached only after a sufficiently long time. It is therefore customary to define the diffusion coefficient in the long-time limit:

$$\boxed{D = \lim_{t\to\infty} \frac{\langle(\mathbf{r} - \mathbf{r}')^2\rangle}{6t} \quad \text{long-time diffusion coefficient}} \tag{3.38}$$

for dynamics in three dimensions. The denominator is $2 \times$ (dimensions) $\times\, t$. This diffusion coefficient is called the **long-time diffusion coefficient**. The dynamics may have different diffusion coefficients in other time scales, or it may not be diffusional. The plot of $\langle(\mathbf{r} - \mathbf{r}')^2\rangle$ versus t will tell the nature of the dynamics. We will see variations of dynamics in different time scales in Sections 3.4 and 4.3.

In Section 1.5, we learned that the mean square end-to-end distance $\langle R_F^2\rangle$ of a wormlike chain becomes proportional to the contour length as the chain becomes longer. The tendency for $\langle(\mathbf{r} - \mathbf{r}')^2\rangle$ to become proportional to t in a long time is parallel to the tendency for $\langle R_F^2\rangle$ of the wormlike chain.

3.2.5 Diffusion and DLS

3.2.5.1 Dynamic Structure Factor and Mean Square Displacement Here we learn how $|g_1(\tau)|$ obtained in DLS gives an estimate of the diffusion coefficient. We are concerned with dilute solutions here. Hence, $|g_1(\tau)| = S_1(\mathbf{k}, \tau)$.

In Eq. 3.26, we use the Taylor expansion at low scattering angles: $\exp[i\mathbf{k}\cdot(\mathbf{r} - \mathbf{r}')] = 1 + i\mathbf{k}\cdot(\mathbf{r} - \mathbf{r}') - (1/2)[\mathbf{k}\cdot(\mathbf{r} - \mathbf{r}')]^2 + \cdots$. Then $S_1(\mathbf{k}, \tau)$ is transformed to

$$S_1(\mathbf{k}, \tau) = 1 - \tfrac{1}{6}\mathbf{k}^2\langle(\mathbf{r} - \mathbf{r}')^2\rangle + \cdots \cong \exp\left[-\tfrac{1}{6}\mathbf{k}^2\langle(\mathbf{r} - \mathbf{r}')^2\rangle\right] \tag{3.39}$$

where $\langle\mathbf{r} - \mathbf{r}'\rangle = 0$, and $\langle(x - x')^2\rangle = \langle(y - y')^2\rangle = \langle(z - z')^2\rangle = \langle(\mathbf{r} - \mathbf{r}')^2\rangle/3$, $\langle(x - x')(y - y')\rangle = 0$, and so forth were used. This $|g_1(\tau)| = S_1(\mathbf{k}, \tau)$ is rewritten to

$$\boxed{\langle(\mathbf{r} - \mathbf{r}')^2\rangle = -6\ln|g_1(\tau)|/\mathbf{k}^2 \quad \text{small } k} \tag{3.40}$$

If plots of $\ln|g_1(\tau)|/\mathbf{k}^2$ vs. τ measured at different angles overlap each other, then k is already sufficiently small. Typically, $k \times$ (size of the particle) < 1 qualifies as small k.

The mean square displacement in time τ is evaluated by using Eq. 3.40. The slope in the plot is equal to $6D$. It is, however, more common to follow the approach described below.

3.2.5.2 Dynamic Structure Factor of a Diffusing Particle More often than not, the particles move according to the diffusion equation. The transition probability is given by Eq. 3.30. Then

$$\begin{aligned} S_1(\mathbf{k}, \tau) &= \int \exp[i\mathbf{k}\cdot(\mathbf{r} - \mathbf{r}')](4\pi D\tau)^{-3/2} \exp\left(-\frac{(\mathbf{r} - \mathbf{r}')^2}{4D\tau}\right) d\mathbf{r} \\ &= \int (4\pi D\tau)^{-3/2} \exp\left(-\frac{(\mathbf{r} - \mathbf{r}' - i\mathbf{k}\cdot 2D\tau)^2}{4D\tau} - D\tau\mathbf{k}^2\right) d\mathbf{r} = \exp(-D\tau\mathbf{k}^2) \end{aligned} \tag{3.41}$$

Thus, $|g_1(\tau)|$ is an exponentially decaying function with a decay constant of $D\mathbf{k}^2$. It is customary to first introduce the **decay rate** Γ of $|g_1(\tau)|$ by

$$\boxed{|g_1(\tau)| = \exp(-\Gamma\tau)} \tag{3.42}$$

and then relate Γ to $\mathbf{k}^2$ as

$$\boxed{\Gamma = D\mathbf{k}^2 \quad \text{decay rate for diffusion}} \tag{3.43}$$

for the diffusional motion. It is apparent that $|g_1(\tau)|$ decays faster at a higher scattering angle.

The procedure to obtain the diffusion coefficient D is as follows. First, measure the autocorrelation function at different angles. Second, obtain Γ as the negative of the slope in the semi-logarithmic plot of $|g_1(\tau)|$ as shown in Figure 3.9. Third, plot

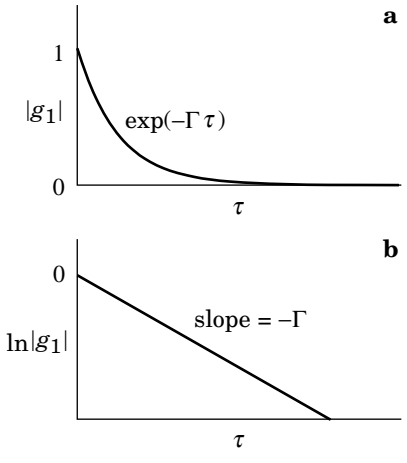

Figure 3.9. When $|g_1(\tau)|$ decays in a single exponential (a), the plot of $\ln|g_1(\tau)|$ is a straight line with a slope of $-\Gamma$ (b).

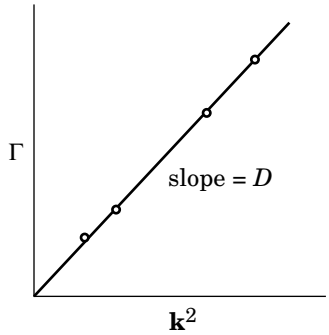

Figure 3.10. Decay rate Γ of $|g_1(\tau)|$, plotted as a function of $\mathbf{k}^2$. If the particles move by diffusion, the plot is on a straight line through the origin with a slope equal to the diffusion coefficient D.

Γ as a function of $\mathbf{k}^2$. The plot should be approximated by a straight line through the origin (see Fig. 3.10). The slope of the line is D. We can show that conversely, if the measured Γ versus $\mathbf{k}^2$ is on a straight line through the origin, then the dynamics is diffusional (Problem 3.3).

When the suspension is not spherical or, in general, is a particle with an internal structure such as a linear polymer chain, the decay rate deviates from the one given by Eq. 3.43 at higher scattering angles. The diffusion coefficient defined in the low $\mathbf{k}$ limit refers to the overall displacement of the molecule, i.e., the motion for the center of mass.

3.2.6 Dynamic Structure Factor of a Polymer Solution

3.2.6.1 Dynamic Structure Factor The electric field of the light scattered by a volume that contains n_P chains ($n_P \gg 1$), each consisting of N beads, can be written in the same way as Eq. 3.15. The dynamic structure factor is now given as

$$\boxed{S_1(\mathbf{k}, \tau) = \frac{1}{N_P N} \sum_{m,n=1}^{N_P} \sum_{i,j=1}^{N} \langle \exp[i\mathbf{k} \cdot (\mathbf{r}_{mi}(0) - \mathbf{r}_{nj}(\tau))] \rangle} \quad \begin{matrix}\text{dynamic structure factor} \\ \text{polymer solution}\end{matrix} \tag{3.44}$$

which is decomposed into two parts:

$$S(\mathbf{k}, \tau) = S_1(\mathbf{k}, \tau) + \frac{n_P}{N} \sum_{i,j=1}^{N} \langle \exp[i\mathbf{k} \cdot (\mathbf{r}_{1i}(0) - \mathbf{r}_{2j}(\tau))] \rangle \tag{3.45}$$

where $S_1(\mathbf{k}, \tau)$ is the single-chain dynamic structure factor:

$$\boxed{S_1(\mathbf{k}, \tau) = \frac{1}{N} \sum_{i,j=1}^{N} \langle \exp[i\mathbf{k} \cdot (\mathbf{r}_{1i}(0) - \mathbf{r}_{1j}(\tau))] \rangle} \quad \begin{matrix}\text{single-chain} \\ \text{dynamic structure factor}\end{matrix} \tag{3.46}$$

At $\tau = 0$, the dynamic structure factors are identical to the static structure factors (Eqs. 2.59 and 2.60):

$$S(\mathbf{k}, 0) = S(\mathbf{k}), \qquad S_1(\mathbf{k}, 0) = S_1(\mathbf{k}) \tag{3.47}$$

Thus, $|g_1(\tau)| = S_1(\mathbf{k}, \tau)/S_1(\mathbf{k}, 0)$ when each polymer chain moves independently of other chains at low concentrations.

3.2.6.2 Long-Time Behavior In a short time scale, $S_1(\mathbf{k},\tau)$ exhibits a complicated pattern, reflecting complex motions of different parts of the polymer chain. Over a long time, however, the motion is simplified. It is dominated by the translation of the chain as a whole in the solution for any conformation. We can prove the dominance of the center-of-mass motion as follows.

In Eq. 3.46, the displacement $\mathbf{r}_{1i}(0) - \mathbf{r}_{1j}(\tau)$ between bead i at time 0 and bead j at time τ on chain 1 consists of three parts:

$$\mathbf{r}_{1i}(0) - \mathbf{r}_{1j}(\tau) = [\mathbf{r}_{1i}(0) - \mathbf{r}_{1G}(0)] + [\mathbf{r}_{1G}(0) - \mathbf{r}_{1G}(\tau)] + [\mathbf{r}_{1G}(\tau) - \mathbf{r}_{1j}(\tau)] \tag{3.48}$$

where $\mathbf{r}_{1G}(0)$ and $\mathbf{r}_{1G}(\tau)$ are the center of mass positions of the chain at time 0 and τ, respectively. The three parts are represented by three vectors in Figure 3.11. Initially, the three parts are correlated. As τ increases, the chain conformation becomes randomized, and the three vectors become more irrelevant to each other. For instance, $\mathbf{r}_{1i}(0) - \mathbf{r}_{1G}(0)$ becomes uncorrelated to $\mathbf{r}_{1G}(\tau) - \mathbf{r}_{1j}(\tau)$ regardless of $i = j$ or not. Thus the statistical average of the square is

$$\begin{aligned}\langle[\mathbf{r}_{1i}(0) - \mathbf{r}_{1j}(\tau)]^2\rangle = \langle[\mathbf{r}_{1i}(0) - \mathbf{r}_{1G}(0)]^2\rangle + \langle[\mathbf{r}_{1G}(0) - \mathbf{r}_{1G}(\tau)]^2\rangle \\ + \langle[\mathbf{r}_{1G}(\tau) - \mathbf{r}_{1j}(\tau)]^2\rangle\end{aligned} \tag{3.49}$$

The first and third terms are equal to R_g^2 by definition. Only the second term grows with time because of diffusion of the chain as a whole. After a long time, the

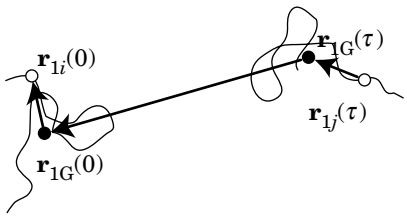

Figure 3.11. The polymer chain moves its center of mass and changes its orientation and internal arrangement. The displacement between monomers i and j, $\mathbf{r}_{1i}(0) - \mathbf{r}_{1j}(\tau)$, is decomposed into three parts indicated by the arrows. Only the center-of-mass distance keeps growing with time.

second term becomes dominant. Thus,

$$-6\ln|g_1(\tau)|/\mathbf{k}^2 = \langle[\mathbf{r}_{1i}(0) - \mathbf{r}_{1j}(\tau)]^2\rangle \rightarrow \langle[\mathbf{r}_{1G}(0) - \mathbf{r}_{1G}(\tau)]^2\rangle \tag{3.50}$$

and therefore $|g_1(\tau)|$ gives the **center-of-mass diffusion coefficient.**

The above discussion applies only to a long time. In a short time, $\ln|g_1(\tau)|$ may exhibit non-$\mathbf{k}^2$ behavior. In Section 3.4, we will learn in more details how $S_1(\mathbf{k},\tau)$ depends on $\mathbf{k}$ and τ for a bead-spring model.

3.2.7 Hydrodynamic Radius

3.2.7.1 Stokes-Einstein Equation To drag a particle suspended in a viscous medium at a constant velocity $\mathbf{v}$, a constant force of $\mathbf{F} = \zeta\mathbf{v}$ must be applied to the particle (Fig. 3.12). The coefficient ζ is called the friction coefficient. Einstein showed that the diffusion coefficient D of the particle in a quiescent solution at temperature T is related to ζ by

$$\boxed{D = \frac{k_B T}{\zeta} \quad \text{Nernst–Einstein equation}} \tag{3.51}$$

This equation is the simplest form of the so-called fluctuation-dissipation theorem. The diffusion, which is a typical equilibrium phenomenon, is related to the friction, a typical energy dissipation phenomenon.

Stokes showed that the friction coefficient for a sphere of radius R_S is given by

$$\zeta = 6\pi\eta_s R_S \tag{3.52}$$

in a solvent of viscosity η_s. The viscosity of a fluid expresses how difficult it is to flow the fluid. We will learn the exact definition of viscosity in Section 3.3.1. Combining the above two equations gives the **Stokes-Einstein** equation:

$$\boxed{D = \frac{k_B T}{6\pi\eta_s R_S} \quad \text{diffusion coefficient of a sphere}} \tag{3.53}$$

The radius R_S is called the **Stokes radius**. The diffusion is faster at a higher temperature, in a less viscous solvent, and for a smaller particle.

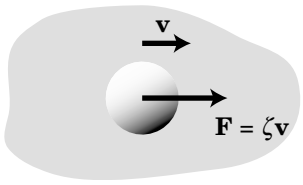

Figure 3.12. A particle moving at a constant velocity $\mathbf{v}$ in a viscous liquid needs to be pulled by force $\mathbf{F} = \zeta\mathbf{v}$.

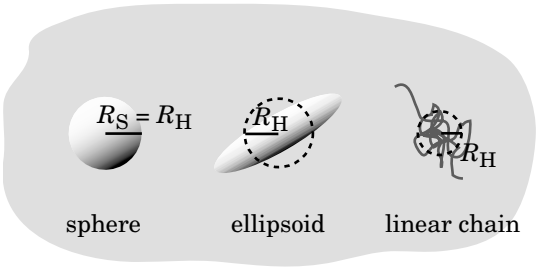

Figure 3.13. For the center-of-mass motion, an ellipsoid with a hydrodynamic radius R_H receives the same friction as a sphere of radius R_H does. Likewise, a linear chain with a hydrodynamic radius R_H diffuses with the same diffusion coefficient as the sphere of radius R_H.

We now extend the concept of the Stokes radius to nonspherical suspensions and molecules (Fig. 3.13). Once the center-of-mass diffusion coefficient D is measured for the suspension or the molecule, we can introduce the **hydrodynamic radius** R_H by

$$\boxed{R_H = \frac{k_B T}{6\pi\eta_s D} \quad \text{hydrodynamic radius}} \tag{3.54}$$

For the spherical suspension, $R_H = R_S$. We can regard R_H as another quantity to characterize the dimension of the molecule.

3.2.7.2 Hydrodynamic Radius of a Polymer Chain For a linear chain molecule, R_H is proportional to R_g and R_F. Therefore, $R_H \propto N^\nu$, where $\nu = 1/2$ in the theta solvent and $\nu \cong 0.59$ or $3/5$ in the good solvent. We can prove the proportionality, as shown below.

When all of the N monomers in the polymer chain move, each monomer receives a friction from the solvent. The overall friction, however, is not proportional to N but rather is proportional to N^ν. Because $\nu < 1$, $N^\nu < N$. The friction of the chain molecule is smaller than the friction nonbonded, independently moving N monomers receive. It is explained as follows. The motion of one of the monomers accompanies motions of adjacent solvent molecules in the same direction, and their effect propagates to another monomer to facilitate its motion in the same direction in an otherwise stagnant solvent (Fig. 3.14). This interaction is called **hydrodynamic interaction**. It is different from the other interactions we have seen so far. It exists only when the particles move. Static properties such as the osmotic pressure are not affected by the hydrodynamic interactions. They only affect dynamic properties, such as diffusion, but do so strongly.

Oseen found that the magnitude of the hydrodynamic interaction between two particles at $\mathbf{r}$ and $\mathbf{r}'$ is proportional to $|\mathbf{r} - \mathbf{r}'|^{-1}$. The interaction decays only algebraically with a small exponent of -1 and therefore is long ranged. In a chain molecule, all monomers affect all other monomers because they are close to each other.

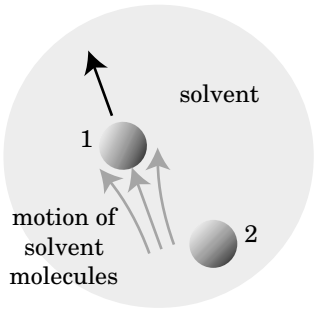

Figure 3.14. Movement of particle 1 generates the motion of solvent molecules, which eases the motion of particle 2 in the same direction. Thus, the hydrodynamic interaction reduces friction.

In Section 3.4.6, we will learn that $1/R_{\mathrm{H}}$ of the chain molecule is given as the average of the reciprocal of the distance between two monomers on the chain:

$$\boxed{\frac{1}{R_{\mathrm{H}}} = \left\langle \frac{1}{|\mathbf{r}_m - \mathbf{r}_n|} \right\rangle \quad \begin{array}{l}\text{hydrodynamic radius}\\ \text{of a polymer chain}\end{array}} \tag{3.55}$$

The average is taken with respect to possible positions of the two monomers m and n ($m \neq n$) and then with respect to m and n that run over all monomers of the chain.

Here we calculate R_{H} of a chain with a Gaussian conformation. Using the Gaussian distribution given by Eq. 1.34, $\langle|\mathbf{r}_m - \mathbf{r}_n|^{-1}\rangle_{mn}$ for a given m and n is calculated as

$$\begin{aligned}\left\langle \frac{1}{|\mathbf{r}_m - \mathbf{r}_n|} \right\rangle_{mn} &= \int_0^\infty (2\pi|n-m|b^2/3)^{-3/2} \exp\left(-\frac{3r^2}{2|n-m|b^2}\right) 4\pi r^2 \frac{1}{r}\,\mathrm{d}r \\ &= (2\pi|n-m|b^2/3)^{-3/2} 4\pi \cdot |n-m|b^2/3 = (6/\pi)^{1/2} b^{-1} |n-m|^{-1/2}\end{aligned} \tag{3.56}$$

The average of $|n-m|^{-1/2}$ with respect to m and n is calculated as

$$N^{-2}\int_0^N \mathrm{d}n \int_0^N \mathrm{d}m |n-m|^{-1/2} = 2N^{-2}\int_0^N 2n^{1/2}\mathrm{d}n = (8/3)N^{-1/2} \tag{3.57}$$

Thus, R_{H} is given by

$$\frac{1}{R_{\mathrm{H}}} = \left(\frac{6}{\pi}\right)^{1/2} \frac{1}{b} \times \frac{8}{3} N^{-1/2} = 8\left(\frac{2}{3\pi}\right)^{1/2} \frac{1}{bN^{1/2}} \tag{3.58}$$

R_{H} is quite small compared with R_{F}: $R_{\mathrm{H}}/R_{\mathrm{F}} = (3\pi/2)^{1/2}/8 \cong 0.271$. R_{H} is smaller than R_{g}: $R_{\mathrm{H}}/R_{\mathrm{g}} = (3/8)\pi^{1/2} \cong 0.665$. Thus, $R_{\mathrm{H}} < R_{\mathrm{g}} < R_{\mathrm{F}}$ for a chain with a Gaussian conformation.

The real chain has $R_{\mathrm{H}} \cong bN^{\nu}$, since $\langle|\mathbf{r}_m - \mathbf{r}_n|^{-1}\rangle_{mn} \cong b^{-1}|n-m|^{-\nu}$. More exact results for polymer chains in a good solvent were obtained in the renormalization

Table 3.1 Various Measures of the Chain Dimension

Polymer Chain	R_H/R_g	R_H/R_F	R_F/R_g
Ideal/theta solvent*	0.665 $(=(3/8)\pi^{1/2})$	0.271 $(=(3\pi/2)^{1/2}/8)$	2.45 $(=6^{1/2})$
Real (good solvent)	0.640	0.255	2.51
Rod-like	$3^{1/2}/(\ln(L/b)-\gamma)$**	$1/[2(\ln(L/b)-\gamma)]$**	3.46 $(=12^{1/2})$

*Chains with an ideal-chain conformation.
**Depends on the rod length L and rod diameter b. $\gamma \cong 0.3$.

group theory and will be given in Section 3.4. The relationship, $R_H < R_g < R_F$, is the same as for the Gaussian chain.

Table 3.1 compares various measures of the dimension for chains with an ideal-chain conformation (or at the theta condition), excluded-volume chains, and rodlike molecules. The latter will be considered in Section 3.5.

Figure 3.15 shows examples of R_H measured by using DLS for different molecular weight fractions. Panel a was obtained for polystyrene in 2-fluorotoluene at

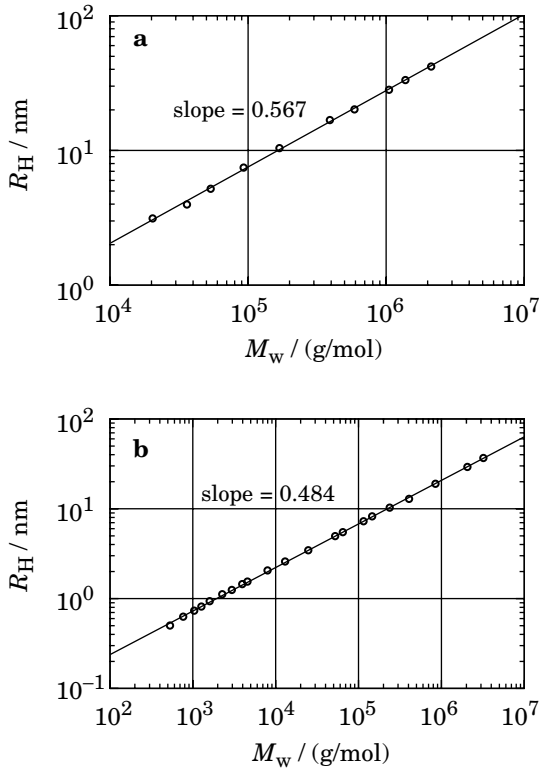

Figure 3.15. Hydrodynamic radius R_H of different molecular weights of a polymer. a: Polystyrene in 2-fluorotoluene at 42.6°C (good solvent). (From Ref. 30.) b: Poly(α-methyl styrene) in cyclohexane at 30.5°C (theta solvent). (From Ref. 31.)

42.6°C (good solvent),[30] and panel b was obtained for poly(α-methyl styrene) in cyclohexane at 30.5°C (theta condition).[31] In the two panels of the figure, the plots are on a straight line, in agreement with the predicted power relationship, $R_H \propto N^{-\nu}$. The exponents ν obtained in the fitting are 0.567 and 0.484, slightly smaller than the values predicted for the two environments.

3.2.8 Particle Sizing

3.2.8.1 Distribution of Particle Size It is all but impossible that every solute molecule or particle has exactly the same hydrodynamic radius in a given solution. There is always a distribution in R_H, as illustrated in Figure 3.16. The peak position and width of the distribution vary from sample to sample. The distribution in R_H leads to a distribution in the diffusion coefficient and therefore a distribution in the decay rate Γ of $|g_1(\tau)|$. Then, $|g_1(\tau)|$ is not a simple exponential decay.

A particle with Γ contributes to the measured $|g_1(\tau)|$ with $\exp(-\Gamma\tau)$. Therefore, the measured $|g_1(\tau)|$ is a superposition of $\exp(-\Gamma\tau)$ with different values of Γ:

$$|g_1(\tau)| = \int G(\Gamma) \exp(-\Gamma\tau) \, d\Gamma \tag{3.59}$$

where $G(\Gamma)$ represents the contribution of each Γ and is normalized, i.e., $\int G(\Gamma) d\Gamma = 1$. The magnitude of the electric-field autocorrelation function is proportional to the scattering intensity ($I \propto E^2$). After normalization to $g_1(\tau)$, each contribution from a different Γ is still weighted by the scattering intensity of particles that exhibit the decay rate of Γ. Thus, $G(\Gamma)$ is the scattering intensity-weighted distribution.

3.2.8.2 Inverse-Laplace Transform The distribution makes $|g_1(\tau)|$ deviate from a single exponential decay, as illustrated in Figure 3.17a. Conversely the analysis of the deviation allows estimation of $G(\Gamma)$. Mathematically, $|g_1(\tau)|$ is the Laplace transform of $G(\Gamma)$, as Eq. 3.59 shows. Then, the procedure to estimate $G(\Gamma)$ from

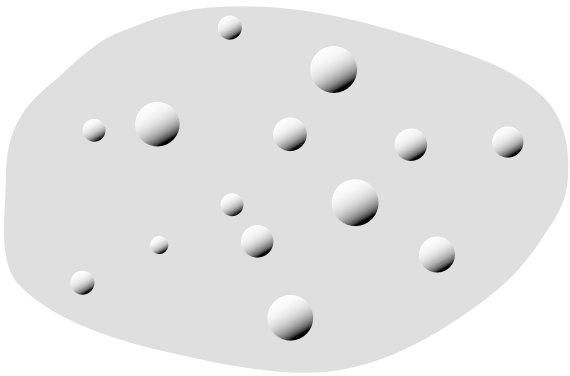

Figure 3.16. Suspension of particles with different diameters.

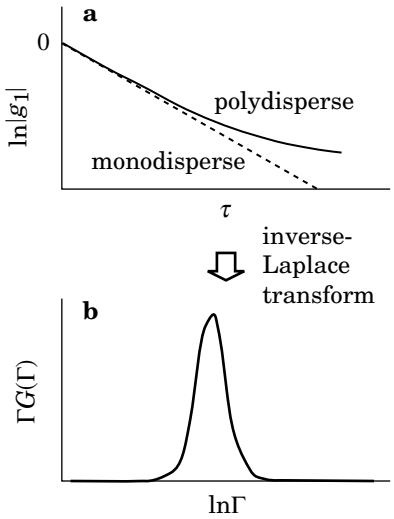

Figure 3.17. a: In a suspension of monodisperse particles, the plot of $\ln|g_1|$ is a straight line (dashed line). Polydispersity of the particle size deviates $\ln|g_1|$ (solid line) from the straight line. b: The inverse Laplace transform of $|g_1(\tau)|$ gives the distribution of the decay rate Γ.

$|g_1(\tau)|$ is **inverse-Laplace transform**. There are computer program packages available for the procedure. Among others, CONTIN[32] has been most frequently used and implemented in commercial DLS measurement systems. The result of the transformation is displayed in $\Gamma G(\Gamma)$ on a logarithmic scale of Γ (Fig. 3.17b). The following equation explains why $\Gamma G(\Gamma)$ is plotted, not just $G(\Gamma)$:

$$|g_1(\tau)| = \int \Gamma G(\Gamma) \exp(-\Gamma\tau)\, \mathrm{d}\ln\Gamma \tag{3.60}$$

The autocorrelator computes $|g_1(\tau)|$ for a finite range of τ, from $\tau_{\min}$ to $\tau_{\max}$. Therefore, $G(\Gamma)$ can be estimated only in a finite range of Γ. Usually, the lower and upper limits of the integral in Eq. 3.59 are $1/\tau_{\max}$ and $1/\tau_{\min}$, respectively.

3.2.8.3 Cumulant Expansion The inverse-Laplace transform is a convenient analysis method when the distribution is broad, especially bimodal or trimodal. When the distribution is narrow and $|g_1(\tau)|$ is close to a single exponential decay, a simpler analysis method, called a **cumulant expansion**, is more useful. In this method, $\ln|g_1(\tau)|$ is approximated by a polynomial of τ, typically of the second order. The first two coefficients represent the mean and the variance of Γ:

$$\boxed{\ln|g_1(\tau)| = -\langle\Gamma\rangle\tau + \tfrac{1}{2}\langle\Delta\Gamma^2\rangle\tau^2 - \tfrac{1}{6}\langle\Delta\Gamma^3\rangle\tau^3 + \cdots \text{ cumulant expansion}} \tag{3.61}$$

where $\Delta\Gamma = \Gamma - \langle\Gamma\rangle$ and the averages are weighted with $G(\Gamma)$:

$$\langle\Gamma\rangle = \int \Gamma G(\Gamma)\, d\Gamma, \quad \langle\Delta\Gamma^2\rangle = \int \Delta\Gamma^2 G(\Gamma)\, d\Gamma, \ldots \tag{3.62}$$

Problem 3.8 proves this expansion. In the absence of distribution, i.e., $\Delta\Gamma = 0$, the second- and higher-order terms disappear, and $\ln |g_1(\tau)|$ is a straight line. Curve-fitting of the measured $\ln |g_1(\tau)|$ by a polynomial gives an estimate of $\langle\Gamma\rangle$ and $\langle\Delta\Gamma^2\rangle$. As found in Problem 3.10, the diffusion coefficient estimated from $\langle\Gamma\rangle$ for a solution of a polydisperse polymer is a z-average diffusion coefficient. Often, we use a simple symbol of Γ for $\langle\Gamma\rangle$.

3.2.8.4 Example Figure 3.18 shows an example of $g_2(\tau)$ ($|g_1(\tau)|$ on the right axis) obtained by a commercial particle-sizing system (Beckman-Coulter, N4Plus) for a 6.9 g/L solution of a polystyrene standard ($M_w = 1.7 \times 10^5$ g/mol) in toluene at 30°C ($\lambda = 632.8$ nm). The scattering angles were 14.0, 20.5, 26.7, and 65.6°. On a logarithmic scale of the ordinate, $g_2(\tau)$ [and $|g_1(\tau)|$] is mostly straight at the four scattering angles, indicating a narrow distribution in $G(\Gamma)$. In the particle-sizing system, the distribution of Γ is converted to a distribution G_d of the apparent particle diameter d_{app} by $d_{app} = k_B T/[3\pi\eta_s(\Gamma/\mathbf{k}^2)]$. In the small k limit and the low concentration limit, $d_{app} = 2R_H$. Figure 3.19 displays $G_d(d_{app})$ on the logarithmic scale of d_{app}, obtained from the $|g_1(\tau)|$ data in Figure 3.18. As expected, the CONTIN analysis returns a single peak. The peak position and width are the same within experimental errors for the measurements at the four angles, indicating that the decay

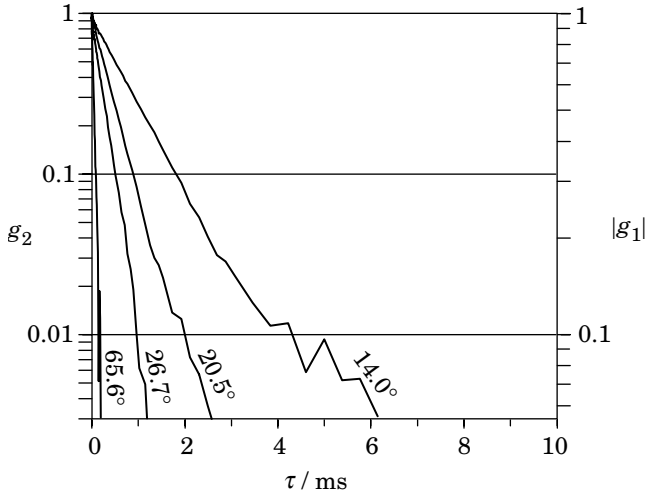

Figure 3.18. Example of autocorrelation functions $g_2(\tau)$ and $|g_1(\tau)|$ obtained in DLS measurements at four scattering angles for a dilute solution of polystyrene in toluene. The two autocorrelation functions differ in the ordinate scale only.

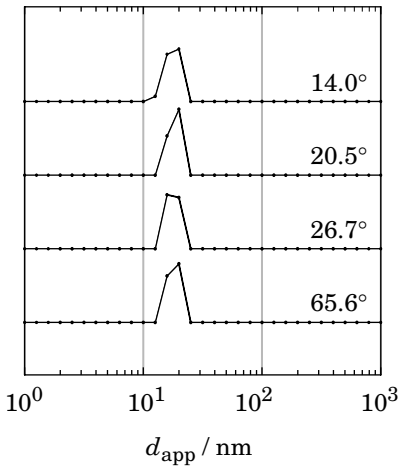

Figure 3.19. CONTIN analysis results for the autocorrelation functions shown in Fig. 3.18. The distribution of the apparent diameter d_{app} is plotted as a function of d_{app} in a logarithmic scale.

of $g_2(\tau)$ is due to the center-of-mass diffusion of the polystyrene molecules and that the measurement was carried out in the range of a sufficiently small k. In fact, $kR_H = 0.056$ at $\theta = 26.7°$, for instance. Displaying $G_d(d_{app})$ in place of $G(\Gamma)$ or the distribution of the diffusion coefficient is handy when results from measurements in different solvents and/or at different temperatures need to be compared.

3.2.9 Diffusion From Equation of Motion

Here we look at the diffusion from another perspective. We will obtain the diffusional behavior, i.e., $\langle[\mathbf{r}(t) - \mathbf{r}(0)]^2\rangle \propto t$, from the equation of motion.

A particle suspended in a liquid receives a random force $\mathbf{f}(t)$ when solvent molecules collide with the particle. We assume that the random force has the following statistical properties:

$$\langle \mathbf{f}(t) \rangle = 0 \tag{3.63}$$

$$\langle \mathbf{f}(t) \cdot \mathbf{f}(t') \rangle = A\delta(t - t') \tag{3.64}$$

where A is a constant yet to be determined. The random force is, on average, zero. It loses its memory instantaneously [$\delta(t - t')$]. The force at a given time has nothing to do with the force at the next moment. Figure 3.20 shows an example of such a force (white noise).

In a viscous solvent, the motion of the particle is overdamped. Then, the equation of motion of the particle has the friction term and the force term only:

$$\zeta \frac{d\mathbf{r}}{dt} = \mathbf{f}(t) \tag{3.65}$$

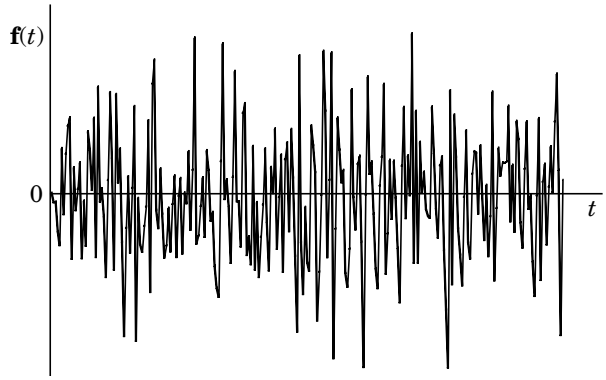

Figure 3.20. Example of a random force $\mathbf{f}(t)$ (its x component) with zero mean and no memory.

The mean square displacement in time t is calculated from

$$\langle[\mathbf{r}(t) - \mathbf{r}(0)]^2\rangle = \frac{1}{\zeta^2}\left\langle \int_0^t \mathbf{f}(t_1)\,\mathrm{d}t_1 \cdot \int_0^t \mathbf{f}(t_2)\,\mathrm{d}t_2 \right\rangle \tag{3.66}$$

We exchange the order of the integration and the averaging:

$$\langle[\mathbf{r}(t) - \mathbf{r}(0)]^2\rangle = \frac{1}{\zeta^2}\int_0^t \mathrm{d}t_1 \int_0^t \mathrm{d}t_2 \langle \mathbf{f}(t_1)\cdot\mathbf{f}(t_2)\rangle \tag{3.67}$$

With Eq. 3.64,

$$\langle[\mathbf{r}(t) - \mathbf{r}(0)]^2\rangle = \frac{1}{\zeta^2}\int_0^t \mathrm{d}t_1 \int_0^t \mathrm{d}t_2 A\delta(t_1 - t_2) = \frac{A}{\zeta^2}\int_0^t \mathrm{d}t_1 = \frac{A}{\zeta^2}t \tag{3.68}$$

The mean square displacement is proportional to t. The particle makes a diffusional motion on all time scales. We also find that the average displacement is zero:

$$\langle \mathbf{r}(t) - \mathbf{r}(0)\rangle = \frac{1}{\zeta}\int_0^t \mathrm{d}t \langle \mathbf{f}(t)\rangle = 0 \tag{3.69}$$

For the mean and variance of the displacement to be identical to those of the diffusion with diffusion coefficient D, $6D = A/\zeta^2$. Thus,

$$A = 6D\zeta^2 = 6\frac{k_\mathrm{B}T}{\zeta}\zeta^2 = 6k_\mathrm{B}T\zeta \tag{3.70}$$

Thus, the random force satisfies

$$\langle \mathbf{f}(t)\cdot\mathbf{f}(t')\rangle = 6k_\mathrm{B}T\zeta\,\delta(t - t') \tag{3.71}$$

The magnitude of the random force is greater for a particle with a larger friction coefficient, typically a larger particle. This random force satisfies the requirement of the equipartition law: thermal energy per degree of freedom is $k_B T/2$ (Problem 3.13).

3.2.10 Diffusion as Kinetics

3.2.10.1 Fick's Law Here, we look at the diffusion from a phenomenological point of view. The treatment in Sections 3.2.4 and 3.2.9 needs tracing each particle and therefore is microscopic.

We consider a container consisting of two parts that hold the solutions of the same solute at different concentrations (see Figure 3.21). The concentration is uniform in each part. As soon as the partition is quietly removed, the solute starts to move from the right compartment where the concentration is higher to the left compartment where it is lower. The distinct boundary becomes fuzzy. After a long time, the concentration becomes uniform throughout the container. The figure shows also a snapshot of the concentration profile during the equilibration process. There is a natural tendency for the system to become uniform as it maximizes its entropy toward the equilibrium. A spatial variation in the concentration $c(\mathbf{r})$ promotes a transfer of the solute from the more concentrated region to the less concentrated region.

The rate of transfer is called a **flux** (also called a flow; but it is necessary to avoid confusion from the macroscopic flow of the fluid). The transfer occurs in the absence of the solvent flow as well as in the presence of the solvent flow. The flux is defined as the mass of the solute that moves across a unit area in a unit time. The direction of the flux is the same as that of the velocity $\mathbf{v}(\mathbf{r})$ of the solute molecules. By definition, the flux $\mathbf{j}(\mathbf{r})$ is related to $\mathbf{v}(\mathbf{r})$ by

$$\mathbf{j}(\mathbf{r}) = c(\mathbf{r})\mathbf{v}(\mathbf{r}) \tag{3.72}$$

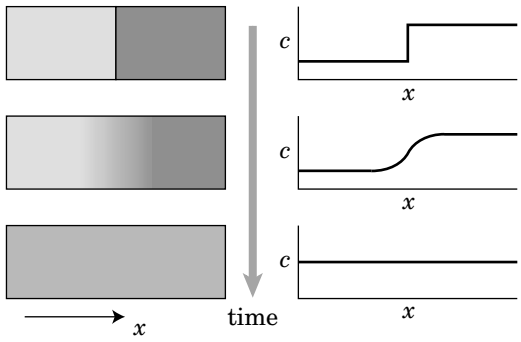

Figure 3.21. When the partition is removed, solute molecules move from the higher-concentration zone to the lower-concentration zone. The concentration profiles before the partition removal, during equilibration, and at equilibrium are shown on the right.

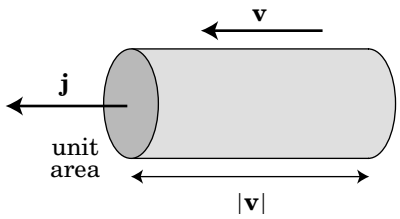

Figure 3.22. Flux **j** is defined as the number of solute molecules that pass the cross section of a unit area in a unit time. The solute molecules in the cylinder of height $|\mathbf{v}|$ pass the cross section in the next unit time.

Figure 3.22 will help us understand this relationship. The solute molecules in a cylinder that has a base of a unit area and a height of $|\mathbf{v}|$ pass the base in the next unit time. The mass of solute molecules in the cylinder, $c|\mathbf{v}|$, is by definition equal to $|\mathbf{j}|$. In the following, we consider a quiescent solution.

The local concentration variation is represented by the **concentration gradient** $\nabla c(\mathbf{r})$. In one dimension, it is $\partial c/\partial x$ (Fig. 3.23). When ∇c is sufficiently small, the flux $\mathbf{j}(\mathbf{r})$ is proportional to $\nabla c(\mathbf{r})$ (Fick's law). In the absence of the concentration

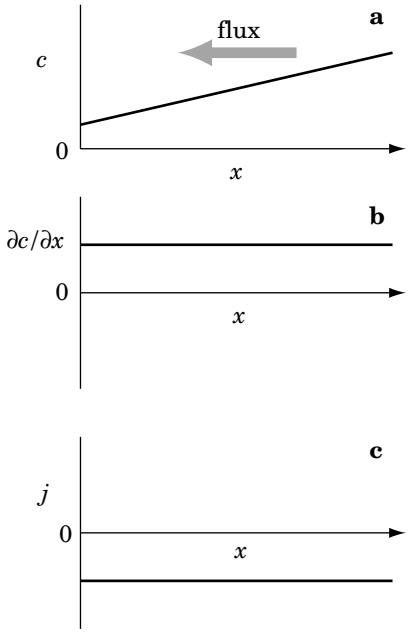

Figure 3.23. Concentration gradient causes a flux. The illustration is for one dimension. a: Profile of concentration c. b: Concentration gradient $\partial c/\partial x$. c: Flux j.

gradient, there is no flux. On reversal of the sign of ∇c, $\mathbf{j}$ also changes its sign. We introduce the diffusion coefficient D as the proportionality constant in

$$\boxed{\mathbf{j} = -D\nabla c \quad \text{Fick's law}} \tag{3.73}$$

The minus sign is necessary to account for the transfer from the high-c region to the low-c region. In one dimension, the flux is negative when $\partial c/\partial x > 0$ as indicated in the figure. We will soon find that the diffusion coefficient defined in this way is equivalent to the one we defined microscopically in Section 3.2.4. The diffusion that follows this equation is called a Fickian diffusion.

3.2.10.2 Diffusion Equation The other equation that relates $\mathbf{j}$ and c is from the conservation of mass. We consider a small fixed volume V (Fig. 3.24). The rate of change in the total mass of the solute in the volume, $V(\partial c/\partial t)$, is equal to the negative of the integral of the surface-normal component of $\mathbf{j}$ over the surface of the volume:

$$V\frac{\partial c}{\partial t} = -\int_{\text{surface}} \mathbf{j}\cdot d\mathbf{S} \tag{3.74}$$

Note that $\mathbf{j}\cdot d\mathbf{S}$ accounts for the mass of the solute molecules that leave the volume through a small area $d\mathbf{S}$. The minus sign is needed because a positive $\mathbf{j}\cdot d\mathbf{S}$ means an outflow. By Green's theorem, the surface integral is converted to the volume integral. In the limit of small V,

$$\int_{\text{surface}} \mathbf{j}\cdot d\mathbf{S} = \int_V \nabla\cdot\mathbf{j}\, d\mathbf{r} = V\nabla\cdot\mathbf{j} \tag{3.75}$$

Combining the two equations, we obtain the law of mass conservation:

$$\boxed{\frac{\partial c}{\partial t} + \nabla\cdot\mathbf{j} = 0 \quad \text{mass conservation}} \tag{3.76}$$

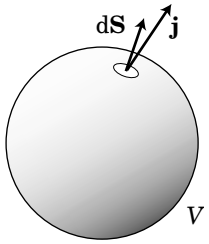

Figure 3.24. Flux $\mathbf{j}$ and the surface normal $d\mathbf{S}$ on a sphere of a small volume V.

With Fick's law, we can obtain the diffusion equation:

$$\boxed{\frac{\partial c}{\partial t} = -\nabla \cdot \mathbf{j} = D\nabla \cdot \nabla c = D\nabla^2 c} \tag{3.77}$$

which is identical to Eq. 3.37. The phenomenological definition of the diffusion coefficient is equivalent to the microscopic definition of the diffusion coefficient.

3.2.10.3 Chemical Potential Gradient With Eq. 3.72, Fick's law can be rewritten to

$$\mathbf{v}(\mathbf{r}) = -D\nabla \ln(c/c^\circ) \tag{3.78}$$

where c° is a reference concentration. We recall that $D = k_B T/\zeta$ (Eq. 3.51). In a solution of a uniform temperature, Eq. 3.78 is converted to

$$\zeta \mathbf{v}(\mathbf{r}) = -\nabla[k_B T \ln(c(\mathbf{r})/c^\circ)] \tag{3.79}$$

In the right-hand side, $k_B T \ln(c/c^\circ)$ is the chemical potential in an ideal solution. This equation dictates a balance in the forces acting on the solute molecule at $\mathbf{r}$. The friction $\zeta \mathbf{v}(\mathbf{r})$ is balanced by the chemical potential gradient, resulting in the velocity $\mathbf{v}(\mathbf{r})$ of the solute molecule. The chemical potential gradient causes a transfer of matter from a higher potential to a lower potential, just as a force on the particle moves it.

3.2.11 Concentration Effect on Diffusion

3.2.11.1 Self-Diffusion and Mutual Diffusion When each suspension or solute molecule is moving independently, the diffusion is a single-particle phenomenon. The latter is observed in the dilute solution limit where there are no other solute molecules in the neighborhood. When other solute molecules are nearby, the diffusion is strongly affected by the other solute molecules. The second terms in Eqs. 3.17 and 3.45 are not negligible any more. What DLS measures is $S(\mathbf{k}, \tau)$, not $S_1(\mathbf{k}, \tau)$. Only when $c \ll c^*$, $S(\mathbf{k}, \tau)$ is equal to $S_1(\mathbf{k}, \tau)$. Otherwise, the apparent diffusion coefficient D estimated from the slope of $|g_1(\tau)|$ depends on c. We will learn how the apparent D depends on c.

To have an intuitive understanding of the concentration effect, we consider a suspension of hard spheres. Suppose that a portion of the suspension acquires temporarily a higher concentration than the surrounding, as shown in Figure 3.25a. The particles in the locally concentrated region tend to move away from each other, resulting in the collision of black particles with white particles (Fig. 3.25b). Upon collision, the particles bounce back, although the motion is overdamped in a viscous environment (Fig. 3.25c). When we trace the motion of each black particle, the collision makes the square displacement smaller compared with the one in the absence of collisions. The effect of the local concentration fluctuation is, however,

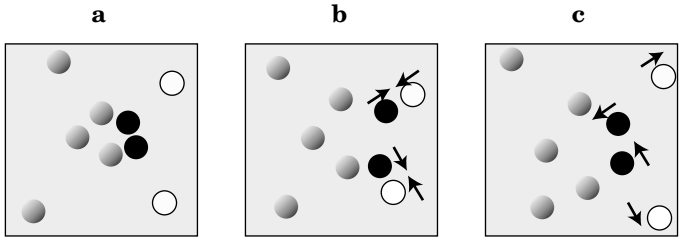

Figure 3.25. A temporary local congestion of spherical particles is dispersed by diffusion and collisions. Black spheres (in a) move to collide with white spheres (b) and bounce back (c). Propagation of the local concentration fluctuation (in a) is carried faster and farther by the white spheres (c).

transmitted farther by the white particles because of the collisions. When we trace the distance between the black particle and the white particle, the collision increases the distance more quickly compared with the counterpart in the absence of collisions.

The first concept, tracing each particle, is for the **self-diffusion**, and the second for the **mutual diffusion**. The **self-diffusion coefficient** D_s is defined for the motion of a given particle as

$$\boxed{D_s = \lim_{t \to \infty} \frac{\langle [\mathbf{r}_1(t) - \mathbf{r}_1(0)]^2 \rangle}{6t} \qquad \text{self-diffusion coefficient}} \tag{3.80}$$

and the **mutual diffusion coefficient** D_m is defined for the motion of two particles as

$$\boxed{D_m = \lim_{t \to \infty} \frac{\langle [\mathbf{r}_1(t) - \mathbf{r}_2(0)]^2 \rangle}{6t} \qquad \text{mutual diffusion coefficient}} \tag{3.81}$$

At sufficiently low concentrations, both D_s and D_m are equal to D_0, the diffusion coefficient of an isolated solute (Problem 3.14). With an increasing concentration, D_s tends to decrease but D_m tends to increase (Fig. 3.26). There are exceptions.

3.2.11.2 Measurement of Self-Diffusion Coefficient What is measured in DLS is D_m. DLS cannot measure D_s because it does not distinguish one solute from another. It is necessary to use other more specialized techniques such as **forced Rayleigh scattering** (FRS), **fluorescence recovery after photo-bleaching** (FRAP), and **pulsed-field gradient nuclear magnetic resonance** (PFG-NMR).

The details of the instruments for the first two optical methods are explained, for instance, in Ref. 33. In short, FRS creates a temporary diffraction grating by intersecting two beams (write-beam) split from a strong, short-wavelength laser at a low angle. The polymer molecules must be labeled with a fluorescent dye. The grating is an alternate pattern of ground-state molecules and excited-state molecules. After the write-beam is turned off, a weak read beam is fired onto the grating to monitor

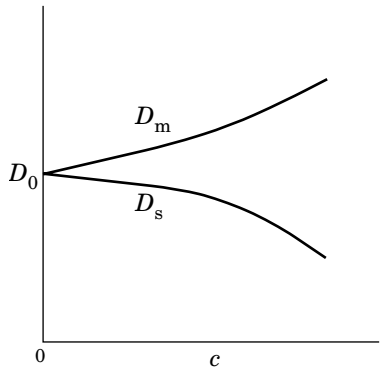

Figure 3.26. As the solute concentration c increases, the mutual diffusion coefficient D_m usually increases and the self-diffusion coefficient D_s decreases. In the low concentration limit, D_m and D_s are equal to D_0.

the decay in the intensity of the diffracted beam as the polymer chains diffuse to diminish the contrast. The decay rate gives an estimate of the self-diffusion coefficient. In FRAP, typically a circular spot beam bleaches the dyes attached to polymer chains. After the laser is turned off, the unbleached polymers sitting outside the spot diffuses into the circular domain to recover a uniform dye distribution. The build-up transient of the dye concentration in the circle gives an estimate of the self-diffusion coefficient. However, instruments that use these techniques are not commercially available.

In PFG-NMR, a pulsed gradient magnetic field is applied across a sample in phase to a spin-echo RF pulse sequence. The amplitude of the free induction decay is given by $S_1(q, \tau)$ with $q = \gamma\delta g$, where γ is the magnetogyric ratio of the nucleus measured, δ is the duration of the gradient field, g is the field gradient, and τ is the separation between successive field pulses. By changing the field gradient, the scattering function is measured at different wave vectors, allowing the user to estimate D_s.

Although D_s cannot be measured in DLS, a closely related **tracer diffusion coefficient** D_t can be measured. In the tracer diffusion, the motion of a labeled solute called a **probe** or a **tracer** is traced selectively. A second solute called a **matrix** is added to the solution and its concentration is varied, whereas the concentration of the probe molecules is held low. The matrix must be invisible, and the probe must be visible. We can give a large contrast between the matrix and probe by choosing a pair of solvent and matrix that are nearly **isorefractive**, i.e., having the same refractive index. Then, the light scattering will look at the probe molecules only. For instance, we can follow the tracer diffusion of polystyrene in a matrix solution of poly(dimethyl siloxane) in tetrahydrofuran.

3.2.11.3 Concentration Dependence of the Diffusion Coefficients Now we consider the effect of the concentration on the diffusion coefficients quantitatively.

First, we consider the concentration effect on the self-diffusion coefficient. Other molecules tend to interrupt the otherwise free diffusion of a given solute molecule. In effect, the presence of other molecules increases the friction coefficient:

$$\zeta = \zeta_0(1 + \zeta_1 c + \cdots) \tag{3.82}$$

where ζ_0 is the friction coefficient in the dilute solution limit, and $\zeta_0\zeta_1$ (>0) is the first-order concentration coefficient. Then,

$$D_s = \frac{k_B T}{\zeta} = \frac{k_B T}{\zeta_0}(1 - \zeta_1 c + \cdots) \tag{3.83}$$

The self-diffusion coefficient decreases linearly with c at low concentrations.

For the mutual diffusion coefficient, we start with generalizing Eq. 3.79 to an equation that applies to nonideal solutions:

$$\zeta \mathbf{v}(\mathbf{r}) = -\nabla\mu(\mathbf{r}) \tag{3.84}$$

In terms of flux,

$$\boxed{\mathbf{j}(\mathbf{r}) = -\frac{c(\mathbf{r})}{\zeta}\nabla\mu(\mathbf{r})} \tag{3.85}$$

Now we use the virial expansion for μ (Problem 2.9):

$$\mu = k_B T[\ln(c/c^\circ) + (2A_2M - v_{sp})c + \cdots] \tag{3.86}$$

Its gradient is given as

$$\nabla\mu = k_B T[c^{-1} + (2A_2M - v_{sp}) + \cdots]\nabla c \tag{3.87}$$

Then,

$$\mathbf{j} = -\frac{k_B T}{\zeta}(1 + (2A_2M - v_{sp})c + \cdots)\nabla c = -\frac{k_B T}{\zeta_0}[1 + (2A_2M - \zeta_1 - v_{sp})c + \cdots]\nabla c \tag{3.88}$$

where Eq. 3. 82 was used for ζ. Thus, D_m changes with c as

$$\boxed{D_m = D_0(1 + k_D c + \cdots) \qquad \text{low concentrations}} \tag{3.89}$$

with a linear coefficient k_D given by

$$\boxed{k_D = 2A_2M - \zeta_1 - v_{sp} \qquad \text{linear coefficient}} \tag{3.90}$$

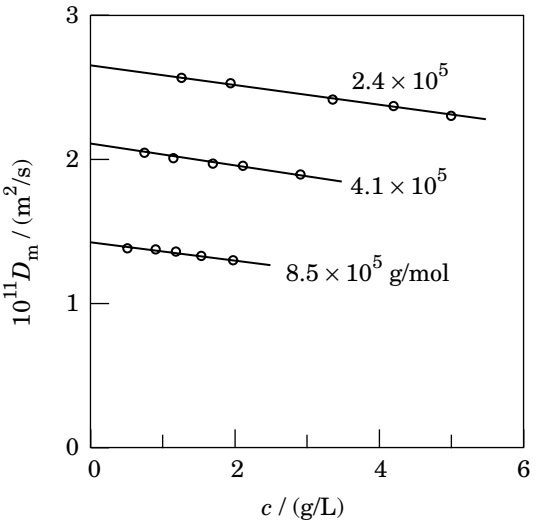

Figure 3.27. Mutual diffusion coefficient D_m of poly(α-methyl styrene) in a theta solvent at different concentrations in the dilute regime. The molecular weight of the polymer is indicated adjacent to each plot. (From Ref. 31.)

In a sufficiently good solvent, $2A_2M > \zeta_1 + v_{sp}$ and therefore D_m increases with c. As the solvent quality becomes poorer, A_2 decreases and therefore k_D becomes eventually negative.

Figure 3.27 shows an example of the concentration dependence of D_m in a theta solvent condition.[31] The light-scattering autocorrelation functions were measured for solutions of poly(α-methyl styrene) fractions of different molecular weights in the theta solvent of cyclohexane at 30.5°C. The first-order concentration coefficient is negative because $A_2 = 0$ at this temperature and therefore $k_D = -(\zeta_1 + v_{sp}) < 0$.

So far, we have assumed that the solvent remains quiescent while the solute molecules move. There is, however, always a backflow of solvent molecules into the space originally occupied by the solute. This effect is to decrease D_m/D_0 by $v_{sp}c$, where $v_{sp}c$ is the fraction of the volume occupied by the polymer in solution. Then,

$$\boxed{k_D = 2A_2M - \zeta_1 - 2v_{sp} \quad \text{with backflow correction}} \tag{3.91}$$

3.2.12 Diffusion in a Nonuniform System

In some systems, the chemical potential depends explicitly on **r**, not only through $c(\mathbf{r})$. An example is charged colloidal particles in an electric field. Here, we consider diffusion of particles in an external field such as an electric field. We limit the discussion to the low concentration limit.

When a stationary external field is applied, the chemical potential has an extra term $U_E(\mathbf{r})$ due to the field:

$$\mu/k_BT = \ln(c/c^\circ) + U_E(\mathbf{r})/k_BT \tag{3.92}$$

Charged particles will experience $U_E(\mathbf{r})$ = (charge) × (electrostatic potential at $\mathbf{r}$), for instance. The diffusion equation is rewritten to

$$\frac{\partial c}{\partial t} = D\nabla\cdot(\nabla c + c\nabla U_E/k_BT) \tag{3.93}$$

We can immediately obtain the equilibrium distribution $c_{eq}(\mathbf{r})$ from $\nabla c_{eq} + c_{eq}\nabla U_E/k_BT = 0$ as

$$c_{eq}(\mathbf{r}) = \text{const.} \times \exp(-U_E(\mathbf{r})/k_BT) \tag{3.94}$$

which is the Boltzmann distribution for particles with space-dependent energy of $U_E(\mathbf{r})$.

3.2.13 PROBLEM

Problem 3.1: We consider a walk on a cubic lattice. Its ith step motion $\Delta\mathbf{r}_i$ in step time t_1 satisfies

$$\langle\Delta\mathbf{r}_i\rangle = 0$$

$$\langle\Delta\mathbf{r}_i\cdot\Delta\mathbf{r}_j\rangle = \begin{cases} b^2 & (i=j) \\ pb^2 & (|i-j|=1) \\ 0 & (\text{otherwise}) \end{cases}$$

where $p < 1$ is a constant. What is the mean square displacement in N steps? Can we define the long-time diffusion coefficient? If yes, what is it?

Solution 3.1: The mean square displacement of N steps is

$$\langle\Delta\mathbf{r}^2\rangle = \sum_{i,j=1}^{N}\langle\Delta\mathbf{r}_i\cdot\Delta\mathbf{r}_j\rangle = \sum_{i=1}^{N}\langle\Delta\mathbf{r}_i{}^2\rangle + \sum_{i=1}^{N-1}\langle\Delta\mathbf{r}_{i+1}\cdot\Delta\mathbf{r}_i\rangle + \sum_{i=2}^{N}\langle\Delta\mathbf{r}_{i-1}\cdot\Delta\mathbf{r}_i\rangle$$
$$= Nb^2 + 2(N-1)pb^2 = b^2[(2p+1)N - 2p]$$

For $N \gg 1$, $\langle\Delta\mathbf{r}^2\rangle = b^2(2p+1)N$. Therefore, the long-time diffusion coefficient D can be defined. It is

$$D = \frac{\langle\Delta\mathbf{r}^2\rangle}{6Nt_1} = \frac{b^2(2p+1)}{6t_1}$$

Problem 3.2: Use the definition of $S_1(\mathbf{k}, \tau)$ (Eq. 3.26) and the diffusion equation for $P(\mathbf{r}, \mathbf{r}'; \tau)$ (Eq. 3.35) to show that $S_1(\mathbf{k}, \tau) = S_1(\mathbf{k}, 0)\exp(-D\mathbf{k}^2\tau)$.

Solution 3.2: From Eqs. 3.26 and 3.35,

$$\frac{\partial}{\partial \tau} S_1(\mathbf{k}, \tau) = \int d\mathbf{r} \exp[i\mathbf{k}\cdot(\mathbf{r} - \mathbf{r}')] \frac{\partial}{\partial \tau} P(\mathbf{r}, \mathbf{r}'; \tau)$$
$$= \int d\mathbf{r} \exp[i\mathbf{k}\cdot(\mathbf{r} - \mathbf{r}')] D\nabla^2 P(\mathbf{r}, \mathbf{r}'; \tau)$$

Integral by parts yields

$$\frac{\partial}{\partial \tau} S_1(\mathbf{k}, \tau) = D\int d\mathbf{r} P(\mathbf{r}, \mathbf{r}'; \tau)\nabla^2 \exp[i\mathbf{k}\cdot(\mathbf{r} - \mathbf{r}')]$$
$$= D\int d\mathbf{r} P(\mathbf{r}, \mathbf{r}'; \tau)(-\mathbf{k}^2 \exp[i\mathbf{k}\cdot(\mathbf{r} - \mathbf{r}')])$$
$$= -D\mathbf{k}^2 \int d\mathbf{r} P(\mathbf{r}, \mathbf{r}'; \tau) \exp[i\mathbf{k}\cdot(\mathbf{r} - \mathbf{r}')] = -D\mathbf{k}^2 S_1$$

The solution of this differential equation is given as

$$S_1(\mathbf{k}, \tau) = S_1(\mathbf{k}, 0) \exp(-D\mathbf{k}^2\tau)$$

Problem 3.3: Use Eq. 3.26 to show that

$$\langle(\mathbf{r} - \mathbf{r}')^2\rangle = -\frac{\partial^2}{\partial \mathbf{k}^2} S_1(\mathbf{k}, \tau)\Big|_{\mathbf{k}=0}$$

without relying on the Taylor expansion.

Solution 3.3: By definition,

$$\langle(\mathbf{r} - \mathbf{r}')^2\rangle = \int d\mathbf{r}(\mathbf{r} - \mathbf{r}')^2 P(\mathbf{r}, \mathbf{r}'; \tau)$$

Because

$$(\mathbf{r} - \mathbf{r}')^2 = -\frac{\partial^2}{\partial \mathbf{k}^2} \exp[i\mathbf{k}\cdot(\mathbf{r} - \mathbf{r}')]\Big|_{\mathbf{k}=0}$$

we obtain

$$\langle(\mathbf{r} - \mathbf{r}')^2\rangle = -\int d\mathbf{r} \frac{\partial^2}{\partial \mathbf{k}^2} \exp[i\mathbf{k}\cdot(\mathbf{r} - \mathbf{r}')]\Big|_{\mathbf{k}=0} P(\mathbf{r}, \mathbf{r}'; \tau)$$
$$= -\frac{\partial^2}{\partial \mathbf{k}^2} \int d\mathbf{r} \exp[i\mathbf{k}\cdot(\mathbf{r} - \mathbf{r}')] P(\mathbf{r}, \mathbf{r}'; \tau)\Big|_{\mathbf{k}=0}$$
$$= -\frac{\partial^2}{\partial \mathbf{k}^2} S_1(\mathbf{k}, \tau)\Big|_{\mathbf{k}=0}$$

Problem 3.4: The viscosity of water is 0.893 cP at 25°C and 0.355 cP at 80°C. How much faster is the diffusion at 80°C compared with 25°C for a particle suspended in water?

Solution 3.4:

$$\frac{D_{80°C}}{D_{25°C}} = \frac{273.15 + 80}{273.15 + 25} \times \frac{0.893\,\text{cP}}{0.355\,\text{cP}} = 2.98$$

Problem 3.5: For the same number of monomers, which conformation has stronger hydrodynamic interactions, flexible or semirigid?

Solution 3.5: Flexible chain; For the same pair of monomers separated by a given distance along the chain contour, the spatial distance between them is shorter in the flexible chain than it is in the semirigid chain.

Problem 3.6: Use Eq. 3.55 to calculate $R_{H,star}$ of a star polymer consisting of n_A arms that have a conformation of a Gaussian chain with N_1 segments of length b. What is $g_H \equiv (R_{H,star}/R_{H,lin})^2$, where $R_{H,lin}$ is for a linear chain of $n_A N_1$ segments? Compare g_H with g_g defined as the ratio of the mean square radii of gyration for the same pair of polymers (Eq. 1.85).

Solution 3.6: We define $\mathbf{r}_{im}$ and $\mathbf{r}_{jn}$ in the same way as we did in Section 1.6. ${R_{H,star}}^{-1} = \langle |\mathbf{r}_{im} - \mathbf{r}_{jn}|^{-1} \rangle$ is calculated separately for $\mathbf{r}_{im}$ and $\mathbf{r}_{jn}$ on the same arm and the pairs on different arms. For the pair on the same arm,

$$\left(\frac{\pi}{6}\right)^{1/2} b \left\langle \frac{1}{|\mathbf{r}_{im} - \mathbf{r}_{in}|} \right\rangle = \frac{1}{N_1^2} \int_0^{N_1} \mathrm{d}n \int_0^{N_1} \mathrm{d}m |n - m|^{-1/2} = \frac{8}{3} \frac{1}{N_1^{1/2}}$$

For pairs on different arms,

$$\left(\frac{\pi}{6}\right)^{1/2} b \left\langle \frac{1}{|\mathbf{r}_{im} - \mathbf{r}_{in}|} \right\rangle = \frac{1}{N_1^2} \int_0^{N_1} \mathrm{d}n \int_0^{N_1} \mathrm{d}m (n + m)^{-1/2} = \frac{8}{3} (2^{1/2} - 1) \frac{1}{N_1^{1/2}}$$

The two types of pairing occur with probabilities of $1/n_A$ and $1 - 1/n_A$, respectively. Then, $R_{H,star}$ is given by

$$\begin{aligned} \frac{1}{R_{H,star}} &= \left(\frac{6}{\pi}\right)^{1/2} \frac{1}{b} \times \frac{8}{3} \frac{1}{N_1^{1/2}} \frac{(2^{1/2} - 1)(2^{1/2} + n_A)}{n_A} \\ &= 8 \left(\frac{2}{3\pi}\right)^{1/2} \frac{1}{b N_1^{1/2}} \frac{(2^{1/2} - 1)(2^{1/2} + n_A)}{n_A} \end{aligned}$$

The R_H of a linear polymer with $n_A N_1$ segments is

$$\frac{1}{R_{H,lin}} = 8 \left(\frac{2}{3\pi}\right)^{1/2} \frac{1}{b(n_A N_1)^{1/2}}$$

The ratio g_{H} is

$$g_{\mathrm{H}} \equiv \left(\frac{R_{\mathrm{H,star}}}{R_{\mathrm{H,lin}}}\right)^2 = \frac{n_A}{[(2^{1/2}-1)(2^{1/2}+n_{\mathrm{A}})]^2}$$

The following figure compares g_{H} with g_{g}:

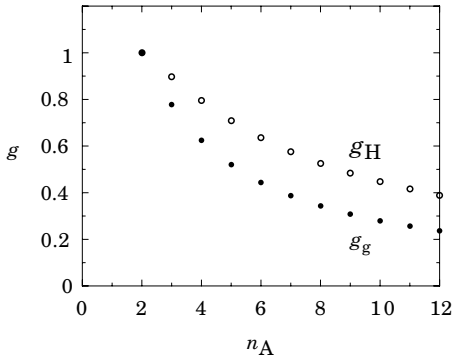

Problem 3.7: What is the addition rule for R_{g} and R_{H} when an a block with R_{ga} and R_{Ha} and a b block with R_{gb} and R_{Hb} are joined to form an a–b diblock copolymer? Assume that the two blocks follow the same chain statistics.

Solution 3.7: The addition rule is

$$R_{\mathrm{g}}{}^{1/\nu} = R_{\mathrm{ga}}{}^{1/\nu} + R_{\mathrm{gb}}{}^{1/\nu}, R_{\mathrm{H}}{}^{1/\nu} = R_{\mathrm{Ha}}{}^{1/\nu} + R_{\mathrm{Hb}}{}^{1/\nu}$$

Problem 3.8: Derive Eq. 3.61 from Eq. 3.59.

Solution 3.8: From Eq. 3.59,

$$\begin{aligned}
\frac{\partial}{\partial\tau}\ln|g_1(\tau)| &= -|g_1(\tau)|^{-1}\int \Gamma G(\Gamma)\exp(-\Gamma\tau)\,\mathrm{d}\Gamma \\
\frac{\partial^2}{\partial\tau^2}\ln|g_1(\tau)| &= |g_1(\tau)|^{-1}\int \Gamma^2 G(\Gamma)\exp(-\Gamma\tau)\,\mathrm{d}\Gamma \\
&\quad -\left(|g_1(\tau)|^{-1}\int \Gamma G(\Gamma)\exp(-\Gamma\tau)\,\mathrm{d}\Gamma\right)^2 \\
\frac{\partial^3}{\partial\tau^3}\ln|g_1(\tau)| &= -|g_1(\tau)|^{-1}\int \Gamma^3 G(\Gamma)\exp(-\Gamma\tau)\,\mathrm{d}\Gamma \\
&\quad + 3|g_1(\tau)|^{-2}\int \Gamma^2 G(\Gamma)\exp(-\Gamma\tau)\,\mathrm{d}\Gamma\int \Gamma G(\Gamma)\exp(-\Gamma\tau)\,\mathrm{d}\Gamma \\
&\quad -2\left(|g_1(\tau)|^{-1}\int \Gamma G(\Gamma)\exp(-\Gamma\tau)\,\mathrm{d}\Gamma\right)^3
\end{aligned}$$

The derivatives at $\tau = 0$ are

$$\frac{\partial}{\partial \tau} \ln|g_1(\tau)|\Big|_{\tau=0} = -\int \Gamma G(\Gamma)\, d\Gamma = -\langle \Gamma \rangle$$

$$\frac{\partial^2}{\partial \tau^2} \ln|g_1(\tau)|\Big|_{\tau=0} = \langle \Gamma^2 \rangle - \langle \Gamma \rangle^2 = \langle \Delta\Gamma^2 \rangle$$

$$\frac{\partial^3}{\partial \tau^3} \ln|g_1(\tau)|\Big|_{\tau=0} = -\langle \Gamma^3 \rangle + 3\langle \Gamma^2 \rangle \langle \Gamma \rangle - 2\langle \Gamma \rangle^3 = -\langle \Delta\Gamma^3 \rangle$$

Thus, the Taylor expansion of $\ln|g_1(\tau)|$ at $\tau = 0$ is expressed as

$$\ln|g_1(\tau)| = -\langle \Gamma \rangle \tau + \tfrac{1}{2}\langle \Delta\Gamma^2 \rangle \tau^2 - \tfrac{1}{6}\langle \Delta\Gamma^3 \rangle \tau^3 + \cdots$$

Problem 3.9: Explain why $|g_1(\tau)|$ deviates upward from the straight line for a polydisperse system?

Solution 3.9: In the final answer of Problem 3.8, the second-order term is always positive.

Problem 3.10: When the DLS measurement is carried out for a solution of a polymer with a molecular weight distribution, how is $G(\Gamma)$ weighted? What average of diffusion coefficient does the initial slope of $|g_1(\tau)|$ give? Component i of the polymer with molecular weight M_i is dissolved in the solution at concentration c_i.

Solution 3.10: The excess scattering intensity I_i by component i is proportional to $c_i M_i$ (Eq. 2.118 with $\mathbf{k} = 0$). Thus, the weight for the component in $G(\Gamma)$ is $c_i M_i$, and

$$|g_1(\tau)| \propto \sum_i c_i M_i \exp(-D_i \mathbf{k}^2 \tau)$$

where D_i is the diffusion coefficient of component i. The initial decay rate is

$$-\frac{\partial}{\partial t} \ln|g_1(\tau)|\Big|_{\tau=0} = \frac{\sum c_i M_i D_i}{\sum c_i M_i} \mathbf{k}^2$$

The average of D is weighted by $c_i M_i$:

$$\langle D \rangle = \frac{\sum_i D_i c_i M_i}{\sum_i c_i M_i}$$

Because $c_i M_i$ is proportional to the product of the weight fraction and M_i, the above average is a z-average.

Problem 3.11: DLS measurement is conducted for a dilute ternary solution of two different polymers a and b in a non-selective solvent. The two polymers are dissolved at concentrations c_a and c_b. The differential refractive index of polymer a in the solvent is dn/dc_a and that of polymer b is dn/dc_b. We assume that the two polymers are monodisperse with molecular weights M_a and M_b, and the decay rates in $|g_1(\tau)|$ measured for a binary solution of polymer a (i.e., polymer a + the same solvent) and another binary solution of polymer b are Γ_a and Γ_b, respectively. Find the apparent distribution $G(\Gamma)$ for the ternary solution. What is $|g_1(\tau)|$ for the solution? Assume that the two polymers are molecularly dispersed in the ternary solution.

Solution 3.11: $G(\Gamma) = G_a\delta(\Gamma - \Gamma_a) + G_b\delta(\Gamma - \Gamma_b)$, where

$$G_a \propto \left(\frac{dn}{dc_a}\right)^2 c_a M_a,\ G_b \propto \left(\frac{dn}{dc_b}\right)^2 c_b M_b$$

Then,

$$G(\Gamma) = \frac{\left(\frac{dn}{dc_a}\right)^2 c_a M_a \delta(\Gamma - \Gamma_a) + \left(\frac{dn}{dc_b}\right)^2 c_b M_b \delta(\Gamma - \Gamma_b)}{\left(\frac{dn}{dc_a}\right)^2 c_a M_a + \left(\frac{dn}{dc_b}\right)^2 c_b M_b}$$

and we obtain

$$|g_1(\tau)| = \frac{\left(\frac{dn}{dc_a}\right)^2 c_a M_a \exp(-\Gamma_a \tau) + \left(\frac{dn}{dc_b}\right)^2 c_b M_b \exp(-\Gamma_b \tau)}{\left(\frac{dn}{dc_a}\right)^2 c_a M_a + \left(\frac{dn}{dc_b}\right)^2 c_b M_b}$$

Solution 3.12: In principle, the particle-sizing system should be able to find the distribution of molecular weight M of a polymer in solution. Assume a narrow distribution of M around $\overline{M}$ given by

$$M^2 f(M)\, d\ln M = (2\pi \overline{M}^2 \sigma^2)^{-1/2} \exp\left(-\frac{\Delta M^2}{2\overline{M}^2\sigma^2}\right) d\Delta M$$

which is obtained from Eq. 1.102 with $M = \overline{M} + \Delta M$ ($|\Delta M/\overline{M}| \ll 1$). The diffusion coefficient D is related to M by $D = \overline{D}(M/\overline{M})^{-\nu}$ where $\overline{D}$ is the

value of D for $M = \overline{M}$. Let $\Delta D = D - \langle D \rangle$, where

$$\langle \cdots \rangle \equiv \int \cdots (2\pi \overline{M}^2 \sigma^2)^{-1/2} \exp\left(-\frac{\Delta M^2}{2\overline{M}^2 \sigma^2} \right) \mathrm{d}\Delta M$$

What is $\langle \Delta D^2 \rangle / \langle D \rangle^2$?

Solution 3.12: With $M = \overline{M}(1 + \Delta M/\overline{M})$, $D = \overline{D}(1 + \Delta M/\overline{M})^{-\nu} \cong \overline{D}(1 - \nu \Delta M/\overline{M})$. Then,

$$\langle D \rangle = \int \overline{D}(1 - \nu \Delta M/\overline{M})(2\pi \overline{M}^2 \sigma^2)^{-1/2} \exp\left(-\frac{\Delta M^2}{2\overline{M}^2 \sigma^2} \right) \mathrm{d}\Delta M = \overline{D}$$

Because $\Delta D = -\overline{D} \nu \Delta M/\overline{\mathrm{M}}$,

$$\langle \Delta D^2 \rangle = \overline{D}^2 \nu^2 \int (\Delta M/\overline{M})^2 (2\pi \overline{M}^2 \sigma^2)^{-1/2} \exp\left(-\frac{\Delta M^2}{2\overline{M}^2 \sigma^2} \right) \mathrm{d}\Delta M = \overline{D}^2 \nu^2 \sigma^2$$

Thus,

$$\langle \Delta D^2 \rangle / \langle D \rangle^2 = \nu^2 \sigma^2$$

Because $\sigma^2 = \ln \mathrm{PDI}$ from Eq. 1.106,

$$\langle \Delta D^2 \rangle / \langle D \rangle^2 = \nu^2 \ln \mathrm{PDI} = \begin{cases} \frac{1}{4} \ln \mathrm{PDI} & \text{(theta solvent)} \\ \frac{9}{25} \ln \mathrm{PDI} & \text{(good solvent)} \end{cases}$$

Note $\langle \Delta D^2 \rangle / \langle D \rangle^2 = \langle \Delta \Gamma^2 \rangle / \langle \Gamma \rangle^2$.

Problem 3.13: Show that, when a particle of mass m receives a random force $\mathbf{f}(t)$ with $\langle \mathbf{f}(t) \rangle = 0$ and $\langle \mathbf{f}(t) \cdot \mathbf{f}(t') \rangle = 6k_\mathrm{B} T \zeta \delta(t - t')$, its average kinetic energy satisfies the equipartition law: $m\langle \mathbf{v}^2 \rangle / 2 = (3/2) k_\mathrm{B} T$ [$k_\mathrm{B} T/2$ per degree of freedom, $(3/2) k_\mathrm{B} T$ for 3D].

Solution 3.13: The equation of motion of the particle (Langevin equation) is

$$\mathbf{f} = m \frac{\mathrm{d}\mathbf{v}}{\mathrm{d}t} + \zeta \mathbf{v}$$

Its solution is given as

$$\mathbf{v}(t) = m^{-1} \int_{-\infty}^{t} \mathbf{f}(t_1) \exp\left[(\zeta/m)(t_1 - t) \right] \mathrm{d}t_1$$

Then,

$$\langle \mathbf{v}(t)^2 \rangle = m^{-2} \int_{-\infty}^{t} dt_1 \int_{-\infty}^{t} dt_2 \langle \mathbf{f}(t_1) \cdot \mathbf{f}(t_2) \rangle \exp\left[(\zeta/m)(t_1 - t + t_2 - t)\right]$$

$$= 6k_B T \zeta m^{-2} \int_{-\infty}^{t} dt_1 \int_{-\infty}^{t} dt_2 \delta(t_1 - t_2) \exp[(\zeta/m)(t_1 - t + t_2 - t)]$$

$$= 6k_B T \zeta m^{-2} \int_{-\infty}^{t} dt_1 \exp\left[(2\zeta/m)(t_1 - t)\right] = \frac{3k_B T}{m}$$

which leads to $m\langle \mathbf{v}^2 \rangle/2 = (3/2)k_B T$.

Problem 3.14: Show that D_m defined by Eq. 3.81 becomes equal to D_0 in the dilute solution limit.

Solution 3.14: In the dilute solution limit, displacement of particle 1 has nothing to do with particle 2. Thus,

$$\langle [\mathbf{r}_1(t) - \mathbf{r}_2(0)]^2 \rangle = \langle [\mathbf{r}_1(t) - \mathbf{r}_1(0) + \mathbf{r}_1(0) - \mathbf{r}_2(0)]^2 \rangle$$

$$= \langle [\mathbf{r}_1(t) - \mathbf{r}_1(0)]^2 \rangle + \langle [\mathbf{r}_1(t) - \mathbf{r}_1(0)][\mathbf{r}_1(0) - \mathbf{r}_2(0)] \rangle + \langle [\mathbf{r}_1(0) - \mathbf{r}_2(0)]^2 \rangle$$

$$= \langle [\mathbf{r}_1(t) - \mathbf{r}_1(0)]^2 \rangle + 0 + \langle [\mathbf{r}_1(0) - \mathbf{r}_2(0)]^2 \rangle$$

When $t \longrightarrow \infty$, the first term is dominant.

Problem 3.15: What is the diffusion equation for a suspension of particles when there is a macroscopic flow $\bar{\mathbf{v}}(\mathbf{r})$ in the fluid?

Solution 3.15: The flow adds a term to the flux $\mathbf{j}$:

$$\mathbf{j} = -D\nabla c + c\bar{\mathbf{v}}$$

With Eq. 3.76,

$$\frac{\partial c}{\partial t} = D\nabla^2 c - \nabla \cdot (c\bar{\mathbf{v}})$$

Problem 3.16: A linear flexible chain is tethered to the surface of a spherical molecule. The sphere-chain molecules are suspended in a solvent that is isorefractive with the chain portion but not with the sphere portion. The solvent is good to both the sphere and the chain. Answer the following questions regarding the static and dynamic light scattering of the solution.

(1) Are the apparent R_g and A_2 estimated in the Zimm plot different from those obtained for solutions of spherical molecules without a tethered chain? If yes, what is the difference?
(2) How about D_0 and k_D in the expression of the mutual diffusion coefficient $D_m = D_0(1 + k_D c)$?

Solution 3.16 (1): Because the scattering comes only from the spheres, R_g is the same. Because $A_{2,\text{sphere}} \ll A_{2,\text{linear}}$, A_2 is greater when a chain is tethered.

Solution 3.16 (2): D_0 is smaller. There is now extra friction. k_D is greater because of the greater A_2.

Problem 3.17: In the preceding problem, another solvent that gives $(dn/dc)_{\text{sphere}} + (dn/dc)_{\text{chain}} = 0$ (the refractive index of the solvent is exactly the average of the refractive indices of the sphere and the chain) was used. The solvent is good to both the sphere and the chain. Answer the following questions.

(1) Are the apparent R_g and A_2 estimated in the Zimm plot different from those obtained for solutions of linear chains without a sphere tag? If yes, what is the difference?
(2) How about D_0 and k_D?

Solution 3.17 (1): R_g is slightly larger because of the sphere tag. A_2 is smaller.

Solution 3.17 (2): D_0 is smaller. k_D is smaller.

3.3 VISCOSITY

3.3.1 Viscosity of Solutions

3.3.1.1 Viscosity of a Fluid Solutions of a high-molecular-weight polymer, even at low concentrations, can flow only slowly. Addition of a small amount of the polymer to the fluid can make it **viscous**, thereby preventing unwanted turbulence in the flow.

Let us consider a fluid filling a space between two parallel plates, as illustrated in Figure 3.28. The bottom plate does not move, but the top plate slides in the y direction without changing the distance to the stationary plate. When the fluid adjacent to the plate sticks to the plate (nonslip boundary condition), the fluid moves in the same direction. Near the bottom plate, the fluid barely moves. However, with an increasing distance from the bottom plate, the fluid moves faster. As long as the flow is sufficiently slow, the fluid flows parallel to the plates. In other words, the velocity of the fluid has only an x component (v_x). This flow mode is called a **laminar flow**. We can regard the fluid as a stack of sheets, each sliding against the sheet beneath it. The velocity of the sheet, v_x, changes linearly with y,

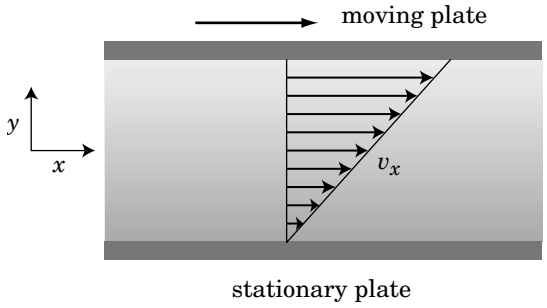

Figure 3.28. Fluid between a stationary bottom plate and a moving top plate. The velocity of the fluid is parallel to the plates and is proportional to the distance from the bottom plate, thereby generating a uniform velocity gradient.

the distance from the stationary plate. The gradient of v_x with respect to y, $\partial v_x/\partial y$, is called the **velocity gradient**.

To move the top plate at a constant velocity, a constant force must be applied in the x direction. The same applies to any small volume of the fluid. We consider a small disk parallel to the plates at distance y from the bottom plate (see Fig. 3.29). The disk has a height of dy. The fluid on the lower base flows at v_x, and the fluid on the upper base flows at $v_x + (\partial v_x/\partial y)\mathrm{d}y$. To make this velocity difference possible, a constant force needs to be exerted on the disk in the x direction. The force per area is called **shear stress** and has a dimension of the pressure. The shear stress σ_{yx} denotes the force per area in the x direction exerted across the plane normal to y. To be precise, σ is a tensor of the second rank. It is symmetric, that is, $\sigma_{yx} = \sigma_{xy}$, and so forth. The regular pressure is expressed as σ_{xx}, σ_{yy}, and σ_{zz}. In the isotropic fluid, $\sigma_{xx} = \sigma_{yy} = \sigma_{zz}$, and it is called hydrostatic pressure.

We next examine the relationship between σ_{yx} and $\partial v_x/\partial y$. When $\partial v_x/\partial y = 0$, $\sigma_{yx} = 0$. If there is no velocity gradient, then no force exists. When flow direction changes, both σ_{yx} and $\partial v_x/\partial y$ change their signs. Therefore, σ_{yx} is proportional to $\partial v_x/\partial y$ when $\partial v_x/\partial y$ is sufficiently small (**Newtonian fluid**):

$$\eta \frac{\partial v_x}{\partial y} = \sigma_{yx} \tag{3.95}$$

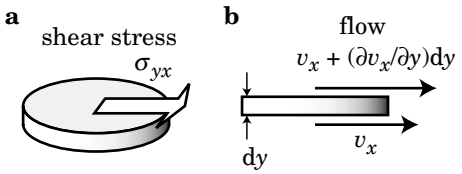

Figure 3.29. A small, thin disk parallel to the plates in Fig. 3.28. a: A shear stress σ_{yx} must be applied to the disk to have a different velocity between the upper base and the lower base. b: Side view.

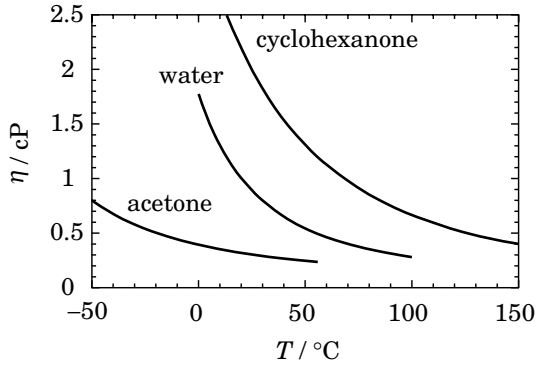

Figure 3.30. Viscosity η of water, acetone, and cyclohexanone at different temperatures.

The proportionality coefficient η is called the **viscosity**. Because $\partial v_x/\partial y$ has a dimension of s^{-1} and σ_{yx} has a dimension of N/m^2, the unit of η is $N\cdot s/m^2 = kg/(m\cdot s)$ in the SI unit. In the cgs system, the unit is $g/(cm\cdot s)$, which defines **poise**. Because most low-molecular-weight liquids have a viscosity of around 0.01 poise at room temperature, centipoise [cP; equal to 0.01 poise] is commonly used for the unit of viscosity. Note that $1\ cP = 10^{-3}\ kg/(m\cdot s)$.

Equation 3.95 illustrates that, to realize the same velocity gradient, a fluid with a greater η needs a larger shear stress. A greater force is needed to move the top plate at the same velocity. The viscosity is a measure for the resistance of the fluid to flow. The viscosity of the fluid sensitively depends on the temperature. Figure 3.30 shows the dependence for water, acetone, and cyclohexanone. The temperature dependence of viscosity is listed in reference books[34] for most organic solvents.

3.3.1.2 Viscosity of a Solution Now we learn how to express the concentration dependence of the viscosity in solutions. When the concentration c, expressed in g/L, is sufficiently low, the viscosity η of the solution is not much different from the viscosity η_s of the pure solvent. The ratio of η to η_s is called the **relative viscosity**. Although the ratio is dimensionless, it is customary to use the symbol η_r for the relative viscosity. When c is low,

$$\eta_r \equiv \frac{\eta}{\eta_s} = 1 + [\eta]c + K_v c^2 + \cdots \quad \text{relative viscosity} \tag{3.96}$$

Figure 3.31 illustrates how η_r changes with c. The linear coefficient $[\eta]$ is called the **intrinsic viscosity**. It can be obtained as the slope in the plot of η_r as a function of c in the low concentration limit:

$$[\eta] \equiv \lim_{c\to 0}\frac{\eta_r - 1}{c} = \lim_{c\to 0}\frac{\eta - \eta_s}{c\eta_s} \quad \text{intrinsic viscosity} \tag{3.97}$$

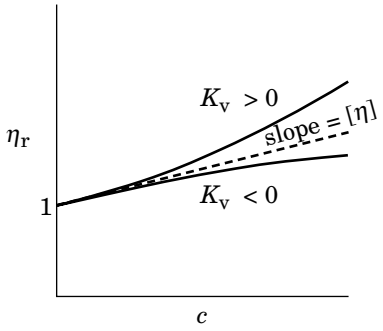

Figure 3.31. Relative viscosity η_r plotted as a function of c. The slope in the low c limit gives $[\eta]$. The plot deviates upward or downward, depending on the sign of K_v.

The dimension of $[\eta]$ is (concentration)$^{-1}$. As we will learn in Section 3.3.3, how $[\eta]$ of the polymer solution depends on the molecular weight of the polymer gives a hint on the conformation of the polymer. The second-order coefficient K_v can be positive or negative.

Sometimes, the **specific viscosity** η_{sp}, defined as $\eta_{sp} \equiv \eta_r - 1$, is used:

$$\eta_{sp} \equiv \eta_r - 1 = \frac{\eta - \eta_s}{\eta_s} = [\eta]c + K_v c^2 + \cdots \quad \text{specific viscosity} \tag{3.98}$$

The **reduced viscosity** η_{red} refers to the ratio of η_{sp} to c:

$$\eta_{red} \equiv \eta_{sp}/c = \frac{\eta - \eta_s}{\eta_s c} = [\eta] + K_v c + \cdots \quad \text{reduced viscosity} \tag{3.99}$$

It has a dimension of (concentration)$^{-1}$. Figure 3.32 illustrates how η_{red} changes with c.

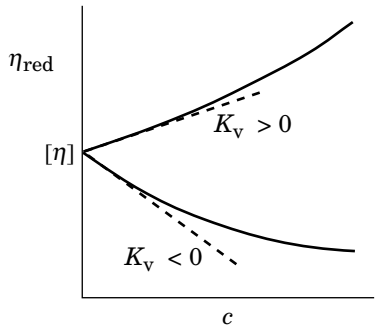

Figure 3.32. Reduced viscosity η_{red} plotted as a function of c. The intercept is $[\eta]$. The slope of the tangent at $c = 0$ gives K_v.

The reciprocal of the intrinsic viscosity is often used to represent the overlap concentration of a given polymer: $c^* = 1/[\eta]$ (Eq. 1.110). It means that we can expect the polymer solution at c^* to be about twice as viscous as the pure solvent.

3.3.2 Measurement of Viscosity

Automated viscometers are commercially available. To measure the viscosity of liquids in the centipoise range, it is, however, more common to use a capillary flow viscometer, unless the measurement is routinely conducted. This classical method is inexpensive, yet can measure the viscosity with a sufficient accuracy.

Figure 3.33 illustrates an **Ubbelohde viscometer**, an improved version of an Ostwald viscometer. The main part on the left has a straight section of capillary and a large cavity above the section. It is imperative that the capillary be straight and its cross section be uniform. Markers are inscribed above and below the cavity. A reservoir is on the bottom of the right side. A fluid is poured into the reservoir and drawn into the cavity by suction. The upper level of the fluid must be raised above the top marker, and the lower level of the fluid must be below the lower end of the capillary. The capillary must be filled with the fluid. The viscometer is held vertically. The suction is then released. As the fluid flows down, the upper level of the fluid passes the top mark and eventually the lower mark as well. The time between these two events, called an efflux time, is recorded. Measurement is carried out in a temperature-controlled bath.

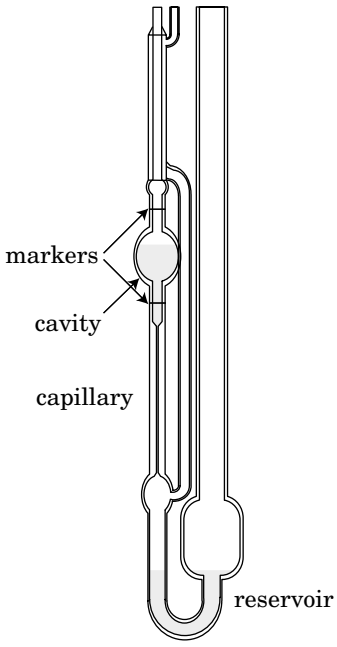

Figure 3.33. Ubbelohde viscometer. The efflux time between the time when the liquid level crosses the upper marker and the time when it crosses the lower marker is measured.

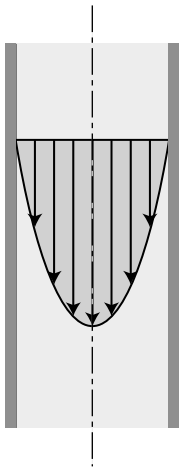

Figure 3.34. Cross section of the flow in the capillary. The flow velocity is parallel to the center line of the capillary. Velocity field is parabolic.

The measurement is based on the capillary flow. If the flow is slow and therefore laminar, the velocity profile in the capillary is of a parabolic cone. The velocity maximizes at the center line and declines to zero toward the wall (Fig. 3.34). The **Poiseuille law** holds for the viscosity of the fluid and the pressure drop ΔP along the length l of the capillary (Fig. 3.35):

$$\eta = \frac{\pi r^4 t \Delta P}{8Vl} \quad \text{Poiseuille flow} \tag{3.100}$$

where r is the radius of the capillary and V is the volume of the fluid that flows in time t. In the viscometer in Figure 3.33, V is the volume of the cavity between the two markers.

The pressure difference can be generated by a liquid pump, but, in the capillary viscometer in the vertical position, it is the gravity that causes ΔP, which is given by

$$\Delta P = \rho_{\text{liq}} g l \tag{3.101}$$

where ρ_{liq} is the density of the liquid, and g is the acceleration by the gravity. Equations 3.100 and 3.101 give the kinematic viscosity ν_{kin} defined as $\nu_{\text{kin}} \equiv \eta/\rho_{\text{liq}}$:

$$\nu_{\text{kin}} \equiv \frac{\eta}{\rho_{\text{liq}}} = \frac{\pi r^4 g}{8V} t \tag{3.102}$$

Note that $\pi r^4 g/(8V)$ is a constant for a given viscometer. The constant can be determined by using a fluid of a known kinematic viscosity. Once calibrated, the

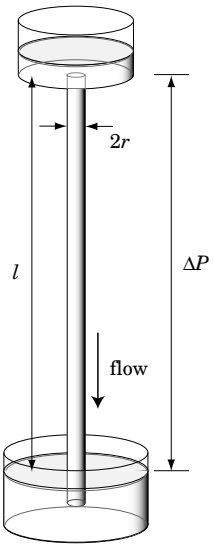

Figure 3.35. Flow in a vertical capillary. The pressure drop ΔP over the length l of the capillary by the gravity causes the flow.

kinematic viscosity can be measured for any fluid from the measurement of the flow time. Together with the density, the viscosity of the fluid can be determined. Alternatively, we can use the formula of

$$\frac{\eta_1}{\eta_2} = \frac{\rho_1 t_1}{\rho_2 t_2} \tag{3.103}$$

to obtain the viscosity η_1 of a solution (density ρ_1) from the measurement of the efflux time t_1, if the efflux time t_2 of a liquid with a known viscosity η_2 and density ρ_2 is measured for the same viscometer. The density of the solution at a given concentration can be estimated from the densities of the solvent and the polymer by assuming additiveness of the volume.

If the fluid is too viscous, the elution takes too long. If it is too fluid, the flow will be too fast, causing a nonlaminar flow. A given viscometer can be used for a finite range of viscosity. To allow for the viscosity measurement of fluids in a wide range of viscosity, Ubbelohde viscometers are available in different radii of the capillary.

3.3.3 Intrinsic Viscosity

The intrinsic viscosity $[\eta]$ is a quantity characteristic of a polymer. It represents an increase in the solution viscosity when the concentration is raised to a certain level. As expected, a polymer molecule with a greater dimension has a larger $[\eta]$.

Table 3.2 Mark-Houwink-Sakurada Exponents

Conformation	α
Linear flexible (theta solvent)	0.5
Linear flexible (good solvent)	0.7–0.8
Rigid	>1

Experimentally, it is expressed by **Mark-Houwink-Sakurada equation**:

$$\boxed{[\eta] = K_{\mathrm{M}}(M/(\mathrm{g/mol}))^{\alpha} \quad \text{Mark-Houwink-Sakurada equation}} \tag{3.104}$$

where K_{M} is a constant of the unit of L/g, and α is called a **Mark-Houwink-Sakurada exponent**. Note that K_{M} and α are different from polymer to polymer and can depend on the solvent as well.

The classical method to determine K_{M} and α of a given polymer is as follows. First, prepare fractions of different molecular weights either by synthesis or by fractionation. Next, make dilute solutions of different concentrations for each fraction. Measure the viscosity of each solution, plot the reduced viscosity as a function of polymer concentration, and estimate $[\eta]$ for each fraction. Plot $[\eta]$ as a function of the molecular weight in a double logarithmic scale. This method has been extensively used to characterize polymer samples because the exponent α provides a measure of the chain rigidity. Values of α are listed in Table 3.2 for some typical shapes and conformations of the polymer. The value of α is around 0.7–0.8 for flexible chains in the good solvent and exceeds 1 for rigid chains. In the theta solvent, the flexible chain has $\alpha = 0.5$.

Apparently, α is greater for a more extended conformation. It is reasonable because a polymer molecule with a greater dimension for a given contour length will experience a greater friction to move in the solvent. We will obtain the formulas of $[\eta]$ for linear flexible chains in the theta solvent and the good solvent in the next section.

SEC equipped with a viscosity detector and a light-scattering detector in tandem with a concentration detector (triple detector SEC) has been recently and increasingly used to obtain the Mark-Houwink-Sakurada plot. Figure 3.36 illustrates the scheme. The advantage is obvious. What is needed for the plot is only one polydisperse fraction of the polymer. As the polymer is separated by the SEC columns according to its dimension, the eluent containing the polymer is immediately led to the detectors in nearly simultaneous measurement of the solution viscosity, the concentration, the molecular weight, and the radius of gyration. Because the concentration is sufficiently low, the second- and higher-order terms are negligible in Eq. 3.96. Then, the ratio of the viscosity of the eluent to that of the pure solvent gives $[\eta]$ with the information of the concentration to be obtained in the concentration detector. Figure 3.37 shows an example of such a measurement.[35] The samples were fractions of poly(vinyl *neo*-decanoate) prepared in radical polymerization and

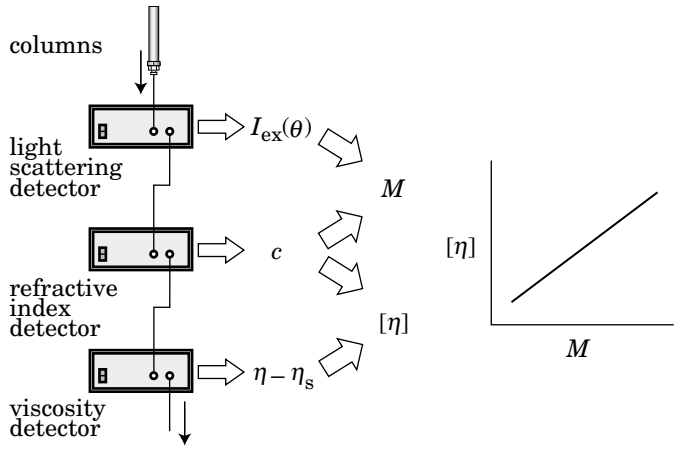

Figure 3.36. Size exclusion chromatography system with an on-line viscometer and a light-scattering detector allows to create the Mark-Houwink-Sakurada plot without fractionating the polymer somewhere else. The concentration is detected by a refractive index detector or an ultraviolet absorption detector.

pulsed laser polymerization. The mobile phase was tetrahydrofuran. The slope α is 0.70 for most of the data, indicating a flexible chain conformation.

3.3.4 Flow Field

In Section 3.3.1, an example of flow fields was shown. We consider a flow $\mathbf{v}$ at $\mathbf{r}$ given as

$$\mathbf{v} = \boldsymbol{\kappa}\mathbf{r} \tag{3.105}$$

where $\boldsymbol{\kappa}$ is the velocity gradient tensor defined as

$$\kappa_{\alpha\beta} = \frac{\partial v_\alpha}{\partial r_\beta} \quad (\alpha, \beta = x, y, z) \tag{3.106}$$

Here, $r_x = x$, for instance. In the example in Section 3.3.1, the flow field was a **shear flow** in the x direction (Fig. 3.38a). Then, $\kappa_{xy} = \kappa$ is the only nonzero element in $\boldsymbol{\kappa}$:

$$\boldsymbol{\kappa} = \begin{bmatrix} 0 & \kappa & 0 \\ 0 & 0 & 0 \\ 0 & 0 & 0 \end{bmatrix} \quad \text{shear flow} \tag{3.107}$$

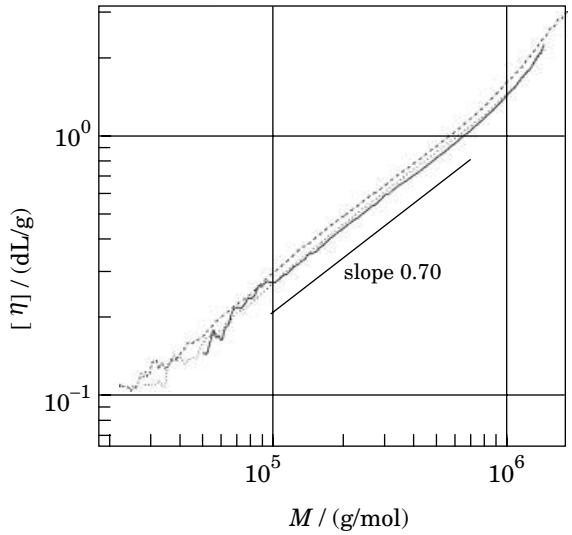

Figure 3.37. Example of the Mark-Houwink-Sakurada plot obtained in size exclusion chromatography. The sample is poly(vinyl *neo*-decanoate) in tetrahydrofuran. The data are along the slope of 0.70, indicating that the polymer is a flexible chain. (From Ref. 35.)

where the velocity gradient κ is also called a **shear rate**. The flow field generated by this κ is

$$\mathbf{v} = \begin{bmatrix} \kappa y \\ 0 \\ 0 \end{bmatrix} \quad \text{shear flow} \tag{3.108}$$

It is convenient to express $[\eta]$ in terms of the shear stress. In the shear flow, the shear stress changes from $\sigma_{yx} = \eta_s \kappa$ for the pure solvent to $\sigma_{yx} + \Delta\sigma_{yx} = \eta\kappa$ for the solution of concentration c ($c \ll c^*$). Then, from Eq. 3.97,

$$[\eta] = \frac{\Delta\sigma_{yx}}{\kappa c \eta_s} = \frac{\Delta\sigma_{xy}}{\kappa c \eta_s} \tag{3.109}$$

When $\Delta\sigma_{yx}$ is calculated up to the linear term of κ, this equation gives κ-independent intrinsic viscosity. The latter is called a **zero-shear viscosity**.

Another flow field often used in theories and experiments is an **elongational flow** (Fig. 3.38b). Its κ is given by

$$\kappa = \begin{bmatrix} -\dot{\varepsilon}/2 & 0 & 0 \\ 0 & -\dot{\varepsilon}/2 & 0 \\ 0 & 0 & \dot{\varepsilon} \end{bmatrix} \quad \text{elongational flow} \tag{3.110}$$

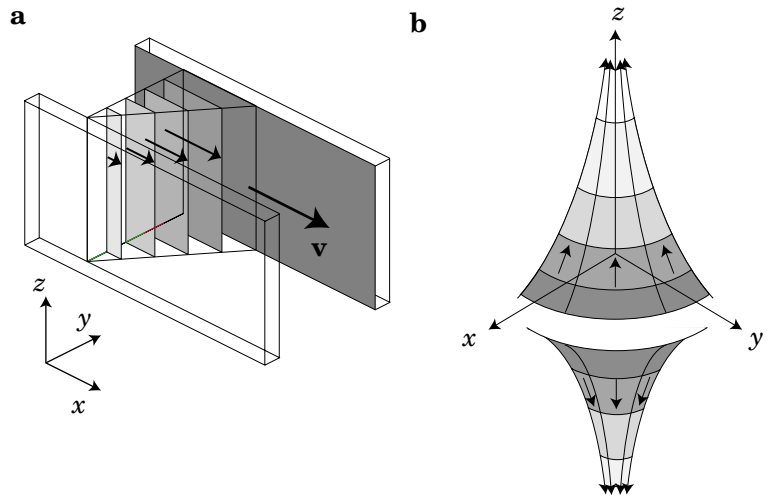

Figure 3.38. Typical flow fields. a: Shear flow. b: Elongational flow.

where $\dot{\varepsilon}$ is called the strain rate. The flow field generated by this κ is

$$\mathbf{v} = \begin{bmatrix} -(\dot{\varepsilon}/2)x \\ -(\dot{\varepsilon}/2)y \\ \dot{\varepsilon}z \end{bmatrix} \quad \text{elongational flow} \tag{3.111}$$

The two velocity fields satisfy the incompressibility requirement:

$$\text{div } \mathbf{v} = 0 \tag{3.112}$$

3.3.5 PROBLEMS

Problem 3.18: It is not easy to place the viscometer in the perfectly vertical position. Evaluate the error in the estimate of η when the viscometer is at angle $\theta \ll 1$ from the vertical.

Solution 3.18: The pressure difference ΔP is smaller. It is now $\rho_{\text{liq}} g l \cos\theta$. Then, Eq. 3.102 changes to

$$\nu_{\text{kin}} = \frac{\pi r^4 g \cos\theta}{8V} t$$

When $\theta \ll 1$, $\cos\theta \cong 1 - \theta^2/2$. The relative error in ν_{kin} is $\sim\theta^2/2$.

Problem 3.19: Measurement of the solution viscosity η at several different concentrations gives information on the state of the polymer chains in solution.

Answer the following questions for linear flexible polymer chains that show $[\eta] \propto M^{0.8}$ when they are molecularly dispersed.

(1) Suppose two polymer chains form an aggregate at low concentrations in a given solvent and behave as if they were a single chain of twice the molecular weight. How does this aggregate change $[\eta]$?

(2) Suppose the polymer chains are molecularly dispersed in the low concentration limit, but tend to form an aggregate of several chains with an increasing concentration. We assume that each aggregate behaves as if it were a single chain that has a molecular weight equal to the total molecular weight of the aggregate. Sketch a plot of η_{red} as a function of c.

Solution 3.19:

(1) When molecularly dispersed, the intrinsic viscosity is $[\eta]_{true} = K_M {M_1}^{0.8}$, where M_1 is the molecular weight of the polymer chain. When dimers (aggregates of two chains) are formed, the apparent intrinsic viscosity changes to $[\eta]_{app} = K_M(2M_1)^{0.8} = 2^{0.8} K_M {M_1}^{0.8} \cong 1.74 \times [\eta]_{true}$.

(2) When n-mers are formed, the apparent intrinsic viscosity changes to $[\eta]_{app} = K_M(nM_1)^{0.8} = n^{0.8}[\eta]_{true}$. The reduced viscosity is therefore, $\eta_{red} \cong n^{0.8}[\eta]_{true.}$ With an increasing c, n increases. Then, η_{red} increases. The plot is similar to the curve for $K_v > 0$ in Fig. 3.32.

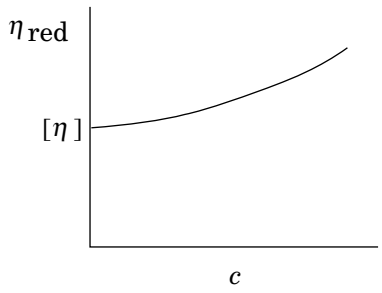

Problem 3.20: A solution of a polydisperse polymer has component i dissolved at concentration c_i. The intrinsic viscosity of component i is given by $[\eta]_i$.

(1) What is $[\eta]$ of the polydisperse polymer?

(2) Each component follows the Mark-Houwink-Sakurada equation: $[\eta]_i = K_M {M_i}^{\alpha}$. What is the molecular weight M_v estimated by assuming that the same equation applies to the polydisperse polymer, i.e., $[\eta] = K_M {M_v}^{\sigma}$. What is the relationship of this M_v to M_n and M_w?

Solution 3.20 (1): For the solution of the polydisperse polymer,

$$\eta = \eta_s\left(1 + \sum_i c_i[\eta]_i + \cdots\right)$$

which we equate to $\eta = \eta_s(1 + c[\eta] + \cdots)$. Then, $\sum_i c_i[\eta]_i = c[\eta] = [\eta]\sum_i c_i$

Thus, $[\eta] = \sum_i c_i[\eta]_i / \sum_i c_i$

Solution 3.20 (2): $K_M M_v{}^{\alpha} = \dfrac{\sum_i c_i K_M M_i{}^{\alpha}}{\sum_i c_i}$ Then, $M_v = \left(\sum_i c_i M_i{}^{\alpha} / \sum_i c_i\right)^{1/\alpha}$

This M_v is another average molecular weight. For polymers with $0 < \alpha < 1$, $M_n < M_v < M_w$.

3.4 NORMAL MODES

3.4.1 Rouse Model

3.4.1.1 Model for Chain Dynamics In Sections 1.2 and 1.3, we learned about the conformation of the ideal chain and obtained the probability distribution of the conformation. The distribution tells how many chains in the system have a certain conformation at a given time. Each chain is moving and changing its conformation all the time. The probability distribution also gives the distribution of the period in which a given chain takes each conformation (ergodicity).

In this section, we learn how fast the conformation changes. To simplify the seemingly complicated motions of the monomers, we employ the bead-spring model of N beads with a spring force constant of $k_{sp} = 3k_BT/b^2$. Figure 3.39 illustrates how the beads move to change the lengths and the orientations of the springs, thereby reshaping the whole chain.

The **Rouse model**[36] is the simplest version of the bead-spring model that can treat the chain dynamics. The model assumes that the beads have no excluded volume (they are essentially a point) and that there are no hydrodynamic interactions

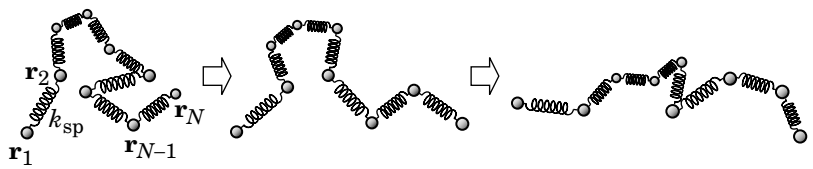

Figure 3.39. A polymer chain of a bead-spring model changes its conformation with time.

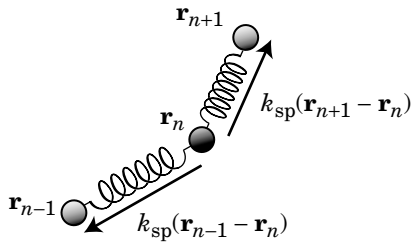

Figure 3.40. Spring force on the nth bead. It is pulled by the two springs.

between the beads. The model was subsequently refined to account for these effects. Unlike the later models, the Rouse model does not provide correct expressions for the center-of-mass diffusion coefficient or the relaxation time for the conformation change. We will learn the Rouse model here in detail, because the way a complicated motion of connected beads is simplified into different modes is noteworthy and used in the later models with modifications. Furthermore, the Rouse-like modes can be observed in solutions at high concentrations and in melts where the hydrodynamic interactions are shielded.

3.4.1.2 Equation of Motion The elastic forces on the nth bead ($n = 2, 3, \ldots, N-1$) are exerted by the two springs that connect the adjacent beads, as illustrated in Figure 3.40. The spring between the $(n-1)$th and the nth beads pulls the bead with the force of $k(\mathbf{r}_{n-1} - \mathbf{r}_n)$. Likewise, the other spring pulls the bead with $k(\mathbf{r}_{n+1} - \mathbf{r}_n)$. In addition, the nth bead receives a random force $\mathbf{f}_n$ that changes with time t from nearby solvent molecules just as a single particle receives the random force (Fig. 3.20). Thus, the equation of motion for the nth bead is given as

$$\zeta \frac{\mathrm{d}\mathbf{r}_n}{\mathrm{d}t} = k_{\rm sp}(\mathbf{r}_{n-1} - \mathbf{r}_n) + k_{\rm sp}(\mathbf{r}_{n+1} - \mathbf{r}_n) + \mathbf{f}_n(t) \quad (n = 2, 3, \ldots, N-1) \tag{3.113}$$

where ζ is the friction coefficient of each bead in the solvent. The mass term (mass $\times$ acceleration) is missing in this equation because the term is negligible on the time scales of our concern (μs to s; the acceleration term is important at high frequencies such as vibrational motion). The motion of the bead is overdamped. A special care is necessary for the terminal beads ($n = 1$ and N). Their equations of motion are

$$\zeta \frac{\mathrm{d}\mathbf{r}_1}{\mathrm{d}t} = k_{\rm sp}(\mathbf{r}_2 - \mathbf{r}_1) + \mathbf{f}_1(t), \; \zeta \frac{\mathrm{d}\mathbf{r}_N}{\mathrm{d}t} = k_{\rm sp}(\mathbf{r}_{N-1} - \mathbf{r}_N) + \mathbf{f}_N(t) \tag{3.114}$$

respectively. By introducing $\mathbf{r}_0 = \mathbf{r}_1$ and $\mathbf{r}_{N+1} = \mathbf{r}_N$, the above two equations become a part of the general equation:

$$\zeta \frac{\mathrm{d}\mathbf{r}_n}{\mathrm{d}t} = k_{\rm sp}(\mathbf{r}_{n-1} + \mathbf{r}_{n+1} - 2\mathbf{r}_n) + \mathbf{f}_n(t) \quad (n = 1, 2, \ldots, N) \quad \text{bead}-\text{spring model} \tag{3.115}$$

The nature of the random force is the same as in Eqs. 3.63 and 3.71:

$$\langle \mathbf{f}_n(t) \rangle = 0 \tag{3.116}$$

$$\langle \mathbf{f}_n(t) \cdot \mathbf{f}_m(t') \rangle = 6\zeta k_B T \delta(t - t')\, \delta_{nm} \tag{3.117}$$

There is no relationship between the forces on difference beads ($\delta_{nm} = 1$ only when $n = m$). The random forces are needed to keep the chain in shape. Without the random forces, the beads would move until all of them collapse onto a single point and the elastic forces disappear.

3.4.2 Normal Coordinates

3.4.2.1 Definition We now need to solve the N equations in Eq. 3.115 simultaneously. The change in $\mathbf{r}_n$ depends on $\mathbf{r}_{n-1}$ and $\mathbf{r}_{n+1}$, and the change in $\mathbf{r}_{n-1}$ depends on $\mathbf{r}_{n-2}$ and $\mathbf{r}_n$, and so forth. Motions of different beads are related to each other. Solving these equations appears difficult, but use of the normal coordinates facilitates it. The ith **normal coordinate** $\mathbf{q}_i(t)$ ($i = 0, 1, \ldots$) is defined as a linear combination of $\mathbf{r}_n(t)$:

$$\boxed{\mathbf{q}_i(t) = \frac{1}{N} \sum_{n=1}^{N} \cos \frac{in\pi}{N} \mathbf{r}_n(t) \qquad \text{normal coordinate}} \tag{3.118}$$

The 0th **normal mode** is essentially the center-of-mass position, $\mathbf{r}_G(t)$, of the N beads:

$$\boxed{\mathbf{q}_0(t) = \frac{1}{N} \sum_{n=1}^{N} \mathbf{r}_n(t) = \mathbf{r}_G(t)} \tag{3.119}$$

Thus $\mathbf{q}_0(t)$ represents the global motion of the bead-spring chain. All the other normal modes represent internal motions. The first and second modes are

$$\begin{aligned} \mathbf{q}_1(t) &= \frac{1}{N} \sum_{n=1}^{N} \cos \frac{n\pi}{N} \mathbf{r}_n(t) \\ &= \frac{1}{N} \left[\cos \frac{\pi}{N} \mathbf{r}_1(t) + \cos \frac{2\pi}{N} \mathbf{r}_2(t) + \cdots + \cos \pi\, \mathbf{r}_N(t) \right] \end{aligned} \tag{3.120}$$

$$\begin{aligned} \mathbf{q}_2(t) &= \frac{1}{N} \sum_{n=1}^{N} \cos \frac{2n\pi}{N} \mathbf{r}_n(t) \\ &= \frac{1}{N} \left[\cos \frac{2\pi}{N} \mathbf{r}_1(t) + \cos \frac{4\pi}{N} \mathbf{r}_2(t) + \cdots + \cos(2\pi)\, \mathbf{r}_N(t) \right] \end{aligned} \tag{3.121}$$

The superposition coefficient $\cos(in\pi/N)$ is plotted in Figure 3.41 as a function of n for $N = 100$ and $i = 1, 2, \ldots, 8$. To be precise, $\cos(in\pi/N)$ is given for integral

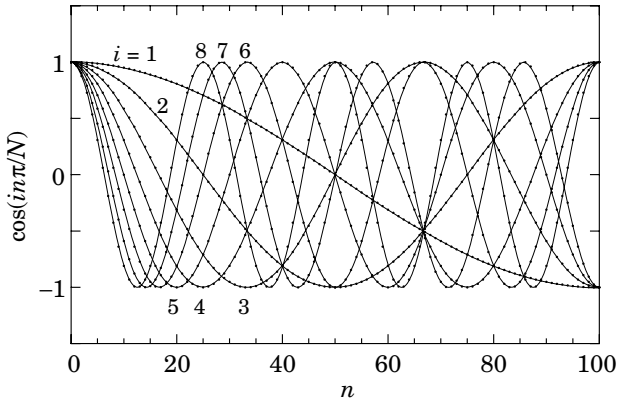

Figure 3.41. Coefficient $\cos(in\pi/N)$ plotted as a function of n for $N = 100$. Curves for $i = 1$ to 8 are shown.

values of n only (small dots on the curves). Figure 3.42 illustrates the sign of $\cos(in\pi/N)$ along the contour of the Rouse chain for $i = 0$ to 6. The zeroth mode is the mean of all $\mathbf{r}_n$. In the first mode, the superposition coefficient changes its sign at the midpoint along the chain contour. In the second mode, the coefficient is positive in the first and last quadrants, and negative in the two middle quadrants. As i increases, the sign alteration becomes more frequent. It is possible to give meanings to these normal modes.

The meaning of the first mode, for instance, may become clearer by considering another superposition coefficient: $+2$ for positive $\cos(in\pi/N)$ and -2 for negative $\cos(in\pi/N)$. Then, $\mathbf{q}_1$ is the vector that connects the centroid of the beads in the first half of the chain and the centroid of the beads in the second half of the chain (see Fig. 3.43a). As the chain makes an overall tumbling motion, $\mathbf{q}_1$ changes its

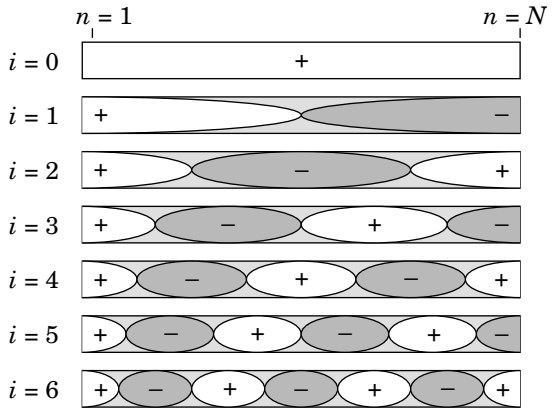

Figure 3.42. Sign of the coefficient $\cos(in\pi/N)$ for $i = 0$ to 6.

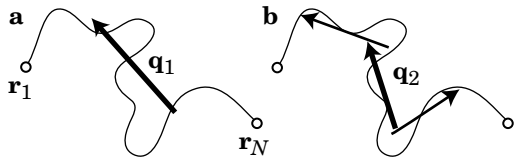

Figure 3.43. Schematic of the first normal mode $\mathbf{q}_1$ (a) and the second normal mode $\mathbf{q}_2$ (b) for a chain conformation given.

orientation. Therefore, we can associate the change in $\mathbf{q}_1$ with rotation of the chain as a whole, although $\mathbf{q}_1$ changes its length by rearrangement of the beads and thus $\mathbf{q}_1$ can change its sign without overall rotation. With the actual coefficient, $\cos(in\pi/N)$, which changes gradually from 1 to -1, $\mathbf{q}_1$ still carries the characteristics that it represents the overall chain orientation.

The next mode $\mathbf{q}_2$ can be viewed as the sum of the two vectors, one drawn from the second quadrant to the first quadrant and the other one drawn from the third quadrant to the fourth quadrant (Fig. 3.43b). Thus $\mathbf{q}_2$ is more sensitive to the local details of the conformation compared with $\mathbf{q}_1$. As we move to $\mathbf{q}_3$, $\mathbf{q}_4, \ldots,$ the mode becomes increasingly sensitive to the local details and less sensitive to the overall conformation. The last mode $\mathbf{q}_N$, defined as

$$\mathbf{q}_N(t) = \frac{1}{N}\sum_{n=1}^{N}\cos(n\pi)\mathbf{r}_n(t) = \frac{1}{N}[-\mathbf{r}_1(t) + \mathbf{r}_2(t) - \cdots + (-1)^N\mathbf{r}_N(t)] \quad (3.122)$$

represents the displacement of even-numbered beads relative to the odd-numbered beads divided by N.

An example of $\mathbf{q}_1$, $\mathbf{q}_2, \ldots$ is shown in Figure 3.44 for a realistic conformation in two dimensions ($N = 32$). We can see that the magnitude of the normal mode tends

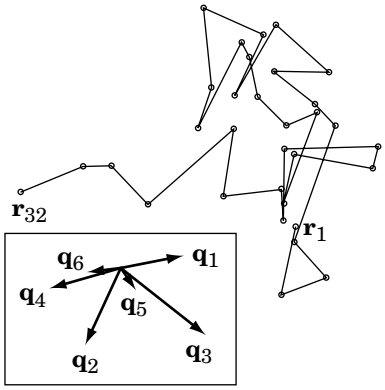

Figure 3.44. Example of a bead-spring model in two dimensions. $N = 32$. The first six normal modes $\mathbf{q}_1$ through $\mathbf{q}_6$ are shown in the inset by vectors (zoomed by a factor of two for easy observation).

to decrease with an increasing mode number i. We expect that $\mathbf{q}_i(t)$ of a higher mode number to change more quickly with time because the mode picks up more localized motions, which do not have to wait for the whole chain to rearrange.

3.4.2.2 Inverse Transformation The normal coordinate is given as a linear combination of the bead positions. Conversely, we can express $\mathbf{r}_n$ as a linear combination of $\mathbf{q}_i$ ($i = 1, 2, \ldots, N$). From Eq. 3.118, we find

$$\begin{aligned} &2\sum_{i=1}^{N-1}\cos\frac{in\pi}{N}\mathbf{q}_i + \mathbf{q}_0 + (-1)^n\mathbf{q}_N \\ &\quad= \frac{1}{N}\sum_{m=1}^{N}\mathbf{r}_m\left(\sum_{i=1}^{N-1}2\cos\frac{im\pi}{N}\cos\frac{in\pi}{N} + 1 + (-1)^{m+n}\right) \\ &\quad= \frac{1}{N}\sum_{m=1}^{N}\mathbf{r}_m\left[\left(\sum_{i=1}^{N-1}\cos\frac{i(m+n)\pi}{N} + \tfrac{1}{2} + \tfrac{1}{2}(-1)^{m+n}\right)\right. \\ &\qquad\left. + \left(\sum_{i=1}^{N-1}\cos\frac{i(m-n)\pi}{N} + \tfrac{1}{2} + \tfrac{1}{2}(-1)^{m-n}\right)\right] \end{aligned} \tag{3.123}$$

Use of the identity

$$\sum_{i=1}^{N-1}\cos\frac{ik\pi}{N} + \tfrac{1}{2} + \tfrac{1}{2}(-1)^k = \begin{cases} N & (k = 0, \pm 2N, \pm 4N, \ldots) \\ 0 & (\text{otherwise}) \end{cases} \tag{3.124}$$

leads Eq. 3.123 to

$$\boxed{\mathbf{r}_n(t) = 2\sum_{i=1}^{N-1}\cos\frac{in\pi}{N}\mathbf{q}_i(t) + \mathbf{q}_0(t) + (-1)^n\mathbf{q}_N(t) \quad (n = 1, 2, \ldots, N-1)} \tag{3.125}$$

Note that the superposition coefficient for $i = 0$ and N is a half of the others. For $n = N$, $\mathbf{r}_N(t)$ is a half of the one given by this equation. We need to treat $\mathbf{r}_N$ separately, because the superposition coefficient, $\cos(in\pi/N)$ in Eq. 3.118 is not symmetric. Fortunately, the effect of the separate treatment is negligible when $N \gg 1$. In the following, we neglect this effect.

3.4.3 Equation of Motion for the Normal Coordinates in the Rouse Model

3.4.3.1 Equation of Motion The equation of motion for $\mathbf{q}_i$ is obtained from Eqs. 3.115 and 3.118 as

$$\begin{aligned} \zeta\frac{\mathrm{d}\mathbf{q}_i}{\mathrm{d}t} &= \frac{1}{N}\sum_{n=1}^{N}\cos\frac{in\pi}{N}\zeta\frac{\mathrm{d}\mathbf{r}_n}{\mathrm{d}t} = \frac{1}{N}\sum_{n=1}^{N}\cos\frac{in\pi}{N}\mathbf{f}_n \\ &\quad + k_{\mathrm{sp}}\frac{1}{N}\sum_{n=1}^{N}\cos\frac{in\pi}{N}(\mathbf{r}_{n-1} + \mathbf{r}_{n+1} - 2\mathbf{r}_n) \end{aligned} \tag{3.126}$$

In the second term,

$$\begin{aligned}\sum_{n=1}^{N}\cos\frac{in\pi}{N}\left(\mathbf{r}_{n-1}+\mathbf{r}_{n+1}-2\mathbf{r}_n\right) &= \sum_{n=0}^{N-1}\cos\frac{i(n+1)\pi}{N}\mathbf{r}_n \\ &+\sum_{n=2}^{N+1}\cos\frac{i(n-1)\pi}{N}\mathbf{r}_n-2\sum_{n=1}^{N}\cos\frac{in\pi}{N}\mathbf{r}_n \\ &\cong \sum_{n=1}^{N}\left(\cos\frac{i(n+1)\pi}{N}+\cos\frac{i(n-1)\pi}{N}-2\cos\frac{in\pi}{N}\right)\mathbf{r}_n\end{aligned} \tag{3.127}$$

Since

$$\begin{aligned}&\cos\frac{i(n+1)\pi}{N}+\cos\frac{i(n-1)\pi}{N}-2\cos\frac{in\pi}{N} \\ &\quad=2\cos\frac{in\pi}{N}\left(\cos\frac{i\pi}{N}-1\right)\cong-\left(\frac{i\pi}{N}\right)^2\cos\frac{in\pi}{N}\end{aligned} \tag{3.128}$$

Eq. 3.126 is rewritten to

$$\zeta\frac{\mathrm{d}\mathbf{q}_i}{\mathrm{d}t}=-k_{\mathrm{sp}}\left(\frac{i\pi}{N}\right)^2\mathbf{q}_i+\frac{1}{N}\sum_{n=1}^{N}\cos\frac{in\pi}{N}\mathbf{f}_n \tag{3.129}$$

For later convenience, we introduce the friction coefficient ζ_i for the ith mode by

$$\zeta_i=\begin{cases}N\zeta & (i=0)\\ 2N\zeta & (i\neq 0)\end{cases}\qquad\text{Rouse model} \tag{3.130}$$

and rewrite Eq. 3.129 to

$$\boxed{\zeta_i\frac{\mathrm{d}\mathbf{q}_i}{\mathrm{d}t}=-k_i\mathbf{q}_i+\mathbf{g}_i\quad(i=0,1,2,\ldots)\quad\text{normal coordinate}} \tag{3.131}$$

Because $k_{\mathrm{sp}}=3k_{\mathrm{B}}T/b^2$, the force constant k_i of the ith mode is given as

$$k_i=k_{\mathrm{sp}}\frac{\zeta_i}{\zeta}\left(\frac{i\pi}{N}\right)^2=\frac{6\pi^2k_{\mathrm{B}}T}{Nb^2}\,i^2\qquad\text{Rouse model} \tag{3.132}$$

The random force $\mathbf{g}_i$ for the ith mode is defined as

$$\mathbf{g}_i(t)=\frac{\zeta_i}{\zeta}\frac{1}{N}\sum_{n=1}^{N}\cos\frac{in\pi}{N}\mathbf{f}_n(t) \tag{3.133}$$

It is now apparent that the equation of motion for $\mathbf{q}_i$ does not depend on other $\mathbf{q}_j$ ($j \neq i$). Each mode is independent (decoupled). With the relaxation time τ_i defined as

$$\tau_i \equiv \zeta_i / k_i \tag{3.134}$$

Eq. 3.131 is further rewritten to

$$\boxed{\frac{\mathrm{d}\mathbf{q}_i}{\mathrm{d}t} = -\frac{1}{\tau_i}\mathbf{q}_i + \frac{1}{\zeta_i}\mathbf{g}_i \quad (i = 0, 1, \ldots) \quad \text{normal coordinate}} \tag{3.135}$$

For the 0th mode, $1/\tau_0 = 0$. Other τ_i are finite:

$$\boxed{\tau_i = \frac{\zeta N^2 b^2}{3\pi^2 k_\mathrm{B} T}\frac{1}{i^2} \quad (i = 1, 2, \ldots) \quad \text{Rouse model}} \tag{3.136}$$

The relaxation time of the normal mode decreases with i as $\tau_i = \tau_1/i^2$ in the Rouse model. The higher-order mode relaxes more quickly.

3.4.3.2 Correlation of Random Force Statistical properties of the random force $\mathbf{g}_i$ are similar to the counterparts of $\mathbf{f}_n$:

$$\langle \mathbf{g}_i(t) \rangle = 0 \tag{3.137}$$

$$\langle \mathbf{g}_i(t) \cdot \mathbf{g}_j(t') \rangle = 6\zeta_i k_\mathrm{B} T \delta(t - t')\delta_{ij} \tag{3.138}$$

The first part is obvious. The second part can be proved as follows:

$$\begin{aligned}
\langle \mathbf{g}_i(t) \cdot \mathbf{g}_j(t') \rangle &= \left(\frac{\zeta_i}{\zeta}\right)^2 \frac{1}{N^2} \sum_{n=1}^{N} \cos\frac{in\pi}{N} \sum_{m=1}^{N} \cos\frac{jm\pi}{N} \langle \mathbf{f}_n(t) \cdot \mathbf{f}_m(t') \rangle \\
&= \left(\frac{\zeta_i}{\zeta}\right)^2 \frac{1}{N^2} \sum_{n=1}^{N} \cos\frac{in\pi}{N} \cos\frac{jn\pi}{N} 6\zeta k_\mathrm{B} T \delta(t - t') \\
&\cong \left(\frac{\zeta_i}{\zeta}\right)^2 6\zeta k_\mathrm{B} T \delta(t - t') \frac{1}{N^2} \int_0^N \cos\frac{in\pi}{N} \cos\frac{jn\pi}{N} \mathrm{d}n
\end{aligned} \tag{3.139}$$

Because

$$\frac{1}{N^2}\int_0^N \cos\frac{in\pi}{N} \cos\frac{jn\pi}{N} \mathrm{d}n = \begin{Bmatrix} 1/N & (i = j = 0) \\ 1/(2N) & (i = j \neq 0) \\ 0 & (i \neq j) \end{Bmatrix} = \frac{\zeta}{\zeta_i}\delta_{ij} \tag{3.140}$$

we obtain Eq. 3.138.

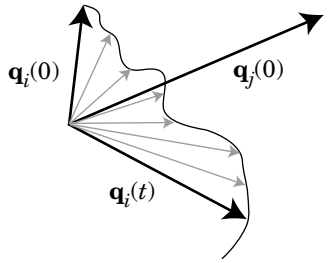

Figure 3.45. Correlation between $\mathbf{q}_i(t)$ and $\mathbf{q}_j(0)$. $\mathbf{q}_i(t)$ changes with time.

3.4.3.3 Formal Solution Equation 3.135 is solved as

$$\mathbf{q}_i(t) = \zeta_i^{-1} \int_{-\infty}^{t} \mathbf{g}_i(t_1) \exp[(t_1 - t)/\tau_i] \mathrm{d}t_1 \quad (i = 0, 1, \ldots) \tag{3.141}$$

This equation includes $i = 0$:

$$\mathbf{q}_0(t) = \zeta_0^{-1} \int_{-\infty}^{t} \mathbf{g}_0(t_1)\, \mathrm{d}t_1 \tag{3.142}$$

Because $\langle \mathbf{g}_i(t) \rangle = 0$, we find the statistical average of $\mathbf{g}_i(t)$ is zero for all modes:

$$\langle \mathbf{q}_i(t) \rangle = 0 \quad (i = 0, 1, \ldots) \tag{3.143}$$

The average of $\mathbf{q}_i(t) \cdot \mathbf{q}_i(0)$ is not zero, as we will see in the next subsection.

Before we look at the correlation of the end-to-end vector and the center-of-mass diffusion for the Rouse model, we derive general formulas for them by using Eqs. 3.135 and 3.138 only. These equations are also valid in the modified versions of the Rouse model. The assumptions specific to the Rouse model, such as $k_{\mathrm{sp}} = 3k_{\mathrm{B}}T/b^2$ and the neglect of the hydrodynamic interactions, show up only in the expressions for the parameters ζ_i, k_i, and τ_i.

3.4.4 Results of the Normal Coordinates

3.4.4.1 Correlation of $q_i(t)$ Although the average is always zero (Eq. 3.143), each $\mathbf{q}_i(t)$ is in general nonzero and changes with time (Fig. 3.45). Here, we consider how $\mathbf{q}_i(t)$ is related to $\mathbf{q}_j(0)$ $(i, j \neq 0)$. When $i = j$, $\langle \mathbf{q}_i(t) \cdot \mathbf{q}_i(0) \rangle$ is the autocorrelation. When $i \neq j$, $\langle \mathbf{q}_i(t) \cdot \mathbf{q}_j(0) \rangle$ is the cross-correlation. Because different modes are irrelevant to each other, the cross-correlation is zero. We use Eq. 3.141 to

calculate the correlation:

$$\begin{aligned}\langle \mathbf{q}_i(t)\cdot\mathbf{q}_j(0)\rangle &= \int_{-\infty}^{t} dt_1 \exp[-(t-t_1)/\tau_i]\int_{-\infty}^{0} dt_2 \exp(t_2/\tau_j)\,\frac{1}{\zeta_i\zeta_j}\,\langle \mathbf{g}_i(t_1)\cdot\mathbf{g}_j(t_2)\rangle \\ &= \int_{-\infty}^{t} dt_1 \exp[-(t-t_1)/\tau_i]\int_{-\infty}^{0} dt_2 \exp(t_2/\tau_j)\,\frac{1}{\zeta_i\zeta_j}\,6\zeta_i\delta_{ij}k_{\mathrm{B}}T\delta(t_1-t_2) \\ &= 6\delta_{ij}k_{\mathrm{B}}T\frac{1}{\zeta_i}\int_{-\infty}^{0} dt_2 \exp[-(t-2t_2)/\tau_i] = \frac{6\delta_{ij}k_{\mathrm{B}}T}{\zeta_i}\,\frac{\tau_i}{2}\exp(-t/\tau_i)\end{aligned} \tag{3.144}$$

for $i, j = 1, 2, \ldots$ Thus

$$\boxed{\langle \mathbf{q}_i(t)\cdot\mathbf{q}_j(0)\rangle = \begin{cases} 3\dfrac{k_{\mathrm{B}}T}{k_i}\exp(-t/\tau_i) & (i=j\neq 0) \\ 0 & (i\neq j)\end{cases} \quad \text{correlation of normal coordinates}} \tag{3.145}$$

In the second case ($i \neq j$), either i or j can be zero; The internal motion is decoupled from the center-of-mass motion. Equation 3.145 indicates that the autocorrelation of $\mathbf{q}_i(t)$ is lost exponentially with a relaxation time of τ_i.

We can obtain the mean square amplitude of $\mathbf{q}_i(t)$ by setting t to 0 in the above equation:

$$\boxed{\langle \mathbf{q}_i^2\rangle = \frac{3k_{\mathrm{B}}T}{k_i} \quad (i=1,2,\ldots) \quad \text{fluctuations of normal coordinate}} \tag{3.146}$$

The higher-order mode has a smaller amplitude, as we will see in the Rouse and other models.

3.4.4.2 End-to-End Vector In place of $\mathbf{r}_N(t) - \mathbf{r}_1(t)$, we calculate $\mathbf{r}_{N-1}(t) - \mathbf{r}_1(t)$ as the end-to-end vector $\mathbf{R}(t)$ of the Rouse chain; the difference is negligible when $N \gg 1$. From Eq. 3.125, $\mathbf{R}(t)$ is expressed by $\mathbf{q}_i$ as

$$\begin{aligned}\mathbf{R}(t) &= 2\sum_{i=1}^{N-1}\left(\cos\frac{i(N-1)\pi}{N} - \cos\frac{i\pi}{N}\right)\mathbf{q}_i(t) \\ &\quad + ((-1)^{N-1}+1)\,\mathbf{q}_N(t) \cong -4\sum_{i:\mathrm{odd}}\mathbf{q}_i(t)\end{aligned} \tag{3.147}$$

where $\cos(i\pi/N) \cong 1$ and $\cos[i(N-1)\pi/N] \cong (-1)^i$ for $N \gg 1$ were used. Note that $\mathbf{R}(t)$ is dominated by $\mathbf{q}_i$ with a small i. As the chain conformation changes, $\mathbf{R}(t)$ changes as well (Fig. 3.46). Its autocorrelation is calculated as

$$\boxed{\langle \mathbf{R}(t)\cdot\mathbf{R}(0)\rangle \cong 16\sum_{i:\mathrm{odd}}\langle \mathbf{q}_i(t)\cdot\mathbf{q}_i(0)\rangle = 16\sum_{i:\mathrm{odd}}\langle \mathbf{q}_i^2\rangle\exp(-t/\tau_i) \quad \text{end-to-end-vector}} \tag{3.148}$$

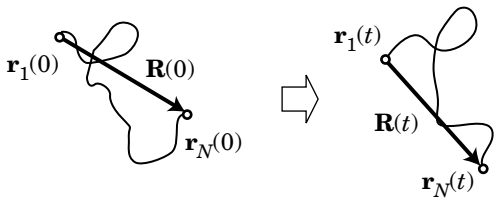

Figure 3.46. End-to-end vector $\mathbf{R}(t)$ changes as the chain conformation changes.

The autocorrelation function of $\mathbf{R}(t)$ is dominated by the first normal mode, as we will see in the Rouse and other models. Thus, $\mathbf{R}(t)$ loses its memory approximately with a relaxation time of τ_1:

$$\boxed{\langle \mathbf{R}(t)\cdot\mathbf{R}(0)\rangle \cong \langle \mathbf{R}^2\rangle \exp(-t/\tau_1) \quad \text{end-to-end vector}} \tag{3.149}$$

Experimentally, $\langle \mathbf{R}(t)\cdot \mathrm{R}(0)\rangle$ can be measured in dielectric relaxation spectroscopy for a polymer molecule that has a nonzero permanent dipole moment along the chain backbone. Other normal modes can also be observed.

3.4.4.3 Center-of-Mass Motion From Eqs. 3.119 and 3.142, the center-of-mass displacement in time t is calculated as

$$\mathbf{r}_{\mathrm{G}}(t) - \mathbf{r}_{\mathrm{G}}(0) = \mathbf{q}_0(t) - \mathbf{q}_0(0) = \frac{1}{\zeta_0}\int_0^t \mathbf{g}_0(t_1)\,\mathrm{d}t_1 \tag{3.150}$$

The mean-square displacement is then calculated as

$$\begin{aligned}\langle [\mathbf{r}_{\mathrm{G}}(t) - \mathbf{r}_{\mathrm{G}}(0)]^2\rangle &= \frac{1}{{\zeta_0}^2}\int_0^t \mathrm{d}t_1 \int_0^t \mathrm{d}t_2 \langle \mathbf{g}_0(t_1)\cdot\mathbf{g}_0(t_2)\rangle \\ &= \frac{1}{{\zeta_0}^2}\int_0^t \mathrm{d}t_1 \int_0^t \mathrm{d}t_2 6\zeta_0 k_{\mathrm{B}}T\delta(t_1 - t_2) = \frac{6k_{\mathrm{B}}T}{\zeta_0}\int_0^t \mathrm{d}t_1 = 6\frac{k_{\mathrm{B}}T}{\zeta_0}t\end{aligned} \tag{3.151}$$

It is proportional to t. The center of mass of the bead-spring chain makes a diffusional motion on all time scales. From this equation, we obtain the center-of-mass diffusion coefficient D_{G}:

$$\boxed{D_{\mathrm{G}} = \frac{k_{\mathrm{B}}T}{\zeta_0} \qquad \text{center-of-mass diffusion}} \tag{3.152}$$

The centroid motion of the bead-spring chain is identical to the motion of a particle that receives a friction of ζ_0. The latter is also evident in Eq. 3.131 with $i = 0$.

3.4.4.4 Evolution of $q_i(t)$ In Section 3.4.4.1, we found that the autocorrelation of $\mathbf{q}_i(t)$ with $\mathbf{q}_i(0)$ is lost over time. We find here the transition probability for $\mathbf{q}_i(t)$

from $\mathbf{q}_i(0)$. From Eq. 3.141,

$$\mathbf{q}_i(t) = \mathbf{q}_i(0)\exp(-t/\tau_i) + \zeta_i^{-1}\int_0^t \mathbf{g}_i(t_1)\exp[(t_1 - t)/\tau_i]\mathrm{d}t_1 \tag{3.153}$$

Because $\langle \mathbf{g}_i(t)\rangle = 0$, the average of $\mathbf{q}_i(t)$ for a given $\mathbf{q}_i(0)$ decays with a time constant τ_i:

$$\langle \mathbf{q}_i(t)\rangle_0 = \mathbf{q}_i(0)\exp(-t/\tau_i) \tag{3.154}$$

where subscript "0" denotes the average for a given $\mathbf{q}_i(0)$.

Now we find the variance. It is calculated as follows.

$$\begin{aligned}\langle[\mathbf{q}_i(t) - \mathbf{q}_i(0)\exp(-t/\tau_i)]^2\rangle &= \zeta_i^{-2}\int_0^t \mathrm{d}t_1\int_0^t \mathrm{d}t_2\langle \mathbf{g}_i(t_1)\cdot\mathbf{g}_i(t_2)\rangle \exp[(t_1 + t_2 - 2t)/\tau_i] \\ &= \zeta_i^{-2}\int_0^t \mathrm{d}t_1\int_0^t \mathrm{d}t_2 6\zeta_i k_\mathrm{B}T\delta(t_1 - t_2)\exp[(t_1 + t_2 - 2t)/\tau_i] \\ &= 6\zeta_i^{-1}k_\mathrm{B}T\int_0^t \exp[2(t_1 - t)/\tau_i]\,\mathrm{d}t_1 = (3\zeta_i^{-1}k_\mathrm{B}T\tau_i)[1 - \exp(-2t/\tau_i)] \\ &= (3k_\mathrm{B}T/k_i)[1 - \exp(-2t/\tau_i)]\end{aligned} \tag{3.155}$$

At $t = 0$, $\langle \mathbf{q}_i(t)\rangle_0 = \mathbf{q}_i(0)$ and the variance is zero. At $t \to \infty$, $\langle \mathbf{q}_i(t)\rangle_0 = 0$ and the variance becomes equal to the square magnitude of $\mathbf{q}_i(t)$ (see Eq. 3.146).

We have calculated the average and variance of $\mathbf{q}_i(t)$ for a given $\mathbf{q}_i(0)$. It can be shown that $\mathbf{q}_i(t)$ follows a normal distribution. Then, the transition probability $P[\mathbf{q}_i, \mathbf{q}_i(0); t]$ for $\mathbf{q}_i$ is given as

$$\begin{aligned}P(\mathbf{q}_i, \mathbf{q}_i(0); t) = {} & [(6\pi k_\mathrm{B}T/k_i)(1 - \exp(-2t/\tau_i))]^{-3/2} \\ & \times\exp\left[-\frac{[\mathbf{q}_i - \mathbf{q}_i(0)\exp(-t/\tau_i)]^2}{(6k_\mathrm{B}T/k_i)(1 - \exp(-2t/\tau_i))}\right]\end{aligned} \tag{3.156}$$

The probability distribution is shown for a few values of t/τ_i in Figure 3.47. The initial sharp peak at $\mathbf{q}_i = \mathbf{q}_i(0)$ gives way to a broader peak at $\mathbf{q}_i = 0$.

3.4.5 Results for the Rouse Model

3.4.5.1 Correlation of the Normal Modes Now we apply the general formulas obtained in the preceding subsection to the Rouse model. First, we study the correlation of $\mathbf{q}_i(t)$. It decays exponentially with a relaxation time τ_i, given by Eq. 3.136. Figure 3.48 compares $\langle \mathbf{q}_i(t)\cdot\mathbf{q}_i(0)\rangle$ for $i = 1$ through 6. Each $\langle \mathbf{q}_i(t)\cdot\mathbf{q}_i(0)\rangle$ is normalized by $\langle \mathbf{q}_1{}^2\rangle$, the square magnitude of the first mode. The decay of $\langle \mathbf{q}_1(t)\cdot\mathbf{q}_1(0)\rangle$ is

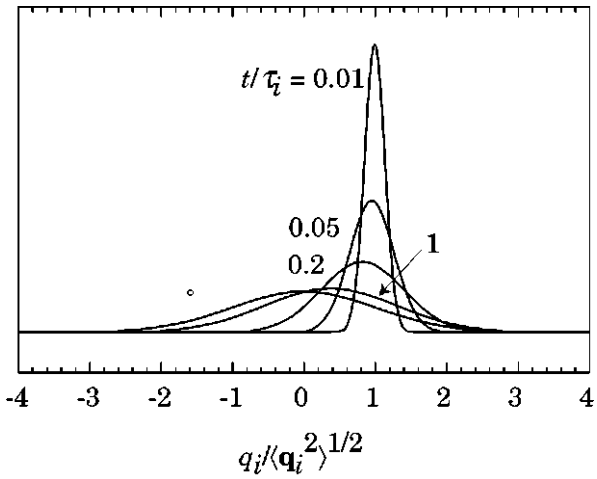

Figure 3.47. Transition probability q_i (one of the x, y, and z components of $\mathbf{q}_i$) for a given $q_i(0)$, plotted at $t/\tau_i = 0.01$, 0.05, 0.2, 1 and ∞. This example has $q_i(0) = \langle \mathbf{q}_i^2 \rangle^{1/2}$.

the slowest. The second normal mode loses its memory four times as fast ($\tau_2 = \tau_1/4$) and the third mode nine times as fast ($\tau_3 = \tau_1/9$).

From Eqs. 3.132 and 3.146, the fluctuations of the normal coordinates are obtained as

$$\langle \mathbf{q}_i^2 \rangle = \frac{Nb^2}{2\pi^2} \frac{1}{i^2} \qquad \text{Rouse model} \tag{3.157}$$

The decrease in the fluctuation for a higher-order mode is manifested in the declining intercept of the curves in the figure.

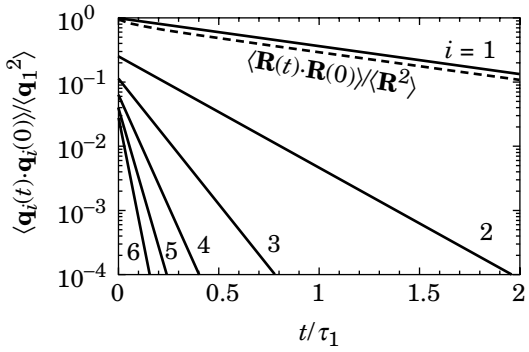

Figure 3.48. Autocorrelation function of $\mathbf{q}_i(t)$ for $i = 1$ to 6, normalized by $\langle \mathbf{q}_1^2 \rangle$. The dashed line represents the autocorrelation of $\mathbf{R}(t)$, normalized by $\langle \mathbf{R}^2 \rangle$.

3.4.5.2 Correlation of the End-to-End Vector With Eqs. 3.148 and 3.157, the autocorrelation of the end-to-end vector is given as

$$\langle \mathbf{R}(t) \cdot \mathbf{R}(0) \rangle \cong \frac{8Nb^2}{\pi} \sum_{i:\text{odd}} \frac{1}{i^2} \exp(-t/\tau_i) \tag{3.158}$$

In the summation, the second term ($i = 3$) has already only $1/9$ of the intensity compared with the first term ($i = 1$). The other terms are even smaller. The first term dominates in the summation. We can then replace $\exp(-t/\tau_i)$ with $\exp(-t/\tau_1)$. Because $\Sigma_{i:\text{odd}} i^{-2} = \pi^2/8$,

$$\langle \mathbf{R}(t) \cdot \mathbf{R}(0) \rangle \cong Nb^2 \exp(-t/\tau_1) \tag{3.159}$$

In Figure 3.48, the exact decay in $\langle \mathbf{R}(t) \cdot \mathbf{R}(0) \rangle / \langle \mathbf{R}^2 \rangle$ is plotted as a dashed line. Except for short times, $\langle \mathbf{R}(t) \cdot \mathbf{R}(0) \rangle$ and $\langle \mathbf{q}_1(t) \cdot \mathbf{q}_1(0) \rangle$ have the same decay rate.

3.4.5.3 Diffusion Coefficient From Eqs. 3.130 and 3.152, the center-of-mass diffusion coefficient D_G of the Rouse model is given as

$$\boxed{D_G \cong \frac{k_B T}{N\zeta} \qquad \text{Rouse model}} \tag{3.160}$$

which is equal to the diffusion coefficient of N connected beads, each of which move with a friction coefficient ζ independently of the other beads.

3.4.5.4 Molecular Weight Dependence Because the Rouse model describes the static conformation of a polymer chain in the theta condition, we expect that the model can also describe the dynamics. However, this expectation is wrong.

In the Rouse model, the relaxation time τ_1 of the first mode is proportional to N^2 (Eq. 3.136). The experimentally observed exponent for a polymer chain in a theta solvent is $3/2$. The discrepancy also exists in the molecular weight dependence of D_G. Experimentally, we observe $D_G \sim M^{-1/2}$ (Section 3.2.7) in the theta solvent. In the Rouse model (Eq. 3.160), $D_G \sim N^{-1}$. The model fails to give the correct exponent. The shortcoming of the model is ascribed to the neglect of hydrodynamic interactions. In the following subsection, we take into account the hydrodynamic interactions. In Section 4.3, we will see an example in which the Rouse model can describe the motion of polymer chains correctly.

3.4.6 Zimm Model

3.4.6.1 Hydrodynamic Interactions B. Zimm[37] improved the Rouse model by taking into account hydrodynamic interactions between beads. He successfully obtained the expressions for the diffusion coefficient and the relaxation times that agree with experimental results.

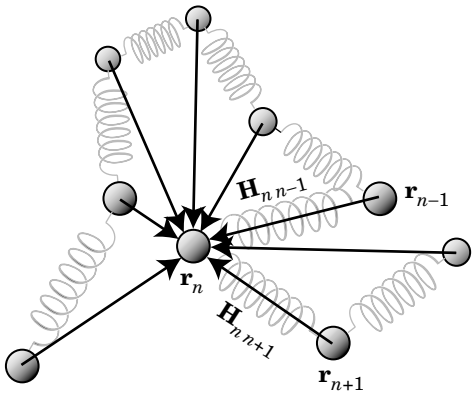

Figure 3.49. Motion of the nth bead is affected by the motion of all the other beads through the hydrodynamic interaction.

In the absence of the hydrodynamic interactions, the motion of the mth bead does not affect other beads except through the spring force. With the hydrodynamic interactions present, the velocity of one of the beads affects all the other beads through the flow of solvent (Fig. 3.49). Alternatively, the equation of motion for $\mathbf{r}_n$ is written as

$$\frac{\mathrm{d}\mathbf{r}_n}{\mathrm{d}t} = \sum_{m=1}^{N} \mathbf{H}_{nm}[k_{\mathrm{sp}}(\mathbf{r}_{m-1} + \mathbf{r}_{m+1} - 2\mathbf{r}_m) + \mathbf{f}_m] \quad (n = 1, 2, \ldots, N) \tag{3.161}$$

where $\mathbf{H}_{nm}$ is a second-rank tensor that represents how the velocity of the mth bead affects the velocity of the nth bead through the solvent between them. In the absence of the hydrodynamic interactions, $\mathbf{H}_{nm} = (\mathbf{I}/\zeta)\delta_{nm}$, where $\mathbf{I}$ is a unit tensor ($I_{\alpha\beta} = \delta_{\alpha\beta}$ with $\alpha, \beta = x, y, z$). Then, Eq. 3.161 reduces to Eq. 3. 115.

Usually, an **Oseen tensor** is used for $\mathbf{H}_{nm}$. Its magnitude is reciprocally proportional to $|\mathbf{r}_n - \mathbf{r}_m|$ and is therefore a function of the chain conformation that changes with time according to Eq. 3.161. Zimm decoupled $\mathbf{H}_{nm}$ from the rest of the equation and replaced it with its average at equilibrium (preaveraging approximation):

$$\frac{\mathrm{d}\mathbf{r}_n}{\mathrm{d}t} = \sum_{m=1}^{N} \langle \mathbf{H}_{nm} \rangle [k_{\mathrm{sp}}(\mathbf{r}_{m-1} + \mathbf{r}_{m+1} - 2\mathbf{r}_m) + \mathbf{f}_m] \quad (n = 1, 2, \ldots, N) \tag{3.162}$$

With the Oseen tensor,

$$\langle \mathbf{H}_{nm} \rangle = \frac{\mathbf{I}}{6\pi\eta_{\mathrm{s}}} \left\langle \frac{1}{|\mathbf{r}_n - \mathbf{r}_m|} \right\rangle_{nm} \tag{3.163}$$

where the statistical average is taken with respect to given n and m.

The right-hand side depends on the chain conformation. We separately consider a polymer chain in the theta solvent and a polymer chain in the good solvent.

3.4.6.2 Zimm Model in the Theta Solvent For a polymer chain in the theta solvent, the Gaussian chain model conveniently gives us an analytical expression of Eq. 3.163. With Eq. 3.56,

$$\langle \mathbf{H}_{nm} \rangle = H_{nm}\mathbf{I} = \frac{\mathbf{I}}{(6\pi^3)^{1/2}\eta_s b|n-m|^{1/2}} \tag{3.164}$$

Because of $|n-m|^{1/2}$ in the denominator, H_{nm} decays only slowly with an increasing $|n-m|$, that is, a distance between the two beads along the chain contour.

Equation 3.164 is not correct for $n = m$. It diverges as n and m approach each other. Upon integration with respect to n and m, however, the singularity is removed. We do not treat H_{nn} separately here. There is no need for that. The sum of the hydrodynamic interactions from other beads far exceeds the friction a given bead would receive in the absence of the hydrodynamic interactions. We will discuss this problem later when we derive the center-of-mass diffusion coefficient.

To convert Eq. 3.162 into equations of motion for the normal coordinate $\mathbf{q}_i$, we first express $\mathbf{r}_{m-1} + \mathbf{r}_{m+1} - 2\mathbf{r}_m$ and $\mathbf{f}_m$ by the normal coordinates $\mathbf{q}_i$ and $\mathbf{g}_i$. From Eq. 3.125,

$$\begin{aligned}\mathbf{r}_{m-1} + \mathbf{r}_{m+1} - 2\mathbf{r}_m &= 2\sum_{j=1}^{N-1}\mathbf{q}_j\left(\cos\frac{j(m-1)\pi}{N} + \cos\frac{j(m+1)\pi}{N} - 2\cos\frac{jm\pi}{N}\right) \\ &\quad + 4(-1)^{m-1}\mathbf{q}_N \cong -2\sum_{j=0}^{N}\mathbf{q}_j\left(\frac{j\pi}{N}\right)^2\cos\frac{jm\pi}{N}\end{aligned} \tag{3.165}$$

For $\mathbf{g}_i$, we use the same definition as Eq. 3.133 with ζ_i/ζ given by Eq. 3.130. It does not mean that ζ_i is the same in the Rouse model and the Zimm model. We just use the same formula in the Zimm model to express the random force in the normal coordinates. As Eq. 3.125 is an inverse transform of Eq. 3.118, the following gives an inverse transform of Eq. 3.133 (Problem 3.21):

$$\mathbf{f}_m = \frac{1}{N}\sum_{j=0}^{N}\mathbf{g}_j\cos\frac{jm\pi}{N} - \frac{(-1)^m}{2N}\mathbf{q}_N \cong \frac{1}{N}\sum_{j=0}^{N}\mathbf{g}_j\cos\frac{jm\pi}{N} \tag{3.166}$$

With Eqs. 3.118, 3.165, and 3.166, Eq. 3.162 is transformed into

$$\frac{d\mathbf{q}_i}{dt} = N\sum_{j=0}^{N}h_{ij}\left(-2k_{sp}\left(\frac{j\pi}{N}\right)^2\mathbf{q}_j + \frac{1}{N}\mathbf{g}_j\right) \tag{3.167}$$

where

$$h_{ij} = \frac{1}{N^2} \sum_{m=1}^{N} \sum_{n=1}^{N} H_{nm} \cos\frac{in\pi}{N} \cos\frac{jm\pi}{N} \tag{3.168}$$

In Eq. 3.167, all of the equations appear to be coupled with each other. Fortunately, they can be decoupled. It can be shown (Problem 3.22) that, when $N \gg 1$, h_{ij} is approximated by

$$h_{ij} \cong \frac{1}{2(3\pi^3 iN)^{1/2}\eta_s b}\delta_{ij} \quad (\text{except } i = j = 0) \tag{3.169}$$

Then, we obtain

$$\zeta_i \frac{d\mathbf{q}_i}{dt} = -k_i \mathbf{q}_i + \mathbf{g}_i \quad (i = 0, 1, \ldots, N) \quad \text{Zimm, theta} \tag{3.170}$$

Formally, the normal modes of the Zimm model follow the same differential equations as those of the Rouse model (Eq. 3.131).

The spring force constant for the ith mode

$$k_i = 2Nk_{sp}\left(\frac{i\pi}{N}\right)^2 = \frac{6\pi^2 k_B T}{Nb^2} i^2 \quad \text{Zimm, theta} \tag{3.171}$$

is identical to the counterpart in the Rouse model (Eq. 3.132) because the hydrodynamic interaction does not alter the equilibrium chain conformation. In the normal coordinate, the two modes are different only in the friction coefficient. Now it is

$$\zeta_i = {h_{ii}}^{-1} = 2(3\pi^3 iN)^{1/2}\eta_s b \quad (i = 1, 2, \ldots, N) \quad \text{Zimm, theta} \tag{3.172}$$

A special care is needed for ζ_0 (Problem 3.23)

$$\zeta_0 = {h_{00}}^{-1} = \tfrac{3}{8}(6\pi^3 N)^{1/2}\eta_s b \quad \text{Zimm, theta} \tag{3.173}$$

Because Eq. 3.170 is identical to Eq. 3.131, we can use the general formulas in Section 3.4.4 to obtain D_G and τ_i for the Zimm model in the theta solvent. The center-of-mass diffusion coefficient is obtained from Eqs. 3.152 and 3.173 as

$$\boxed{D_G = \frac{8}{3(6\pi^3)^{1/2}} \frac{k_B T}{\eta_s b N^{1/2}} = \frac{8}{3(6\pi^3)^{1/2}} \frac{k_B T}{\eta_s R_F} \quad \text{Zimm, theta}} \tag{3.174}$$

Its molecular weight dependence is $D_G \sim N^{-1/2}$. Thus, the hydrodynamic interactions increase the diffusivity of the chain, especially for a long chain, compared with a group of N independently moving beads (Rouse model). The friction on a

bead from the surrounding fluid is therefore much smaller than the sum of the hydrodynamic interactions the bead receives from the other beads. This result justifies our neglect of H_{nn} in deriving Eq. 3.164.

The relaxation time τ_i of the ith mode is calculated from Eqs. 3.171 and 3.172 as

$$\boxed{\tau_i = \frac{\zeta_i}{k_i} = \frac{1}{(3\pi)^{1/2}} \frac{\eta_s b^3 N^{3/2}}{k_B T} i^{-3/2} = \frac{1}{(3\pi)^{1/2}} \frac{\eta_s {R_F}^3}{k_B T} i^{-3/2} \quad \text{Zimm, theta}} \tag{3.175}$$

The Zimm model successfully describes the experimentally observed dependence: $D_G \sim M^{-1/2}$, $\tau_1 \sim M^{3/2}$, and $\tau_i/\tau_1 \sim i^{-3/2}$.

3.4.6.3 Hydrodynamic Radius By definition of h_{00} (Eq. 3.168), we can express D_G as

$$\begin{aligned} D_G &= k_B T h_{00} = k_B T \frac{1}{N^2} \int_0^N dn \int_0^N dm H_{nm} \\ &= k_B T \frac{1}{N^2} \int_0^N dn \int_0^N dm \frac{1}{6\pi\eta_s} \left\langle \frac{1}{|\mathbf{r}_n - \mathbf{r}_m|} \right\rangle_{nm} = \frac{k_B T}{6\pi\eta_s} \left\langle \frac{1}{|\mathbf{r}_n - \mathbf{r}_m|} \right\rangle \end{aligned} \tag{3.176}$$

where Eq. 3.163 was used. In the last line, $\langle \cdots \rangle$ implies a twofold statistical average: The first average is with respect to the positions of given beads n and m, and the second averaging scans n and m. Thus, from the definition of R_H (Eq. 3.54), it is given in the preaveraging approximation by

$$\boxed{\frac{1}{R_H} = \left\langle \frac{1}{|\mathbf{r}_n - \mathbf{r}_m|} \right\rangle \quad \text{hydrodynamic radius, polymer chain}} \tag{3.177}$$

Equation 3.55 was obtained in this way.

3.4.6.4 Zimm Model in the Good Solvent The Zimm model we used for the theta chains needs a small modification when we apply it to the chains in the good solvent. We must give up the numerical coefficients but can still obtain the exponents that agree with experimental results.

First, we work on h_{ij}. In place of $|n - m|^{-1/2}$ in the preaveraged hydrodynamic interaction between the nth and mth beads, we now have $|n - m|^{-\nu}$ with $\nu \cong 3/5$ or 0.59. We can show that h_{ij} is still diagonal, that is, $h_{ij} = 0$ for $i \neq j$, and the friction coefficient $\zeta_i = {h_{ii}}^{-1}$ of the ith mode changes to (Problem 3.24)

$$\zeta_i \cong \eta_s b N^\nu i^{1-\nu} \quad (i = 1, 2, \ldots) \tag{3.178}$$

$$\zeta_0 \cong \eta_s b N^\nu \tag{3.179}$$

Second, the force constant k_i needs some change because the Gaussian chain does not describe the conformation of the real chain. It can be obtained from

Table 3.3 Models for Dynamics

Model	Chain Statistics	Hydrodynamic Interactions	D_G	τ_i	$[\eta]$
Rouse	ideal	absent	M^{-1}	M^2/i^2	M^1
Zimm	ideal	present	$M^{-1/2}$	$M^{3/2}/i^{3/2}$	$M^{1/2}$
Zimm	real	present	$M^{-\nu}$	$M^{3\nu}/i^{3\nu}$	$M^{3\nu-1}$
Kirkwood*	rod	present	$(\ln M - a)/M$	$M^3/[(\ln M - a)$ $i(i+1)]$	$M^2/(\ln M - a)$

*a represents a constant.

Eq. 3.146. Appendix 3.A.1 shows how to evaluate $\langle \mathbf{q}_i^2 \rangle$ for the real chain. With Eq. 3.A.5,

$$k_i \cong \frac{k_B T}{b^2 N^{2\nu}} i^{2\nu+1} \tag{3.180}$$

With these modified ζ_i and k_i, $\mathbf{q}_i$ follows the same equation as in the Zimm model in the theta solvent.

The center-of-mass diffusion coefficient is obtained from Eqs. 3.152 and 3.179 as

$$D_G \cong \frac{k_B T}{\eta_s b N^{\nu}} \cong \frac{k_B T}{\eta_s R_F} \tag{3.181}$$

The relaxation time τ_i is calculated as

$$\tau_i = \frac{\zeta_i}{k_i} \cong \frac{\eta_s b^3 N^{3\nu}}{k_B T} i^{-3\nu} \cong \frac{\eta_s {R_F}^3}{k_B T} i^{-3\nu} \tag{3.182}$$

The Zimm model for the good solvent successfully describes the experimentally observed dependence: $D_G \sim M^{-\nu}$, $\tau_1 \sim M^{3\nu}$, and $\tau_i/\tau_1 \sim i^{-3\nu}$.

According to a more elaborate calculation based on the renormalization group theory,[38]

$$\boxed{D_G \cong 0.0829 \frac{k_B T}{\eta_s R_g} \qquad \text{Zimm, good solvent}} \tag{3.183}$$

Results for D_G, τ_1, τ_i/τ_1 are summarized in Table 3.3. The table also shows the results for the rodlike molecule (Section 3.5) and the M dependence of $[\eta]$ (Section 3.4.7).

3.4.7 Intrinsic Viscosity

3.4.7.1 Extra Stress by Polymers Adding a polymer to a solvent increases its viscosity. Figure 3.50 illustrates a polymer chain in a shear flow. For the portion of

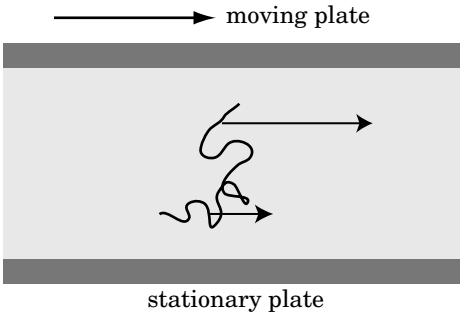

Figure 3.50. Portions of a polymer chain in shear flow experience different velocities depending on the distance from the stationary plate.

the chain closer to the moving plate to move faster compared with the other portion of the chain closer to the stationary plate, extra stress needs to be applied. In another word, flow becomes more difficult because of the polymer chain.

To estimate the intrinsic viscosity in the bead-spring model, we need to find how much the stress tensor in the flowing fluid changes when a unit amount of the polymer is added. At low concentrations, the increase in the stress tensor $\sigma_{\alpha\beta}(\alpha, \beta = x, y, z)$ due to the presence of bead-spring chains is given as

$$\Delta\sigma_{\alpha\beta} = \frac{cN_A}{M}\sum_{n=1}^{N}\left\langle \frac{\partial U}{\partial r_{n\alpha}} r_{n\beta}\right\rangle \tag{3.184}$$

where cN_A/M represents the number of the polymer chains in unit volume and U is the internal energy of the bead-spring model. As illustrated in Figure 3.51, an extra stress needs to be applied across the plane separating the nth bead from the $n-1$th bead in order to move the two beads with $\mathbf{v}(\mathbf{r}_n)$ and $\mathbf{v}(\mathbf{r}_{n-1})$, respectively.

In the Rouse model, there is no excluded volume effect. In the Zimm model for the theta solvent, the chain conformation is the same as that of the Rouse model. For these two models, U is given by a sum of the elastic energy of the springs (Eq. 1.51), and therefore

$$\frac{\partial U}{\partial \mathbf{r}_n} = -k_{sp}(\mathbf{r}_{n-1} + \mathbf{r}_{n+1} - 2\mathbf{r}_n) \tag{3.185}$$

which is equal to the negative of the spring force in Eq. 3.115. Then, Eq. 3.184 leads to

$$\Delta\sigma_{\alpha\beta} = \frac{cN_A}{M} k_{sp}\sum_{n=1}^{N}\langle -(\mathbf{r}_{n-1} + \mathbf{r}_{n+1} - 2\mathbf{r}_n)_\alpha r_{n\beta}\rangle \tag{3.186}$$

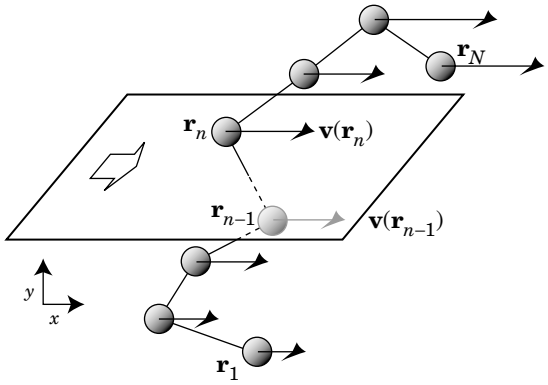

Figure 3.51. The xz plane separating the $n-1$th bead from the nth bead receives a stress in y direction when the bead-spring chain is in a shear flow.

where $\mathbf{r}_\alpha$ is the α component of $\mathbf{r}$ ($\mathbf{r}_x = r_x = x$, for instance). We now use Eqs. 3.125 and 3.165 to express the right-hand side in normal coordinates. Because $\mathbf{q}_i$ and $\mathbf{q}_j$ are irrelevant if $i \neq j$,

$$\langle -(\mathbf{r}_{n-1} + \mathbf{r}_{n+1} - 2\mathbf{r}_n)_\alpha r_{n\beta} \rangle = 4 \sum_{i=1}^{N} \left(\frac{i\pi}{N} \right)^2 \cos^2 \frac{in\pi}{N} \langle q_{i\alpha} q_{i\beta} \rangle \tag{3.187}$$

Then, Eq. 3.186 is rewritten to

$$\Delta\sigma_{\alpha\beta} = \frac{cN_A}{M} k_{sp} 4 \sum_{i=1}^{N} \left(\frac{i\pi}{N} \right)^2 \langle q_{i\alpha} q_{i\beta} \rangle \sum_{n=1}^{N} \cos^2 \frac{in\pi}{N} \cong \frac{cN_A}{M} k_{sp} 2N \sum_{i=1}^{N} \left(\frac{i\pi}{N} \right)^2 \langle q_{i\alpha} q_{i\beta} \rangle \tag{3.188}$$

With Eq. 3.132 and 3.171, this equation is further rewritten to

$$\Delta\sigma_{\alpha\beta} = \frac{cN_A}{M} \sum_{i=1}^{N} k_i \langle q_{i\alpha} q_{i\beta} \rangle \tag{3.189}$$

It is now apparent that $\Delta\sigma_{\alpha\beta} = \Delta\sigma_{\beta\alpha}$, as required. Although the last equation was derived for the ideal chain conformations, it is also valid for real chains with an excluded volume.

3.4.7.2 Intrinsic Viscosity of Polymers In the absence of flow, the solution is isotropic. Each component (x, y, z) of $\mathbf{q}_i$ is independent. Then, $\langle q_{i\alpha}\, q_{i\beta} \rangle = \langle q_{i\alpha} \rangle \langle q_{i\beta} \rangle = 0$. Polymers do not add a stress. Our next job is to find how the flow changes $\langle q_{i\alpha}\, q_{i\beta} \rangle$.

In the presence of flow, the bead at $\mathbf{r}_n$ has an additional velocity $\kappa \mathbf{r}_n$, as we learned in Section 3.3.4 The equation of motion for the nth bead, given by

Eq. 3.161, changes to

$$\frac{\mathrm{d}\mathbf{r}_n}{\mathrm{d}t} = \sum_{m=1}^{N} \mathbf{H}_{nm}[k_{\mathrm{sp}}(\mathbf{r}_{m-1} + \mathbf{r}_{m+1} - 2\mathbf{r}_m) + \mathbf{f}_m] + \boldsymbol{\kappa}\mathbf{r}_n (n = 1, 2, \ldots, N) \tag{3.190}$$

Note that $\boldsymbol{\kappa}\mathbf{r}_n$ is a linear function of $\mathbf{r}_n$. With the preaveraging approximation for $\mathbf{H}_{nm}$ and conversion to the normal coordinates, it is straightforward to see the equation of motion for the ith normal mode acquire an additional term:

$$\frac{\mathrm{d}\mathbf{q}_i}{\mathrm{d}t} = -\frac{k_i}{\zeta_i}\mathbf{q}_i + \frac{1}{\zeta_i}\mathbf{g}_i + \boldsymbol{\kappa}\mathbf{q}_i \quad (i = 0, 1, \ldots) \tag{3.191}$$

Although we have used the Zimm model here, this equation is apparently valid for the Rouse model as well. The off-diagonal elements of the tensor $\boldsymbol{\kappa}$ couple different components (x, y, and z) of $\mathbf{q}_i$, as we will see below, but $\mathbf{q}_i$ of different i are still independent of each other.

Now we consider a steady shear flow: $\partial v_x/\partial y = \kappa_{xy} = \kappa$, other elements are zero, as given by Eq. 3. 107. This tensor couples q_{ix} and q_{iy}:

$$\begin{aligned}\frac{\mathrm{d}}{\mathrm{d}t}\langle q_{ix}q_{iy}\rangle &= \left\langle q_{ix}\left(-\frac{k_i}{\zeta_i}q_{iy} + \frac{1}{\zeta_i}g_{iy} + (\boldsymbol{\kappa}\mathbf{q}_i)_y\right) + q_{iy}\left(-\frac{k_i}{\zeta_i}q_{ix} + \frac{1}{\zeta_i}g_{ix} + (\boldsymbol{\kappa}\mathbf{q}_i)_x\right)\right\rangle \\ &= -2\frac{k_i}{\zeta_i}\langle q_{ix}q_{iy}\rangle + \kappa\langle {q_{iy}}^2\rangle \end{aligned} \tag{3.192}$$

where $\langle q_{ix}\, g_{iy} + q_{iy}\, g_{ix}\rangle = \langle q_{ix}\rangle\langle g_{iy}\rangle + \langle q_{iy}\rangle\langle g_{ix}\rangle = 0$ and $(\boldsymbol{\kappa}\mathbf{q}_i)_y = 0$, $(\boldsymbol{\kappa}\mathbf{q}_i)_x = \kappa \mathrm{q}_{iy}$ were used. The stationary solution ($\mathrm{d}\langle q_{ix}\, q_{iy}\rangle/\mathrm{d}t = 0$) of Eq. 3.192 is

$$\langle q_{ix}\, q_{iy}\rangle = \frac{\kappa\zeta_i}{2k_i}\langle {q_{iy}}^2\rangle \tag{3.193}$$

When the flow is sufficiently slow, the solution is nearly isotropic. Then, $\langle {q_{iy}}^2\rangle = \langle \mathbf{q}_i^2\rangle/3 = k_{\mathrm{B}}T/k_i$ from Eq. 3.146, and we have

$$\langle q_{ix}\, q_{iy}\rangle = \frac{\kappa\ k_{\mathrm{B}}T\zeta_i}{2{k_i}^2} \tag{3.194}$$

Then, from Eq. 3.189,

$$\Delta\sigma_{xy} = \frac{\kappa c N_{\mathrm{A}} k_{\mathrm{B}}T}{2M}\sum_{i=1}^{N}\tau_i \tag{3.195}$$

Finally, we obtain a general expression for the intrinsic viscosity. With Eq. 3.109,

$$\boxed{[\eta] \cong \frac{N_{\mathrm{A}}k_{\mathrm{B}}T}{2M\eta_{\mathrm{s}}}\sum_{i=1}^{N}\tau_i \quad \begin{array}{l}\text{intrinsic viscosity} \\ \text{bead-spring model}\end{array}} \tag{3.196}$$

The explicit expressions for $[\eta]$ for the three cases of the bead-spring model are:

1. Rouse model. With Eq. 3.136,

$$[\eta] \cong \frac{N_A N^2 b^2 \zeta}{M \eta_s} \frac{1}{6\pi^2} \sum_{i=1}^{N} i^{-2} \cong \frac{N_A N^2 b^2 \zeta}{36 M \eta_s} \sim M \tag{3.197}$$

   where the upper limit in the summation was replaced by ∞ and $\Sigma_i i^{-2} = \pi^2/6$ was used.

2. Zimm model, theta solvent. With Eq. 3.175,

$$[\eta] \cong \frac{N_A (bN^{1/2})^3}{2(3\pi)^{1/2} M} \sum_{i=1}^{N} i^{-3/2} \cong 0.425 \times \frac{N_A {R_F}^3}{M} \sim M^{1/2} \tag{3.198}$$

   where $\Sigma_i\, i^{-3/2} \cong 2.612$ was used.

3. Zimm model, good solvent. With Eq. 3.182,

$$[\eta] \cong \frac{N_A (bN^{\nu})^3}{M} \sum_{i=1}^{N} i^{-3\nu} \sim M^{3\nu - 1} \tag{3.199}$$

   The exponent is 0.8 for $\nu = 3/5$ and 0.77 for $\nu = 0.59$ (see Table 3.3). These values agree with experimental results (Fig. 3.37).

3.4.7.3 Universal Calibration Curve in SEC In the Zimm model (theta and good solvents), the intrinsic viscosity is essentially the ratio of the "volume" of the polymer chain, ${R_F}^3$, to the mass of each polymer chain, M/N_A. The solvent viscosity and the temperature do not show up explicitly in the final expression. Thus we can define **hydrodynamic volume** V_{hd} by

$$\boxed{V_{hd} \equiv [\eta] M / N_A \quad \text{hydrodynamic volume}} \tag{3.200}$$

There is a consensus that the retention time t_R in SEC is determined by V_{hd} for a given polymer fraction. The plot of $[\eta]M/N_A$ vs. t_R obtained for different polymers but with the same column fall on a single master curve. In fact, the data for the theta condition and the data for rigid-chain polymers are also on the master curve obtained for flexible chains in good solvents. The curve is called a **universal calibration curve**. An example is shown in Figure 3.52.[39] The existence of the curve proves that the hydrodynamic volume governs the partitioning in the SEC column.

3.4.8 Dynamic Structure Factor

3.4.8.1 General Formula We consider in this subsection the dynamic structure factor of a bead-spring model. For now we do not distinguish the three cases of the model.

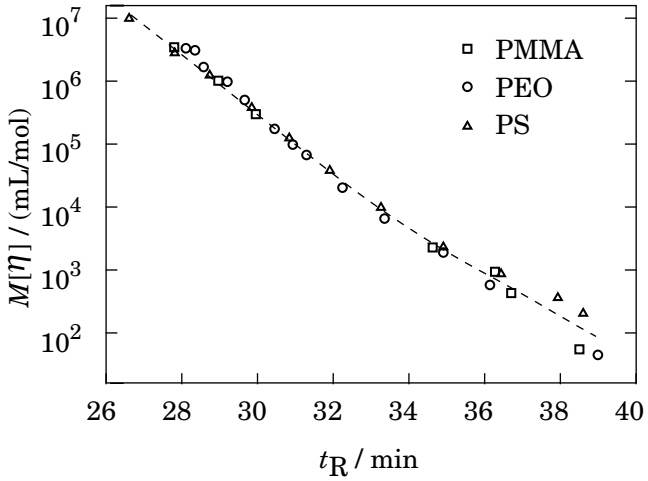

Figure 3.52. Universal calibration curve of SEC. The plots of $M[\eta]$ obtained for poly(methyl methacrylate), poly(ethylene oxide), and polystyrene are on a master curve. The mobile phase was dimethylacetamide. (From Ref. 39.)

We define $\mathbf{r}_{mn}(t) \equiv \mathbf{r}_n(t) - \mathbf{r}_m(0)$, the displacement of the nth bead at time t with respect to the mth bead at time 0 (Fig. 3.53). Using Eq. 3.125, we find that $\mathbf{r}_{mn}(t)$ is given as

$$\mathbf{r}_{mn}(t) = [\mathbf{q}_0(t) - \mathbf{q}_0(0)] + 2\sum_{i=1}^{N-1}\left[\cos\frac{in\pi}{N}\,\mathbf{q}_i(t) - \cos\frac{im\pi}{N}\mathbf{q}_i(0)\right] + [(-1)^n\mathbf{q}_N(t) - (-1)^m\mathbf{q}_N(0)] \tag{3.201}$$

Because different modes are uncorrelated, the average of $\exp[i\mathbf{k}\cdot\mathrm{r}_{mn}(t)]$ for a given m and n is

$$\langle\exp[i\mathbf{k}\cdot\mathbf{r}_{mn}(t)]\rangle_{mn} = \langle\exp[i\mathbf{k}\cdot(\mathbf{q}_0(t) - \mathbf{q}_0(0))]\rangle \times \prod_{i=1}^{N}\left\langle\exp\left[2i\mathbf{k}\cdot\left(\cos\frac{in\pi}{N}\mathbf{q}_i(t) - \cos\frac{im\pi}{N}\mathbf{q}_i(0)\right)\right]\right\rangle \tag{3.202}$$

The last factor for $i = N$ was incorporated into the product. The first factor represents the center-of-mass diffusion:

$$\langle\exp[i\mathbf{k}\cdot(\mathbf{q}_0(t) - \mathbf{q}_0(0))]\rangle = \exp(-D_G t\mathbf{k}^2) \tag{3.203}$$

Using Eq. 3.B.7 in Appendix 3.B [$\sigma^2 = (3k_BT/k_i)/3 = k_BT/k_i$; note Eq. 3.B.3; $\tau = \tau_i$; $A = 2\cos(in\pi/N)$; $B = 2\cos(im\pi/N)$], the ith factor in the N-fold product

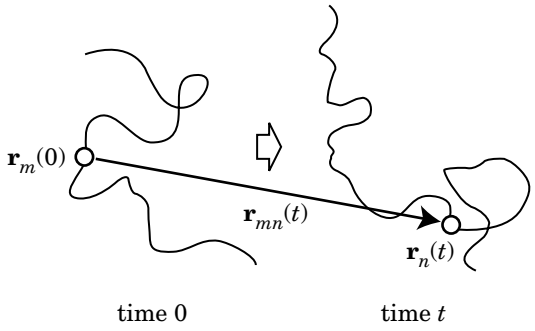

Figure 3.53. $\mathbf{r}_{mn}(t)$ is the distance of the nth bead at time t from the mth bead at time 0.

is transformed to

$$\left\langle \exp\left[i\mathbf{k}\cdot\left(2\cos\frac{in\pi}{N}\mathbf{q}_i(t) - 2\cos\frac{im\pi}{N}\mathbf{q}_i(0)\right)\right]\right\rangle$$
$$= \exp\left[-\frac{2k_BT}{k_i}\mathbf{k}^2\left(\cos^2\frac{in\pi}{N} + \cos^2\frac{im\pi}{N} - 2\cos\frac{in\pi}{N}\cos\frac{im\pi}{N}\exp(-t/\tau_i)\right)\right] \tag{3.204}$$

Thus,

$$\langle \exp[i\mathbf{k}\cdot\mathbf{r}_{mn}(t)]\rangle_{mn}$$
$$= \exp\left[-D_G t\mathbf{k}^2 - 2\mathbf{k}^2\sum_{i=1}^{N}\frac{k_BT}{k_i}\right.$$
$$\left.\times\left(\cos^2\frac{in\pi}{N} + \cos^2\frac{im\pi}{N} - 2\cos\frac{in\pi}{N}\cos\frac{im\pi}{N}\exp(-t/\tau_i)\right)\right] \tag{3.205}$$

At $t = 0$,

$$\langle \exp[i\mathbf{k}\cdot\mathbf{r}_{mn}(0)]\rangle_{mn} = \exp\left[-2\mathbf{k}^2\sum_{i=1}^{N}\frac{k_BT}{k_i}\left(\cos\frac{in\pi}{N} - \cos\frac{im\pi}{N}\right)^2\right] \tag{3.206}$$

Combined,

$$\langle \exp[i\mathbf{k}\cdot\mathbf{r}_{mn}(t)]\rangle_{mn} = \langle \exp[i\mathbf{k}\cdot\mathbf{r}_{mn}(0)]\rangle_{mn}$$
$$\times\exp\left[-D_G t\mathbf{k}^2 - 4\mathbf{k}^2\sum_{i=1}^{N}\frac{k_BT}{k_i}\cos\frac{in\pi}{N}\cos\frac{im\pi}{N}[1 - \exp(-t/\tau_i)]\right] \tag{3.207}$$

The dynamic structure factor of the chain is the average of the above equation with respect of m and n:

$$S_1(\mathbf{k}, t) = \exp(-D_G t\, \mathbf{k}^2) N^{-1} \sum_{m,n=1}^{N} \langle \exp[i\mathbf{k}\cdot\mathbf{r}_{mn}(0)]\rangle_{mn} \exp\left[-4\mathbf{k}^2 \sum_{i=1}^{N} \frac{k_B T}{k_i} \times \cos\frac{in\pi}{N} \cos\frac{im\pi}{N} [1 - \exp(-t/\tau_i)]\right]$$

dynamic structure factor bead-spring model

(3.208)

The long-time behavior is simple. At $t \gg \tau_1$, $1 - \exp(-t/\tau_1) \cong 1$, and therefore the time-dependent factor is $\exp(-D_G \mathbf{k}^2 t)$ only. Then, $S_1(\mathbf{k}, t)$ decays with a decay rate of $D_G \mathbf{k}^2$, indicating center-of-mass diffusion of the whole chain. This feature is common to all of the three models.

The short-time behavior for $t \ll \tau_N$ is different:

$$S_1(\mathbf{k}, t) = \exp(-D_G t \mathbf{k}^2) N^{-1} \times \sum_{m,n=1}^{N} \langle \exp[i\mathbf{k}\cdot\mathbf{r}_{mn}(0)]\rangle_{mn} \exp\left[-4\mathbf{k}^2 t \sum_{i=1}^{N} \frac{k_B T}{\zeta_i} \cos\frac{in\pi}{N} \cos\frac{im\pi}{N}\right] \quad (3.209)$$

The slope of $\ln S_1(\mathbf{k}, t)$ at $t = 0$ is

$$\left.\frac{\partial}{\partial t} \ln S_1(\mathbf{k}, t)\right|_{t=0} = -D_G \mathbf{k}^2 - \frac{4\mathbf{k}^2 \sum_{m,n=1}^{N} \langle \exp[i\mathbf{k}\cdot\mathbf{r}_{mn}(0)]\rangle_{mn} \sum_{i=1}^{N} \frac{k_B T}{\zeta_i} \cos\frac{in\pi}{N} \cos\frac{im\pi}{N}}{\sum_{m,n=1}^{N} \langle \exp[i\mathbf{k}\cdot\mathbf{r}_{mn}(0)]\rangle_{mn}} \quad (3.210)$$

The initial slope may not follow $\sim\mathbf{k}^2$ dependence and is different from model to model.

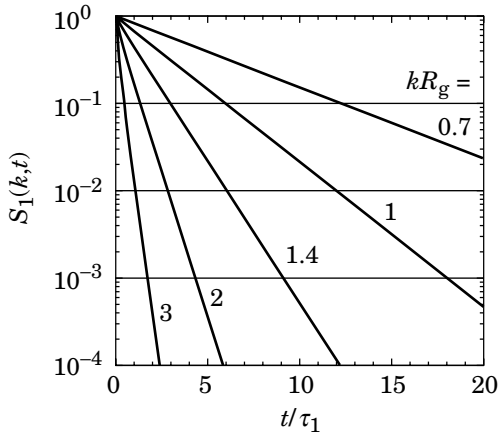

Figure 3.54. Dynamic structure factor $S_1(\mathbf{k}, t)$ is plotted as a function of t/τ_1 for various values of kR_g. Calculation was done by using the Zimm model for the theta solvent.

Figure 3.54 shows how $S_1(\mathbf{k}, t)$ changes with time t in the Zimm model for the theta condition. For $kR_g = 0.7$, $\ln S_1(\mathbf{k}, t)$ is almost straight over the entire range of time; $S_1(\mathbf{k}, t)$ decays with a constant rate of $D_G\mathbf{k}^2$. With an increasing kR_g, the plot deviates from the straight line. The tangential to the curve is steep at near $t = 0$. At long times, $S_1(\mathbf{k}, t)$ decays with $D_G\mathbf{k}^2$. Note that a small change in kR_g results in a large difference in the decay characteristics of $S_1(\mathbf{k}, t)$.

The plots are similar in the Rouse model except that it takes a longer time (in terms of t/τ_1) for $S_1(\mathbf{k}, t)$ to decay to a given level.

In the following, we examine the initial slope of $\ln S_1(\mathbf{k}, t)$ in the three models for the bead-spring chain.

3.4.8.2 Initial Slope in the Rouse Model In the Rouse model, $\langle \exp[i\mathbf{k}\cdot\mathbf{r}_{mn}(0)]\rangle_{mn} = \exp(-b^2\mathbf{k}^2|n-m|/6)$ (Eq. 2.77). The denominator of Eq. 3.210 is equal to $N^2 f_D(kR_g)$, where the Debye function $f_D(x)$ is defined by Eq. 2.79. The numerator is calculated as shown in Appendix 3.C. From Eq. 3.C.3,

$$\text{numerator} \cong 4\mathbf{k}^2N^2\sum_{i=1}^{N}\frac{k_BT}{\zeta_i}\frac{k^2R_g^{\,2}}{(k^2R_g^{\,2})^2 + (i\pi)^2} \tag{3.211}$$

The sum is calculated as follows:

$$\begin{aligned}\sum_{i=1}^{N}\frac{k_BT}{\zeta_i}\frac{k^2R_g^{\,2}}{(k^2R_g^{\,2})^2 + (i\pi)^2} &\cong \frac{k_BT}{2N\zeta}\frac{1}{\pi}\sum_{i=1}^{\infty}\frac{k^2R_g^{\,2}/\pi}{(k^2R_g^{\,2}/\pi)^2 + i^2} \\ &= \frac{k_BT}{2N\zeta}\frac{1}{\pi}\frac{\pi}{2}(\coth k^2R_g^{\,2} - (k^2R_g^{\,2})^{-1}) = \tfrac{1}{4}D_G(\coth k^2R_g^{\,2} - (k^2R_g^{\,2})^{-1})\end{aligned} \tag{3.212}$$

where Eq. A4.1 was used. Thus,

$$\left.\frac{\partial}{\partial t}\ln S_1(\mathbf{k}, t)\right|_{t=0} = -D_G\mathbf{k}^2\left(1 + \frac{\coth k^2R_g^{\,2} - (k^2R_g^{\,2})^{-1}}{f_D(kR_g)}\right) \tag{3.213}$$

Because $\coth x - x^{-1} \cong x/3$ and $f_D(x) \cong 1$ when $x \ll 1$, the initial slope of $\ln S_1(\mathbf{k}, t)$ is $-D_G\mathbf{k}^2$ at small $\mathbf{k}$, the same as the long-time behavior. At large $\mathbf{k}$, the slope is $-(1/2)D_G\mathbf{k}^2(kR_g)^2$, since $\coth x - x^{-1} \cong 1$ and $f_D(x) \cong 2/x^2$ when $x \gg 1$. The initial slope shows a crossover from $\sim -k^2$ to $\sim -k^4$ with an increasing kR_g.

3.4.8.3 Initial Slope in the Zimm Model, Theta Solvent Equation 3.211 is valid also in the Zimm model for the theta solvent because the equation depends on the chain conformation only. However, Eqs. 3.212 and 3.213 are different. We evaluate the sum in Eq. 3.211 for small $\mathbf{k}$ and large $\mathbf{k}$ separately. For small $\mathbf{k}$,

$$\begin{aligned}\sum_{i=1}^{N}\frac{k_BT}{\zeta_i}\frac{k^2R_g^{\,2}}{(k^2R_g^{\,2})^2 + (i\pi)^2} &\cong \frac{3\cdot 2^{1/2}}{16}D_G\frac{1}{\pi}\sum_{i=1}^{N}\frac{k^2R_g^{\,2}/\pi}{i^{1/2}[(k^2R_g^{\,2}/\pi)^2 + i^2]} \\ &\le \frac{3\cdot 2^{1/2}}{16}D_G\frac{1}{\pi}\sum_{i=1}^{\infty}\frac{k^2R_g^{\,2}/\pi}{(k^2R_g^{\,2}/\pi)^2 + i^2} = \frac{3}{16\cdot 2^{1/2}}D_G(\coth k^2R_g^{\,2} - (k^2R_g^{\,2})^{-1})\end{aligned} \tag{3.214}$$

where Eqs. 3.172, 3.174 and A4.1 were used. Then, the second term in Eq. 3.210 is negligible, just as in the Rouse model. The initial slope of $\ln S_1(\mathbf{k}, t)$ is $-D_G\mathbf{k}^2$ at small $\mathbf{k}$.

For large $\mathbf{k}$, the sum is evaluated as follows:

$$\sum_{i=1}^{N} \frac{k_B T}{\zeta_i} \frac{k^2 {R_g}^2}{(k^2 {R_g}^2)^2 + (i\pi)^2} \cong \frac{3 \cdot 2^{1/2}}{16} D_G \frac{1}{\pi} \int_0^\infty \frac{k^2 {R_g}^2/\pi}{i^{1/2}[(k^2 {R_g}^2/\pi)^2 + i^2]} \mathrm{d}i$$

$$= \frac{3 \cdot 2^{1/2}}{16} D_G \frac{1}{\pi} \frac{\pi}{2^{1/2} k R_g / \pi^{1/2}} = \frac{D_G}{k R_g} \frac{3\pi^{1/2}}{16} \tag{3.215}$$

where Eq. A4.2 was used. Thus,

$$\left. \frac{\partial}{\partial t} \ln S_1(\mathbf{k}, t) \right|_{t=0} = -D_G \mathbf{k}^2 \left(1 + \frac{3\pi^{1/2}/4}{k R_g f_D(k R_g)} \right) \quad k R_g \gg 1 \tag{3.216}$$

The initial slope of $\ln S_1(\mathbf{k}, t)$ is $-(3\pi^{1/2}/8) D_G \mathbf{k}^2 k R_g$ at large $\mathbf{k}$.

3.4.8.4 Initial Slope in the Zimm Model, Good Solvent We cannot use Eq. 3.211 because the conformation is not Gaussian. We need to start with Eq. 3.210. For small $\mathbf{k}$, $\langle \exp[\mathrm{i}\mathbf{k} \cdot \mathbf{r}_{mn}(0)] \rangle_{mn} \cong 1$. Therefore, the second term of Eq. 3.210 is

$$\frac{4\mathbf{k}^2}{N^2} k_B T \sum_{i=1}^{N} \frac{1}{\zeta_i} \left(\sum_{n=1}^{N} \cos \frac{in\pi}{N} \right)^2 \cong 0 \tag{3.217}$$

because of Eq. 3.124. Thus, the initial slope of $\ln S_1(\mathbf{k}, t)$ is $-D_G\mathbf{k}^2$ at small $\mathbf{k}$.

For large $\mathbf{k}$, the denominator of the second term of Eq. 3.210 is estimated as

$$\begin{aligned} \sum_{m,n=1}^{N} \langle \exp[\mathrm{i}\mathbf{k} \cdot \mathbf{r}_{mn}(0)] \rangle_{mn} &\cong \int_0^N \mathrm{d}n \int_0^n \mathrm{d}m \exp(-b^2 \mathbf{k}^2 (n - m)^{2\nu}) \\ &\cong \int_0^N \mathrm{d}m (N - m) \exp(-b^2 \mathbf{k}^2 m^{2\nu}) \\ &\cong N(bk)^{-1/\nu} \int_0^\infty \exp(-x^2) x^{1/\nu - 1} \, \mathrm{d}x \cong N(bk)^{-1/\nu} \end{aligned} \tag{3.218}$$

where the variable of integration was changed to $x = bkm^\nu$. For the numerator, we first evaluate the sum with respect to i:

$$\sum_{i=1}^{N} \frac{k_B T}{\zeta_i} \cos \frac{in\pi}{N} \cos \frac{im\pi}{N} \cong \frac{k_B T}{\eta_s b N^\nu} \sum_{i=1}^{N} \frac{1}{i^{1-\nu}} \left[\cos \frac{i(n-m)\pi}{N} + \cos \frac{i(n-m)\pi}{N} \right]$$

$$\cong D_{\mathrm{G}}\left[\delta_{mn}\sum_{i=1}^{N} i^{\nu-1} + (1-\delta_{mn})\int_0^{\infty} x^{\nu-1}\cos\frac{(n-m)\pi}{N}x\,\mathrm{d}x + \int_0^{\infty} x^{\nu-1}\cos\frac{(n+m)\pi}{N}x\,\mathrm{d}x\right]$$

$$\cong D_{\mathrm{G}}N^{\nu}\left[\delta_{mn} + (1-\delta_{mn})\frac{1}{|n-m|^{\nu}} + \frac{1}{|n+m|^{\nu}}\right] \tag{3.219}$$

where Eq. A3.2 was used. Then, the numerator is dominated by the sum of $|n-m|^{-\nu}$ and therefore estimated as

$$k^2\sum_{m,n=1}^{N}\langle\exp[\mathrm{i}\mathbf{k}\cdot\mathbf{r}_{mn}(0)]\rangle_{mn}\frac{D_{\mathrm{G}}N^{\nu}}{|n-m|^{\nu}}$$
$$\cong k^2D_{\mathrm{G}}N^{\nu}\int_0^{N}\mathrm{d}n\int_0^{n}\mathrm{d}m\,\exp(-b^2\mathbf{k}^2|n-m|^{2\nu})\frac{1}{|n-m|^{\nu}}$$
$$\cong k^2D_{\mathrm{G}}N^{\nu}N(bk)^{1-1/\nu}\int_0^{\infty}\exp(-x^2)x^{1/\nu-2}\,\mathrm{d}x \cong k^2D_{\mathrm{G}}N^{\nu}N(bk)^{1-1/\nu} \tag{3.220}$$

Thus, the slope is approximated as

$$\frac{\partial}{\partial t}\ln S_1(\mathbf{k},t)\bigg|_{t=0} \cong -D_{\mathrm{G}}\mathbf{k}^2(1+N^{\nu}kb) \cong -D_{\mathrm{G}}\mathbf{k}^2(1+kR_{\mathrm{g}}) \quad kR_{\mathrm{g}} \gg 1 \tag{3.221}$$

The initial slope of $\ln S_1(\mathbf{k},t)$ is $\sim -D_{\mathrm{G}}\mathbf{k}^2kR_{\mathrm{g}}$ at large $\mathbf{k}$.

The initial decay rate of $S_1(\mathbf{k},t)$, the negative of the initial slope of $\ln S_1(\mathbf{k},t)$, is summarized in Table 3.4. The table includes the result for rodlike molecules (Section 3.5).

3.4.8.5 Initial Slope: Experiments The initial slope of $\ln S_1(\mathbf{k},t)$ is usually measured in DLS. At low concentrations, $|g_1(t)| \propto S_1(\mathbf{k},t)$. Therefore, the initial

Table 3.4 Initial Decay Rate of $|g_1(t)|$

		Short Time	
Model	Long Time	Small $\mathbf{k}$	Large $\mathbf{k}$
Rouse	$D_{\mathrm{G}}\mathbf{k}^2$	$D_{\mathrm{G}}\mathbf{k}^2$	$(1/2)D_{\mathrm{G}}\mathbf{k}^2(kR_{\mathrm{g}})^2$
Zimm, theta solvent	$D_{\mathrm{G}}\mathbf{k}^2$	$D_{\mathrm{G}}\mathbf{k}^2$	$(3\pi^{1/2}/8)D_{\mathrm{G}}\mathbf{k}^2(kR_{\mathrm{g}})$
Zimm, good solvent	$D_{\mathrm{G}}\mathbf{k}^2$	$D_{\mathrm{G}}\mathbf{k}^2$	$\sim D_{\mathrm{G}}\mathbf{k}^2(kR_{\mathrm{g}})$
Kirkwood (rod)	$D_{\mathrm{G}}\mathbf{k}^2$	$D_{\mathrm{G}}\mathbf{k}^2$	$(3/2)D_{\mathrm{G}}\mathbf{k}^2$

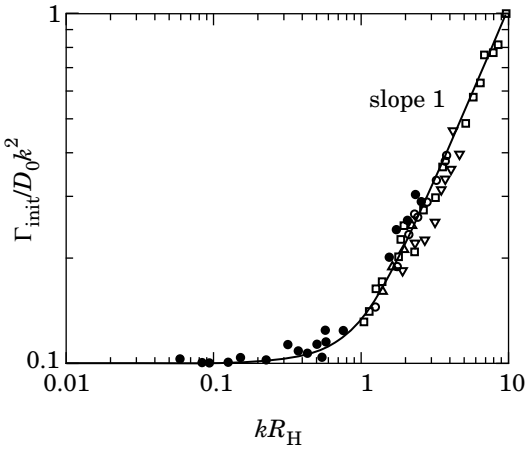

Figure 3.55. Initial decay rate $\Gamma_{\rm init}$ of $|g_1(t)|$, reduced by its low-k asymptote $D_0\mathbf{k}^2$, is plotted as a function of $kR_{\rm H}$. The data obtained for polystyrene in various solvents are on a theoretical curve (solid line) obtained for the Zimm model in the theta solvent. (From Ref. 40.)

decay rate $\Gamma_{\rm init}$ of $|g_1(t)|$ defined as

$$\Gamma_{\rm init} = -\lim_{t\to 0} \frac{\ln|g_1(t)|}{t} \tag{3.222}$$

is equal to the negative of the initial slope of $\ln S_1(\mathbf{k}, t)$.

Figure 3.55 shows $\Gamma_{\rm init}$ obtained in DLS for dilute solutions of polystyrene in various solvents that range from a good solvent to a near-theta solvent.[40] In the ordinate, $\Gamma_{\rm init}$ is reduced by $D_0\mathbf{k}^2$, the rate at low angles. The abscissa is the dimensionless $kR_{\rm H}$. The solid line in the figure was calculated by using Eq. 3.210 for the Zimm model in the theta solvent. The data obtained in good solvents and theta solvents lie on the theoretical curve. At $kR_{\rm H} \ll 1$, $\Gamma_{\rm init} = D_0\mathbf{k}^2$. At $kR_{\rm H} \gg 1$, the master curve has a slope of 1, in agreement with Eqs. 3.216 and 3.221.

3.4.9 Motion of Monomers

3.4.9.1 General Formula In the preceding subsections, we considered the center-of-mass motion and also obtained a general formula for the statistical average of the Fourier transform of $\mathbf{r}_{mn}(t) = \mathbf{r}_n(t) - \mathbf{r}_m(0)$. In this subsection, we look at the motion of the beads (monomers) in different time scales. We first obtain expressions for $\langle[\mathbf{r}_{mn}(t)]^2\rangle_{mn}$, the statistical average of the $[\mathbf{r}_{mn}(t)]^2$ for given m and n, and consider how the average changes with time in the short time. We will then examine how the mean square displacement of the beads $\langle[\mathbf{r}_{mn}(t)]^2\rangle$ changes with time for each model. The displacement of the beads is different from that of the center of mass. In the long time scale ($t \gg \tau_1$), they should be identical, but, in the short time scale, the beads can move more quickly than the center of mass. In this subsection, we consider primarily the Rouse chain and the Zimm model in the theta solvent.

For that purpose, we apply the formula

$$\langle [\mathbf{r}_{mn}(t)]^2 \rangle_{mn} = -\frac{\partial^2}{\partial \mathbf{k}^2} \langle \exp[i\mathbf{k} \cdot \mathbf{r}_{mn}(t)] \rangle_{mn} \Big|_{\mathbf{k}=0} \tag{3.223}$$

to Eq. 3.207 and obtain

$$\langle [\mathbf{r}_{mn}(t)]^2 \rangle_{mn} - \langle [\mathbf{r}_{mn}(0)]^2 \rangle_{mn} = 6D_G t + 24 \sum_{i=1}^{N} \frac{k_B T}{k_i} \times \cos \frac{in\pi}{N} \cos \frac{im\pi}{N} [1 - \exp(-t/\tau_i)] \tag{3.224}$$

where the mean square distance between the two beads is

$$\langle [\mathbf{r}_{mn}(0)]^2 \rangle_{mn} = b^2 |m - n| \tag{3.225}$$

for the ideal-chain conformation. We can use Eq. 3.125 to derive Eq. 3.224 directly (Problem 3.26).

In the short time scale ($t \ll \tau_N$), $1 - \exp(-t/\tau_i) \cong t/\tau_i$ and therefore Eq. 3.224 reduces to

$$\langle [\mathbf{r}_{mn}(t)]^2 \rangle_{mn} - \langle [\mathbf{r}_{mn}(0)]^2 \rangle_{mn} \cong 6t \left[D_G + 4 \sum_{i=1}^{N} \frac{k_B T}{\zeta_i} \cos \frac{in\pi}{N} \cos \frac{im\pi}{N} \right] \text{short time} \tag{3.226}$$

In the long time scale ($t \gg \tau_1$), $1 - \exp(-t/\tau_i) \cong 1$ and therefore Eq. 3.224 reduces to

$$\langle [\mathbf{r}_{mn}(t)]^2 \rangle_{mn} - \langle [\mathbf{r}_{mn}(0)]^2 \rangle_{mn} = 6D_G t + 24 \sum_{i=1}^{N} \frac{k_B T}{k_i} \cos \frac{in\pi}{N} \cos \frac{im\pi}{N} \text{ long time} \tag{3.227}$$

In the long time scale, the first term dominates, and $\langle [\mathbf{r}_{mn}(t)]^2 \rangle_{mn}$ becomes indistinguishable from the center-of-mass diffusion, as expected. The mean square displacement increases linearly with t in the two asymptotes. The motion of the monomers is diffusional in the two asymptotes but with different diffusion coefficients. Then, the motion cannot be diffusional in the intermediate time range.

3.4.9.2 Mean Square Displacement: Short-Time Behavior Between a Pair of Monomers Before considering the mean square displacement of the same beads (monomers) in Section 3.4.9.3, we look at the evolution of $\langle [\mathbf{r}_{mn}(t)]^2 \rangle_{mn}$ for a pair of beads in the short time scale. Because ζ_i is different between the Rouse model and the Zimm model for the theta solvent, we treat them separately.

In the Rouse model, $k_BT/\zeta_i = D_G/2$, and the second term in Eq. 3.226 is calculated as

$$4\sum_{i=1}^{N}\frac{k_BT}{\zeta_i}\cos\frac{in\pi}{N}\cos\frac{im\pi}{N} = D_G\sum_{i=1}^{N}\left[\cos\frac{i(n-m)\pi}{N} + \cos\frac{i(n+m)\pi}{N}\right] \cong D_G N\delta_{nm} \tag{3.228}$$

where Eq. 3.124 was used. Thus, the overall short-time behavior is given as

$$\langle[\mathbf{r}_{mn}(t)]^2\rangle_{mn} \cong b^2|n-m| + 6D_Gt(1+N\delta_{mn}) \qquad \begin{matrix}\text{Rouse model}\\ \text{short time}\end{matrix} \tag{3.229}$$

There is a distinct difference between a different pair ($m \neq n$) and the same pair ($m = n$; self-diffusion of each bead). For the same pair, $\langle[\mathbf{r}_{nn}(t)]^2\rangle_{nn} = 6D_G(N+1)t \cong 6(k_BT/\zeta)t$. It means that each bead moves freely with its own friction coefficient as if the other beads were absent or not connected. For a pair of different beads, the short-time mean square displacement increases as $6D_Gt$, the same as the center of mass diffusion. Different beads are uncorrelated.

In the Zimm model (theta solvent), $k_BT/\zeta_i = (3\cdot 2^{1/2}/16)D_G/i^{1/2}$ from Eqs. 3.172 and 3.174. Therefore, the second term in Eq. 3.226 is calculated as

$$4\sum_{i=1}^{N}\frac{k_BT}{\zeta_i}\cos\frac{in\pi}{N}\cos\frac{im\pi}{N} = \frac{3}{4\cdot 2^{1/2}}D_G\sum_{i=1}^{N}\frac{1}{i^{1/2}}\left[\cos\frac{i(n-m)\pi}{N} + \cos\frac{i(n+m)\pi}{N}\right] \tag{3.230}$$

When $n = m$, $\cos(2in\pi/N)$ is a rapidly changing function of i. The sum will be much smaller compared with the first term, $\Sigma i^{-1/2} \cong 2N^{1/2}$. Thus,

$$\langle[\mathbf{r}_{nn}(t)]^2\rangle_{nn} \cong 6D_Gt\left(1 + \frac{3}{2^{3/2}}N^{1/2}\right) \tag{3.231}$$

When $n \neq m$, the sum is dominated with the first term because $\cos[i(n+m)\pi/N]$ changes between positive and negative more rapidly compared with $\cos[i(n-m)\pi/N]$. From Eq. A3.3 in Appendix A3, we have

$$\langle[\mathbf{r}_{mn}(t)]^2\rangle_{mn} \cong b^2|n-m| + 6D_Gt\left(1 + \frac{3}{8}(N/|n-m|)^{1/2}\right) \qquad \begin{matrix}\text{Zimm, theta}\\ \text{short time}\end{matrix} \tag{3.232}$$

The hydrodynamic interactions allow the distance between a nearby pair of beads to grow more rapidly compared with a distant pair. For the latter, the short-time mean square displacement increases as in the Rouse model.

3.4.9.3 Mean Square Displacement of Monomers Now we trace the motion of the same bead ($m = n$) in all time scales. From Eq. 3.224, the displacement of each

monomer, $\langle[\mathbf{r}_{nn}(t)]^2\rangle_{nn}$, is given as

$$\langle[\mathbf{r}_{nn}(t)]^2\rangle_{nn} = 6D_{\mathrm{G}}t + 24\sum_{i=1}^{N}\frac{k_{\mathrm{B}}T}{k_i}\cos^2\frac{in\pi}{N}[1 - \exp(-t/\tau_i)] \tag{3.233}$$

where $\mathbf{r}_{nn}(t) = \mathbf{r}_n(t) - \mathbf{r}_n(0)$ is the displacement of the nth bead. We denote the average of $\langle[\mathbf{r}_{nn}(t)]^2\rangle_{nn}$ with respect to n by $\langle[\mathbf{r}_{nn}(t)]^2\rangle$ without subscript and calculate it for the short, long, and intermediate time ranges. The average of $\cos^2(in\pi/N)$ with respect to n is $1/2$. Thus,

$$\langle[\mathbf{r}_{nn}(t)]^2\rangle \cong 6D_{\mathrm{G}}t + 12\sum_{i=1}^{N}\frac{k_{\mathrm{B}}T}{k_i}[1 - \exp(-t/\tau_i)] \tag{3.234}$$

In the short time ($t \ll \tau_N$),

$$\langle[\mathbf{r}_{nn}(t)]^2\rangle \cong 6t\left[D_{\mathrm{G}} + 2\sum_{i=1}^{N}\frac{k_{\mathrm{B}}T}{\zeta_i}\right] \quad \text{short time} \tag{3.235}$$

In the long time ($t \gg \tau_1$),

$$\langle[\mathbf{r}_{nn}(t)]^2\rangle \cong 6D_{\mathrm{G}}t + 12\sum_{i=1}^{N}\frac{k_{\mathrm{B}}T}{k_i} \quad \text{long time} \tag{3.236}$$

In the intermediate time range, we need to deal with $1 - \exp(-t/\tau_i)$ as it is.

In the following, we consider $\langle[\mathbf{r}_{nn}(t)]^2\rangle$ for the Rouse model and the Zimm model in the theta solvent separately. We will also briefly consider $\langle[\mathbf{r}_{nn}(t)]^2\rangle$ for the Zimm model in the good solvent.

1. In the Rouse model, $\zeta_i = 2N\zeta$ for $i \neq 0$. Then, the second term in the bracket of Eq. 3.235 is

$$2\sum_{i=1}^{N}\frac{k_{\mathrm{B}}T}{\zeta_i} = \frac{k_{\mathrm{B}}T}{\zeta} \tag{3.237}$$

which is much greater compared with $D_{\mathrm{G}} = k_{\mathrm{B}}T/N\zeta$. Thus, in the short time, monomers move with a diffusion coefficient of $k_{\mathrm{B}}T/\zeta$ as if there were not connected by springs:

$$\langle[\mathbf{r}_{nn}(t)]^2\rangle \cong 6\frac{k_{\mathrm{B}}T}{\zeta}t = 6ND_{\mathrm{G}}t \qquad \begin{matrix}\text{Rouse model}\\ \text{short time}\end{matrix} \tag{3.238}$$

as we have seen in Eq. 3.229.

For the long-time behavior, use of $k_i = 6\pi^2 k_{\mathrm{B}}Ti^2/Nb^2$ (Eq. 3.132) yields

$$12\sum_{i=1}^{N}\frac{k_{\mathrm{B}}T}{k_i} = \frac{2Nb^2}{\pi^2}\sum_{i=1}^{N}\frac{1}{i^2} \cong \frac{2Nb^2}{\pi^2}\sum_{i=1}^{\infty}\frac{1}{i^2} = \frac{2Nb^2}{\pi^2}\frac{\pi^2}{6} = \frac{1}{3}Nb^2 \tag{3.239}$$

Then, Eq. 3.236 is

$$\langle [\mathbf{r}_{nn}(t)]^2 \rangle \cong 6D_G t + \frac{1}{3} Nb^2 \qquad \begin{matrix}\text{Rouse model} \\ \text{long time}\end{matrix} \tag{3.240}$$

For the intermediate time range, we use $\tau_i = \tau_1/i^2$ to calculate Eq. 3.234 as follows:

$$\langle [\mathbf{r}_{nn}(t)]^2 \rangle \cong 6D_G t + \frac{2Nb^2}{\pi^2} \sum_{i=1}^{N} \frac{1}{i^2} [1 - \exp(-i^2 t/\tau_1)] \tag{3.241}$$

We approximate the sum by an integral. Integral by parts yields

$$\sum_{i=1}^{N} \frac{1}{i^2} [1 - \exp(-i^2 t/\tau_1)] \cong \int_0^{\infty} \frac{1}{i^2} [1 - \exp(-i^2 t/\tau_1)] \, \mathrm{d}i = (\pi t/\tau_1)^{1/2} \tag{3.242}$$

Thus,

$$\langle [\mathbf{r}_{nn}(t)]^2 \rangle \cong 6D_G t + (2Nb^2/\pi^2)(\pi t/\tau_1)^{1/2} \qquad \begin{matrix}\text{Rouse model} \\ \text{intermediate time}\end{matrix} \tag{3.243}$$

Figure 3.56 illustrates how $\langle [\mathbf{r}_{nn}(t)]^2 \rangle$ changes with time t. The boundaries of the three time regimes can also be obtained as an interaction between two lines that correspond to the relevant sections and their extrapolates (Problem 3.27). The diffusion characteristics show a crossover from the single-bead diffusion to the N-bead

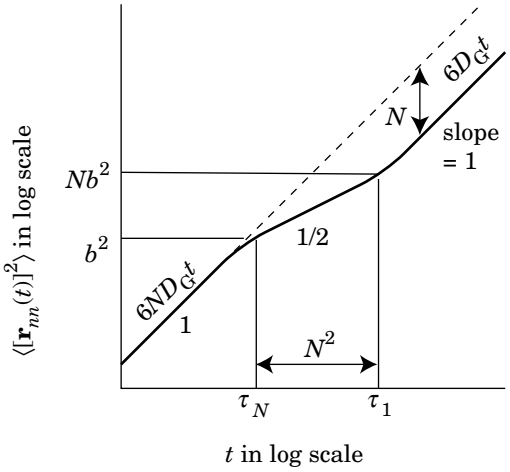

Figure 3.56. Mean square displacement of the beads on the Rouse chain, $\langle [\mathbf{r}_{nn}(t)]^2 \rangle$, is plotted as a function of time t. The plot has three distinct regions. In $t \ll \tau_N$ and $t \gg \tau_1$, the dynamics is diffusional with diffusion coefficients ND_G and D_G, respectively. In the time range between them, $\langle [\mathbf{r}_{nn}(t)]^2 \rangle \sim t^{1/2}$.

diffusion. The latter is slower by a factor of N. Between the two diffusional asymptotes, the mean square displacement of the monomers on the Rouse chain increases in a power of $t^{1/2}$. The range of time that exhibits the power is roughly between τ_N and τ_1. The mean square displacement is b^2 and Nb^2 at the two boundaries of the range.

2. In the Zimm model for the theta solvent, $k_B T/\zeta_i = (3\cdot 2^{1/2}/16)D_G/i^{1/2}$. The second term of Eq. 3.235 is calculated as

$$2\sum_{i=1}^{N}\frac{k_B T}{\zeta_i} = \frac{3\cdot 2^{1/2}}{8}D_G\sum_{i=1}^{N} i^{-1/2} \cong \frac{3\cdot 2^{1/2}}{4}D_G N^{1/2} \tag{3.244}$$

where the sum was approximated by the integral. This term is much greater compared with the first term, D_G. Thus, in the short time, monomers move with a diffusion coefficient of $(3/4)(2N)^{1/2}D_G$. From Eq. 3.174, we find this diffusion coefficient is equal to $4(3/\pi)^{1/2}k_B T/(6\pi\eta_s b) \cong 3.9 \times k_B T/(6\pi\eta_s b)$. Thus, the monomers move as if there were not connected by springs and with a diffusion coefficient about four times as large as that of a sphere of radius b:

$$\langle[\mathbf{r}_{nn}(t)]^2\rangle \cong 9(N/2)^{1/2}D_G t = 6\cdot 4(3/\pi)^{1/2}\frac{k_B T}{6\pi\eta_s b}t \qquad \begin{matrix}\text{Zimm, theta}\\ \text{short time}\end{matrix} \tag{3.245}$$

The expression for $\langle[\mathbf{r}_{nn}(t)]^2\rangle$ in the long time is the same as that of the Rouse model, because k_i is common between the two models. Thus, Eq. 3.240 holds as it does for the Zimm model in the theta solvent. Note, however, that D_G is different between the two models.

For the intermediate time range, we use $\tau_i = \tau_1/i^{3/2}$ to evaluate Eq. 3.234 as follows:

$$\langle[\mathbf{r}_{nn}(t)]^2\rangle \cong 6D_G t + \frac{2Nb^2}{\pi^2}\sum_{i=1}^{N}\frac{1}{i^2}[1 - \exp(-i^{3/2}t/\tau_1)] \tag{3.246}$$

We approximate the sum by an integral. Integral by parts yields

$$\sum_{i=1}^{N}\frac{1}{i^2}[1 - \exp(-i^{3/2}t/\tau_1)] \cong \int_0^{\infty}\frac{1}{i^2}[1 - \exp(-i^{3/2}t/\tau_1)]\mathrm{d}i = \Gamma_{1/3}(t/\tau_1)^{2/3} \tag{3.247}$$

where $\Gamma_{1/3} = \Gamma(1/3) \cong 2.679$ (see Eq. A3.6). Thus,

$$\langle[\mathbf{r}_{nn}(t)]^2\rangle \cong 6D_G t + (2\Gamma_{1/3}/\pi^2)Nb^2(t/\tau_1)^{2/3} \qquad \begin{matrix}\text{Zimm, theta}\\ \text{intermediate time}\end{matrix} \tag{3.248}$$

Figure 3.57 illustrates how $\langle[\mathbf{r}_{nn}(t)]^2\rangle$ changes with time t in the Zimm model. The monomer motion is diffusional in the two asymptotes. Between them, $\langle[\mathbf{r}_{nn}(t)]^2\rangle \sim t^{2/3}$.

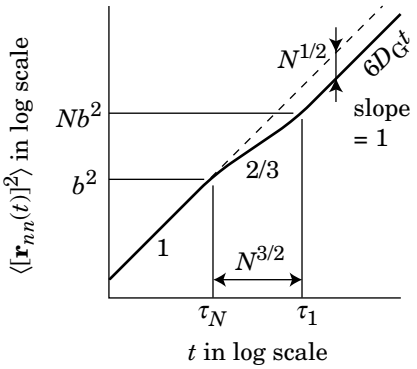

Figure 3.57. Mean square displacement of the beads on the chain for the Zimm model in the theta solvent, $\langle[\mathbf{r}_{nn}(t)]^2\rangle$

3. In the Zimm model for the good solvent, our discussion is limited to power relationships. For the short-time behavior, we note $k_B T/\zeta_i \cong i^{\nu-1} D_G$. Then, in Eq. 3.235,

$$\sum_{i=1}^{N} \frac{k_B T}{\zeta_i} \cong D_G \sum_{i=1}^{N} i^{\nu-1} \cong D_G N^{\nu} \tag{3.249}$$

which is much greater than D_G. Therefore, the short-time behavior is given as

$$\langle[\mathbf{r}_{nn}(t)]^2\rangle \cong N^{\nu} D_G t \cong \frac{k_B T}{\eta_s b} t \qquad \begin{matrix}\text{Zimm, good} \\ \text{short time}\end{matrix} \tag{3.250}$$

The bead moves as if it were not connected with other beads.

The expression for the long-time behavior is almost the same as that for the other two models, namely,

$$\langle[\mathbf{r}_{nn}(t)]^2\rangle \cong 6D_G t + N^{2\nu} b^2 \qquad \begin{matrix}\text{Zimm, good} \\ \text{long time}\end{matrix} \tag{3.251}$$

For the intermediate time range, we evaluate the following:

$$\langle[\mathbf{r}_{nn}(t)]^2\rangle \cong 6D_G t + N^{2\nu} b^2 \sum_{i=1}^{N} \frac{1}{i^{2\nu+1}} [1 - \exp(-i^{3\nu} t/\tau_1)] \tag{3.252}$$

By replacing the sum with an integral and using integral by parts, we obtain

$$\langle[\mathbf{r}_{nn}(t)]^2\rangle \cong 6D_G t + N^{2\nu} b^2 (t/\tau_1)^{2/3} \qquad \begin{matrix}\text{Zimm, good} \\ \text{intermediate}\end{matrix} \tag{3.253}$$

The exponent $2/3$ is the same as the one we obtained for the theta solvent condition.

3.4.10 PROBLEMS

Problem 3.21: Show the inverse transform of Eq. 3.133:

$$\mathbf{f}_n = \frac{1}{N}\sum_{j=0}^{N} \mathbf{g}_j \cos\frac{jn\pi}{N} - \frac{(-1)^n}{2N}\mathbf{g}_N$$

Solution 3.21: We rewrite Eq. 3.133 to

$$\frac{\zeta}{\zeta_i}\mathbf{g}_i(t) = \frac{1}{N}\sum_{n=1}^{N} \cos\frac{in\pi}{N}\mathbf{f}_n(t)$$

This conversion has the same structure as Eq. 3.118 with $(\zeta/\zeta_i)\mathbf{g}_i$ replacing $\mathbf{q}_i$. Then, we can apply the inverse transform, Eq. 3.125, as it is:

$$\mathbf{f}_n(t) = 2\sum_{i=1}^{N-1} \cos\frac{in\pi}{N}\frac{\zeta}{\zeta_i}\mathbf{g}_i(t) + \frac{\zeta}{\zeta_0}\mathbf{g}_0(t) + (-1)^n\frac{\zeta}{\zeta_N}\mathbf{g}_N(t)$$

Because $\zeta_0 = N\zeta$ and $\zeta_i = 2N\zeta$ $(i \geqslant 1)$

$$\begin{aligned}\mathbf{f}_n(t) &= \frac{1}{N}\sum_{i=1}^{N-1} \cos\frac{in\pi}{N}\mathbf{g}_i(t) + \frac{1}{N}\mathbf{g}_0(t) + (-1)^n\frac{1}{2N}\mathbf{g}_N(t)\\ &= \frac{1}{N}\sum_{j=0}^{N} \mathbf{g}_j \cos\frac{jn\pi}{N} - \frac{(-1)^n}{2N}\mathbf{g}_N\end{aligned}$$

Problem 3.22: Show that, in the Zimm model for the theta solvent,

$$h_{ij} \cong \frac{1}{2(3\pi^3 iN)^{1/2}\eta_s b}\delta_{ij} \quad \text{(except } i = j = 0\text{)}$$

Solution 3.22: From Eqs. 3.164 and 3.168,

$$h_{ij} = \frac{1}{N^2}\frac{1}{(6\pi^3)^{1/2}\eta_s b}\int_0^N \mathrm{d}n \int_0^N \mathrm{d}m|n - m|^{-1/2}\cos\frac{in\pi}{N}\cos\frac{jm\pi}{N}$$

The integral with respect to m is calculated as

$$\begin{aligned}&\int_0^N \mathrm{d}m|n - m|^{-1/2}\cos\frac{jm\pi}{N}\\ &= \int_{n-N}^{n} \mathrm{d}(n-m)|n-m|^{-1/2}\left(\cos\frac{jn\pi}{N}\cos\frac{j(n-m)\pi}{N} + \sin\frac{jn\pi}{N}\sin\frac{j(n-m)\pi}{N}\right)\end{aligned}$$

$$\cong \cos\frac{jn\pi}{N}\int_{-\infty}^{\infty} \mathrm{d}(n-m)|n-m|^{-1/2}\cos\frac{j(n-m)\pi}{N}$$
$$+ \sin\frac{jn\pi}{N}\int_{-\infty}^{\infty} \mathrm{d}(n-m)|n-m|^{-1/2}\sin\frac{j(n-m)\pi}{N}$$
$$\cong 2\cos\frac{jn\pi}{N}\int_{0}^{\infty} \mathrm{d}(n-m)|n-m|^{-1/2}\cos\frac{j(n-m)\pi}{N} = 2\cos\frac{jn\pi}{N}\left(\frac{N}{2j}\right)^{1/2}$$

where the lower and upper limits of the integral are set to $-\infty$ and ∞, because frequent alterations of the sign in $\cos[j(n-m)\pi/N]$ and $\sin[j(n-m)\pi/N]$ at large values of $|n-m|$ make its contribution much smaller compared with the contribution from small values of $|n-m|$. Equation A3.3 was used in the last equality. Then,

$$h_{ij} = \frac{1}{N}\frac{1}{(6\pi^3)^{1/2}\eta_s b}\left(\frac{N}{2j}\right)^{1/2}\frac{1}{N}\int_0^N 2\cos\frac{in\pi}{N}\cos\frac{jn\pi}{N}\,\mathrm{d}n$$
$$= \frac{1}{N}\frac{1}{(6\pi^3)^{1/2}\eta_s b}\left(\frac{N}{2j}\right)^{1/2}\delta_{ij} = \frac{1}{2(3\pi^3 Ni)^{1/2}\eta_s b}\,\delta_{ij}$$

Problem 3.23: Show that, in the Zimm model for the theta solvent,

$$h_{00} = \frac{8}{3}\frac{1}{(6\pi^3 N)^{1/2}\eta_s b}$$

Solution 3.23: From Eqs. 3.164 and 3.168,

$$h_{00} = \frac{1}{N^2}\frac{1}{(6\pi^3)^{1/2}\eta_s b}\int_0^N \mathrm{d}n\int_0^N \mathrm{d}m|n-m|^{-1/2}$$

The integral is calculated as

$$\int_0^N \mathrm{d}n\int_0^N \mathrm{d}m|n-m|^{-1/2} = 2\int_0^N \mathrm{d}n\int_0^n \mathrm{d}m(n-m)^{-1/2} = 2\int_0^N \mathrm{d}n\, 2n^{1/2} = \tfrac{8}{3}N^{3/2}$$

Problem 3.24: Show that, in the Zimm model for the good solvent,

$$h_{ij} \cong \frac{1}{N^{\nu} i^{1-\nu}\eta_s b}\,\delta_{ij} \quad (\text{except } i=j=0)$$
$$h_{00} = \frac{1}{\eta_s b N^{\nu}}$$

Solution 3.24:

$$h_{ij} \cong \frac{1}{N^2}\frac{1}{\eta_s b}\int_0^N \mathrm{d}n \int_0^N \mathrm{d}m |n-m|^{-\nu} \cos\frac{in\pi}{N}\cos\frac{jm\pi}{N}$$

The integral with respect to m is calculated as

$$\begin{aligned}
&\int_0^N \mathrm{d}m|n-m|^{-\nu}\cos\frac{jm\pi}{N} \\
&= \int_{n-N}^{n} \mathrm{d}(n-m)|n-m|^{-\nu}\left(\cos\frac{jn\pi}{N}\cos\frac{j(n-m)\pi}{N}\right. \\
&\quad \left. + \sin\frac{jn\pi}{N}\sin\frac{j(n-m)\pi}{N}\right) \cong \cos\frac{jn\pi}{N}\int_{-\infty}^{\infty}\mathrm{d}(n-m)|n-m|^{-\nu}\cos\frac{j(n-m)\pi}{N} \\
&\quad + \sin\frac{jn\pi}{N}\int_{-\infty}^{\infty}\mathrm{d}(n-m)|n-m|^{-1/2}\sin\frac{j(n-m)\pi}{N} \\
&\cong 2\cos\frac{jn\pi}{N}\int_0^{\infty}\mathrm{d}(n-m)|n-m|^{-\nu}\cos\frac{j(n-m)\pi}{N} \\
&= 2\cos\frac{jn\pi}{N}\times\frac{\Gamma(1-\nu)}{(j\pi/N)^{1-\nu}}\cos\frac{(1-\nu)\pi}{2} \cong \cos\frac{jn\pi}{N}\left(\frac{N}{j}\right)^{1-\nu}
\end{aligned}$$

where the lower and upper limits of the integral are set to $-\infty$ and ∞ , because frequent alterations of the sign in $\cos[j(n-m)\pi/N]$ and $\sin[j(n-m)\pi/N]$ at large values of $|n-m|$ make its contribution much smaller compared with the contribution from small values of $|n-m|$. Equation A3.2 was used in the last equality. Then,

$$\begin{aligned}
h_{ij} &\cong \frac{1}{N}\frac{1}{\eta_s b}\left(\frac{N}{j}\right)^{1-\nu}\frac{1}{N}\int_0^N \mathrm{d}n\cos\frac{in\pi}{N}\cos\frac{jn\pi}{N} \\
&\cong \frac{1}{N}\frac{1}{\eta_s b}\left(\frac{N}{j}\right)^{1-\nu}\delta_{ij} = \frac{1}{N^{\nu} i^{1-\nu}\eta_s b}\delta_{ij}
\end{aligned}$$

For h_{00},

$$h_{00} \cong \frac{1}{N^2}\frac{1}{\eta_s b}\int_0^N \mathrm{d}n\int_0^N \mathrm{d}m|n-m|^{-\nu}$$

The integral is calculated as

$$\begin{aligned}
\int_0^N \mathrm{d}n\int_0^N \mathrm{d}m|n-m|^{-\nu} &= 2\int_0^N \mathrm{d}n\int_0^n \mathrm{d}m(n-m)^{-\nu} \\
&= \frac{2}{1-\nu}\int_0^N \mathrm{d}n\, n^{1-\nu} = \frac{2}{1-\nu}\frac{1}{2-\nu}N^{2-\nu}
\end{aligned}$$

Problem 3.25: Estimate D_G and τ_1 for a polymer chain with $R_F = 100$ nm in a solvent of $\eta_s = 1.0$ cP at 25°C using the Zimm model for the theta solvent.

Solution 3.25:

$$D_G = \frac{8}{3(6\pi^3)^{1/2}} \frac{k_B T}{\eta_s R_F} = \frac{8}{3(6\pi^3)^{1/2}} \times \frac{1.38 \times 10^{-23}\,\text{J/K} \times 298.15\,\text{K}}{1.0 \times 10^{-3}\,\text{kg/(m·s)} \times 10^{-7}\,\text{m}}$$
$$= 8.0 \times 10^{-12}\,\text{m}^2/\text{s}$$
$$\tau_1 = \frac{1}{(3\pi)^{1/2}} \frac{\eta_s R_F^3}{k_B T} = \frac{1}{(3\pi)^{1/2}} \times \frac{1.0 \times 10^{-3}\,\text{kg/(m·s)} \times (10^{-7}\,\text{m})^3}{1.38 \times 10^{-23}\,\text{J/K} \times 298.15\,\text{K}} = 79\,\mu\text{s}$$

Problem 3.26: Use Eq. 3.125 to derive Eq. 3.224 directly.

Solution 3.26: From Eq. 3.125,

$$\langle [\mathbf{r}_{mn}(t)]^2 \rangle_{mn} = \langle [\mathbf{q}_0(t) - \mathbf{q}_0(0)]^2 \rangle$$
$$+4\sum_{i=1}^{N} \left\langle \cos^2 \frac{in\pi}{N} [\mathbf{q}_i(t)]^2 + \cos^2 \frac{im\pi}{N} [\mathbf{q}_i(0)]^2 - 2\cos \frac{in\pi}{N} \cos \frac{im\pi}{N} \mathbf{q}_i(t) \cdot \mathbf{q}_i(0) \right\rangle$$

where term of $\mathbf{q}_N$ was incorporated into the sum. The first term is the center-of-mass diffusion. Here, we use Eqs. 3.145, 3.146, and 3.151. Then, the above equation is rewritten to

$$\langle [\mathbf{r}_{mn}(t)]^2 \rangle_{mn} = 6D_G t + 12\sum_{i=1}^{N} \frac{k_B T}{k_i}$$
$$\times \left[\cos^2 \frac{in\pi}{N} + \cos^2 \frac{im\pi}{N} - 2\cos \frac{in\pi}{N} \cos \frac{im\pi}{N} \exp(-t/\tau_i) \right]$$

At $t = 0$,

$$\langle [\mathbf{r}_{mn}(0)]^2 \rangle_{mn} = 12\sum_{i=1}^{N} \frac{k_B T}{k_i} \left(\cos \frac{in\pi}{N} - \cos \frac{im\pi}{N} \right)^2$$

Thus, the evolution of $\langle [\mathbf{r}_{mn}(t)]^2 \rangle_{mn}$ from its value at $t = 0$ is given as

$$\langle [\mathbf{r}_{mn}(t)]^2 \rangle_{mn} - \langle [\mathbf{r}_{mn}(0)]^2 \rangle_{mn} = 6D_G t + 24\sum_{i=1}^{N} \frac{k_B T}{k_i}$$
$$\times \cos \frac{in\pi}{N} \cos \frac{im\pi}{N} [1 - \exp(-t/\tau_i)]$$

Problem 3.27: Where are the intersections between two adjacent time ranges in Figure 3.56?

Solution 3.27: Around τ_N: the time t at the intersection between Eqs. 3.238 and 3.243 is obtained from

$$6ND_G t = 6D_G t + (2Nb^2/\pi^2)(\pi t/\tau_1)^{1/2}$$

Because $N \gg 1$, it is rewritten to $3D_G t = (b^2/\pi^2)(\pi t/\tau_1)^{1/2}$, which leads to

$$t = \frac{b^4}{9\pi^3 {D_G}^2 \tau_1} = \frac{b^4}{9\pi^3} \frac{(N\zeta)^2}{(k_B T)^2} \frac{3\pi^2 k_B T}{\zeta N^2 b^2} = \frac{1}{3\pi} \frac{b^2 \zeta}{k_B T} = \pi \tau_N$$

Thus we find that the first section extends to $\sim\tau_N$.

Around τ_1: the time t at the intersection between Eqs. 3.240 and 3.243 is obtained from

$$6D_G t + (2Nb^2/\pi^2)(\pi t/\tau_1)^{1/2} = 6D_G t + \frac{1}{3} Nb^2$$

which is converted to

$$t = \frac{\pi^3}{36} \tau_1 \cong 0.86\tau_1$$

The boundary between the second and third sections is around τ_1.

Problem 3.28: Where are the intersections between two adjacent time ranges in Figure 3.57?

Solution 3.28: Around τ_N: the time t at the intersection between Eqs. 3.245 and 3.248 is obtained from

$$9(N/2)^{1/2} D_G t = 6D_G t + (2\Gamma_{1/3}/\pi^2) Nb^2 (t/\tau_1)^{2/3}$$

Because $N \gg 1$, the first term on the right-hand side is negligible. Then,

$$t = \left(\frac{2^{3/2} \Gamma_{1/3}}{9\pi^2} \right)^3 \frac{b^6 N^{3/2}}{{D_G}^3 \tau_1^2} = \frac{\eta_s b^3}{k_B T} \frac{(\Gamma_{1/3})^3}{8(3\pi)^{1/2}} = \frac{(\Gamma_{1/3})^3}{8} \tau_N \cong 2.4\tau_N$$

Thus we find that the first section extends to $\sim\tau_N$.

Around τ_1: the time t at the intersection between Eqs. 3.240 and 3.248 is obtained from

$$6D_G t + (2\Gamma_{1/3}/\pi^2) Nb^2 (t/\tau_1)^{2/3} = 6D_G t + \frac{1}{3} Nb^2$$

which is converted to

$$t = \left(\frac{\pi^2}{6\Gamma_{1/3}}\right)^{3/2} \tau_1 \cong 0.48\tau_1$$

The boundary between the second and third sections is around τ_1.

3.5 DYNAMICS OF RODLIKE MOLECULES

3.5.1 Diffusion Coefficients

Dynamics of rodlike molecules is quite different from that of linear flexible chains. The rodlike molecule exhibits a well-defined rotational motion in addition to the center-of-mass motion (Fig. 3.58). The latter has two components: parallel to the rod axis and perpendicular to the rod axis. The expressions for the **translational diffusion coefficients** $D_\parallel$ and $D_\perp$ in the directions parallel and perpendicular to the rod axis and the **rotational diffusion coefficient** D_r were obtained by Kirkwood[41] for a model that consists of N beads in a straight line.

The diffusion along the rod axis is one-dimensional, and the diffusion in the direction perpendicular to the axis is two-dimensional, because the degree of freedom is 1 and 2 in the two directions, respectively. The three-dimensional diffusion coefficient D_G of the center of mass is the isotropic mean of $D_\parallel$ and $D_\perp$, that is, $D_G = (D_\parallel + 2D_\perp)/3$. It is expressed as

$$\boxed{D_G = \frac{k_B T[\ln(L/b) - \gamma]}{3\pi\eta_s L} \qquad \text{rodlike molecule}} \tag{3.254}$$

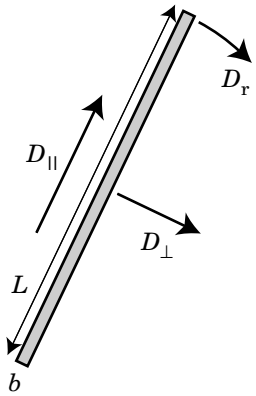

Figure 3.58. Rodlike molecule of length L and diameter b. The center-of-mass translation has two components, parallel and perpendicular to the rod axis, with the diffusion coefficients $D_\parallel$ and $D_\perp$. The rod can also rotate around the center with diffusion coefficient D_r.

where L is the rod length, b is the rod diameter ($b \ll L$), and γ is a constant. In the numerator, $\ln(L/b)$ is the result of hydrodynamic interactions between different parts of the rod; without its correction, $D_G \sim 1/L$ and thus D_G would be equal to the diffusion coefficient of N connected, independent beads (Problem 3.29). The constant γ, a result of the end effect, is around 0.3. The diffusion coefficients $D_\parallel$ and $D_\perp$ are

$$D_\parallel = \tfrac{3}{2} D_G, \qquad D_\perp = \tfrac{3}{4} D_G \tag{3.255}$$

The diffusion is faster in the parallel direction than it is in the perpendicular direction. The difference is rather small; $D_\parallel$ is only twice as large as $D_\perp$.

From Eq. 3.254, we find that the hydrodynamic radius R_H of the rodlike molecule is given as

$$R_H = \frac{L/2}{\ln(L/b) - \gamma} \tag{3.256}$$

Because the denominator depends only weakly on L, R_H increases nearly linearly with molecular weight. The dependence is much stronger compared with a linear flexible chain.

The rotational diffusion coefficient D_r was obtained as

$$\boxed{D_r = \frac{3k_B T[\ln(L/b) - \gamma]}{\pi \eta_s L^3} \qquad \text{rodlike molecule}} \tag{3.257}$$

and is related to D_G by $D_r = 9D_G/L^2$. Note that D_r has a dimension of s^{-1}. The rotational diffusion coefficient has an extremely steep dependence on the molecular weight. A rod twice as long can rotate only at the rate of $1/8$ of the shorter rod.

3.5.2 Rotational Diffusion

3.5.2.1 Pure Rotational Diffusion Here we consider the rotational motion of the rodlike molecule in details. We do not pay attention to the center-of-mass position. Let us define by $\mathbf{u}(t)$ the unit vector along the rod axis at time t and place the rodlike molecule in the spherical polar coordinate system (Fig. 3.59). The orientation vector $\mathbf{u}(t)$ is represented by the polar angle θ and the azimuthal angle φ. We define the probability density $\psi(\theta,\varphi; t)$ for the distribution of $\mathbf{u}(t)$ in the same way as the concentration represents the population of solute molecules per volume. The probability to find $\mathbf{u}(t)$ between θ and $\theta + d\theta$ and between φ and $\varphi + d\varphi$ is $\psi(\theta,\varphi; t)\sin\theta d\theta d\varphi$.

The rotational part of the motion is described by the **rotational diffusion equation** for $\psi(\theta,\varphi; t)$:

$$\frac{\partial \psi}{\partial t} = D_r\left(\frac{1}{\sin\theta}\frac{\partial}{\partial\theta}\sin\theta\frac{\partial}{\partial\theta} + \frac{1}{\sin^2\theta}\frac{\partial^2}{\partial\varphi^2}\right)\psi \tag{3.258}$$

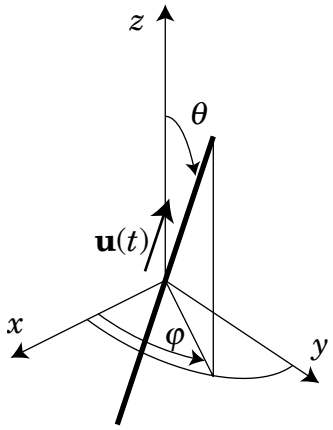

Figure 3.59. Rodlike molecule in the spherical polar coordinate system. The orientation of the rod, **u**, is expressed by θ and φ.

where the operator in the parenthesis is the orientational part of the Laplacian ∇^2 in the polar coordinate system. The solution of the diffusion equation is, in general, given as

$$\psi(\theta,\varphi;t) = \sum_{l=0}^{\infty} \sum_{m=-l}^{l} a_{lm}(t) Y_l^m(\theta,\varphi) \tag{3.259}$$

where $Y_l^m(\theta, \varphi)$ is the spherical harmonic function ($l = 0, 1, 2, \ldots; m = -l, -l + 1, \ldots, l$) and $a_{lm}(t)$ is the expansion coefficient. The same diffusion equation applies to the transition probability $P(\theta,\varphi; \theta',\varphi'; t)$ from (θ', φ') to (θ, φ).

In some systems, $\psi(\theta,\varphi; t)$ does not depend on φ. For instance, when we consider how the probability density $\psi(\mathbf{u}; t)$ evolves for a rod with $\mathbf{u}(0)$ parallel to the polar axis, the distribution is a function of θ and t only. Another example is a rodlike molecule that has a permanent dipole moment along the axis in an electric field. The natural choice of the polar axis is the direction of the electric field. When ψ depends on θ and t only, the rotational diffusion equation is simplified to

$$\boxed{\frac{\partial \psi}{\partial t} = D_r \frac{1}{\sin\theta} \frac{\partial}{\partial \theta} \sin\theta \frac{\partial \psi}{\partial \theta} \qquad \text{rotational diffusion, uniaxial}} \tag{3.260}$$

Then, $\psi(\theta,\varphi; t)$ is expanded in $Y_l^0(\theta, \varphi) \propto P_l(\cos\theta)$ only:

$$\psi(\theta; t) = \sum_{l=0}^{\infty} a_l(t) P_l(\cos\theta) \tag{3.261}$$

where $P_l(x)$ is the lth Legendre polynomial ($l = 0,1,2,\ldots$). The first few functions are $P_0(x) = 1$, $P_1(x) = x$, $P_2(x) = (3x^2 - 1)/2$.

We apply Eq. 3.260 to consider how fast the correlation of the rod orientation is lost. We place the polar axis in the direction of $\mathbf{u}(0)$ and consider how $\langle \mathbf{u}(t)\cdot\mathbf{u}(0)\rangle = \langle\cos\theta\rangle = \langle P_1(\cos\theta)\rangle$ changes with time. The statistical average is calculated with a weight of $\sin\theta$. From Eq. 3.260,

$$\begin{aligned}\frac{\mathrm{d}\langle\cos\theta\rangle}{\mathrm{d}t} &= \frac{\mathrm{d}}{\mathrm{d}t}\int_0^\pi \cos\theta\psi\sin\theta\mathrm{d}\theta = D_\mathrm{r}\int_0^\pi \sin\theta\cos\theta\frac{1}{\sin\theta}\frac{\partial}{\partial\theta}\sin\theta\frac{\partial\psi}{\partial\theta}\mathrm{d}\theta \\ &= -2D_\mathrm{r}\int_0^\pi \cos\theta\psi\sin\theta\mathrm{d}\theta = -2D_\mathrm{r}\langle\cos\theta\rangle\end{aligned} \tag{3.262}$$

where integration by parts was used twice. Likewise, we can show that (Problem 3.20)

$$\frac{\mathrm{d}\langle P_l(\cos\theta)\rangle}{\mathrm{d}t} = -l(l+1)D_\mathrm{r}\langle P_l(\cos\theta)\rangle \tag{3.263}$$

Note that, at $t = 0$, $\langle P_l(\cos\theta)\rangle = \langle P_l(1)\rangle = 1$. Then, $\langle P_l(\cos\theta)\rangle$ relaxes with time according to

$$\langle P_l(\cos\theta)\rangle = \exp(-t/\tau_l) \tag{3.264}$$

with a relaxation time $\tau_l = [l(l+1)D_\mathrm{r}]^{-1}$. The lth orientational correlation is lost with τ_l.

Rotational motion of the rodlike molecule can be viewed as the motion of its end point on the surface of a sphere with the rod as its diameter (Fig. 3.60). Over a short period of time ($D_\mathrm{r}t \ll 1$), $\theta \ll 1$ and therefore $\langle P_l(\cos\theta)\rangle = \langle\cos\theta\rangle \cong \langle 1 - \theta^2/2\rangle = 1 - \langle\theta^2/2\rangle$. The right-hand side of Eq. 3.264 is $\cong 1 - t/\tau_1 = 1 - 2D_\mathrm{r}t$. Thus, $\langle\theta^2\rangle = 4D_\mathrm{r}t$. The end point makes a two-dimensional diffusion. Over a longer period of

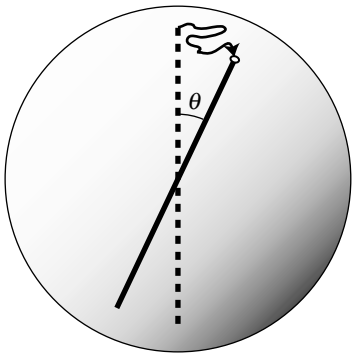

Figure 3.60. Rotational motion a rodlike molecule can be regarded as the motion of its end point on the sphere surface.

time, however, the mean square displacement loses a meaning in the rotational diffusion.

3.5.2.2 Translation-Rotational Diffusion We consider both the center-of-mass translation and the rotation now. The transition probability $P(\mathbf{r}_G,\mathbf{u};\mathbf{r}'_G,\mathbf{u}';t)$ from $(\mathbf{r}'_G,\mathbf{u}')$ at time 0 to $(\mathbf{r}_G,\mathbf{u})$ at time t follows the diffusion equation:

$$\frac{\partial P}{\partial t} = D_r \nabla_{\mathbf{u}}{}^2 P + \frac{\partial}{\partial \mathbf{r}_G} \cdot [D_\parallel \mathbf{uu} + D_\perp (\mathbf{I} - \mathbf{uu})] \cdot \frac{\partial P}{\partial \mathbf{r}_G} \tag{3.265}$$

where $\nabla_{\mathbf{u}}{}^2$ represents the differential operator in Eq. 3.258. The diffusivity is now anisotropic. The centroid diffusion constant $D = D_\parallel \mathbf{uu} + D_\perp(\mathbf{I} - \mathbf{uu})$ is not a simple scaler but a tensor of the second rank. Note that, in the polar spherical coordinate system,

$$\mathbf{uu} = \begin{bmatrix} 1 & 0 & 0 \\ 0 & 0 & 0 \\ 0 & 0 & 0 \end{bmatrix}, \quad \mathbf{I} - \mathbf{uu} = \begin{bmatrix} 0 & 0 & 0 \\ 0 & 1 & 0 \\ 0 & 0 & 1 \end{bmatrix} \tag{3.266}$$

Therefore, $D = D_\parallel$ in the direction of $\mathbf{u}$, and $D = D_\perp$ in the direction perpendicular to $\mathbf{u}$. Upon integrating with respect to $\mathbf{r}_G$, Eq. 3.265 reduces to Eq. 3.258.

3.5.3 Dynamic Structure Factor

We consider the dynamic structure factor of a rodlike molecule. The long-time behavior is rather trivial. The orientational distribution will be averaged, and the center-of-mass diffusion alone will survive. Then,

$$S_1(\mathbf{k},t)/S_1(\mathbf{k},0) \cong \exp(-D_G \mathbf{k}^2 t) \qquad \text{long time} \tag{3.267}$$

The short-time behavior in the small $\mathbf{k}$ limit is also given by this equation. To consider the short-time behavior for large $\mathbf{k}$, we first rewrite Eq. 3.46 into

$$S_1(\mathbf{k},t) = \frac{1}{N} \sum_{m,n=1}^{N} \langle \exp[i\mathbf{k} \cdot (\mathbf{r}_m(t) - \mathbf{r}_n(0))] \rangle \tag{3.268}$$

where monomers m and n are distributed uniformly along the rod. For the short-time behavior, we can write

$$\mathbf{r}_m(t) - \mathbf{r}_n(0) = x_{mn}(0)\mathbf{u} + \mathbf{u}\Delta x + \Delta \mathbf{v} + r_m \Delta \mathbf{u} \tag{3.269}$$

where $\mathbf{u}$ is the rod orientation at time zero, $x_{mn}(0)$ is the distance between the two monomers at time zero. The center-of-mass displacement in time t is Δx along the

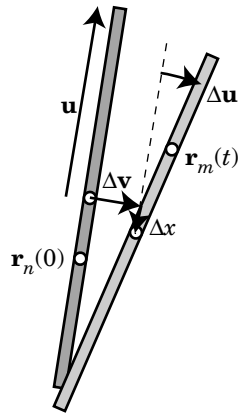

Figure 3.61. Short time motion of the rodlike molecule consists of the center-of-mass translation (Δx and $\Delta\mathbf{v}$ in the directions parallel and perpendicular to the rod axis) and rotation $\Delta\mathbf{u}$.

rod axis and $\Delta\mathbf{v}$ in the perpendicular direction. Rotation in time t is $\Delta\mathbf{u}$, and r_m is the distance of the mth bead from the center (see Fig. 3.61).

The center-of-mass motions in the two directions and the rotational motion are mutually independent. For a given $\mathbf{u}$,

$$\begin{aligned}\langle \exp(\mathrm{i}\mathbf{k}\cdot[\mathbf{r}_m(t) - \mathbf{r}_n(0)])\rangle_{\mathbf{u}} = {} & \langle \exp[\mathrm{i}\mathbf{k}\cdot\mathbf{u}x_{mn}(0)]\rangle_{\mathbf{u}}\langle \exp(\mathrm{i}\mathbf{k}\cdot\mathbf{u}\Delta x)\rangle_{\mathbf{u}} \\ & \times\langle \exp(\mathrm{i}\mathbf{k}\cdot\Delta\mathbf{v})\rangle_{\mathbf{u}}\langle \exp(\mathrm{i}\mathbf{k}\cdot\Delta\mathbf{u}\, r_m)\rangle_{\mathbf{u}}\end{aligned} \tag{3.270}$$

We calculate each term separately. When $\mathbf{k}$ is large, $\exp(\mathrm{i}\mathbf{k}\cdot\mathbf{u}\Delta x)$ is a rapidly varying function. Its average is contributed mostly from small Δx. Then, we can regard that the random variable Δx is distributed with a normal distribution that has a zero mean and a variance of $2D_\parallel t$. Thus

$$\begin{aligned}\langle \exp(\mathrm{i}\mathbf{k}\cdot\mathbf{u}\Delta x)\rangle_{\mathbf{u}} &= \int_{-\infty}^{\infty} \exp(\mathrm{i}k_\parallel \Delta x)\,(4\pi D_\parallel t)^{-1/2} \exp\left(-\frac{\Delta x^2}{4D_\parallel t}\right)\mathrm{d}\Delta x \\ &= \exp(-D_\parallel {k_\parallel}^2 t)\end{aligned} \tag{3.271}$$

where $k_\parallel = \mathbf{k}\cdot\mathbf{u}$ is the parallel component of $\mathbf{k}$. Likewise, the random variable $\Delta\mathbf{v}$ is distributed with a two-dimensional normal distribution that has a zero mean and a variance of $4D_\perp t$. Thus

$$\langle \exp(\mathrm{i}\mathbf{k}\cdot\Delta\mathbf{v})\rangle_{\mathbf{u}} = \int_{-\infty}^{\infty} \exp(\mathrm{i}\mathbf{k}\cdot\Delta\mathbf{v})(4\pi D_\perp t)^{-1} \exp\left(-\frac{\Delta\mathbf{v}^2}{4D_\perp t}\right)\mathrm{d}\Delta\mathbf{v} = \exp(-D_\perp {k_\perp}^2 t) \tag{3.272}$$

where $k_\perp{}^2 = \mathbf{k}^2 - (\mathbf{k}\cdot\mathbf{u})^2$ is the square of the perpendicular component of $\mathbf{k}$. Likewise, $\Delta\mathbf{u}$ is distributed with a two-dimensional normal distribution that has a zero mean and a variance of $4D_r t$. Thus

$$\begin{aligned}\langle \exp(i\mathbf{k}\cdot\Delta\mathbf{u}\, r_m)\rangle_{\mathbf{u}} &= \int_{-\infty}^{\infty} \exp(i\mathbf{k}\cdot\Delta\mathbf{u} r_m)(4\pi D_r t)^{-1}\exp\left(-\frac{\Delta\mathbf{u}^2}{4D_r t}\right)d\Delta\mathbf{u} \\ &= \exp(-D_r k_\perp{}^2 t\, r_m{}^2) \end{aligned} \tag{3.273}$$

All combined,

$$\langle \exp(i\mathbf{k}\cdot[\mathbf{r}_m(t) - \mathbf{r}_n(0)])\rangle_{\mathbf{u}} = \langle \exp[i\mathbf{k}\cdot\mathbf{u}x_{mn}(0)]\rangle_{\mathbf{u}} \exp(-D_\parallel k_\parallel{}^2 t - (D_\perp + D_r r_m{}^2)k_\perp{}^2 t) \tag{3.274}$$

Averaging with respect to r_m cannot be done analytically. We evaluate the initial slope of $\ln S_1(\mathbf{k}, t)$. It is equal to the initial slope of $\langle \exp(i\mathbf{k}\cdot[\mathbf{r}_m(t) - \mathbf{r}_n(0)])\rangle_{\mathbf{u}}$:

$$\frac{\partial}{\partial t}\langle \exp(i\mathbf{k}\cdot[\mathbf{r}_m(t) - \mathbf{r}_n(0)])\rangle_{\mathbf{u}}\bigg|_{t=0} = -D_\parallel k_\parallel{}^2 - (D_\perp + D_r r_m{}^2)k_\perp{}^2 \tag{3.275}$$

for given $\mathbf{u}$ and r_m. Now we take the average with respect to $\mathbf{u}$ and r_m. First, r_m is uniformly distributed in $[-L/2, L/2]$. Therefore, the average of $r_m{}^2$ is $L^2/12$. The average of $k_\parallel{}^2$ with respect to $\mathbf{u}$ is calculated as

$$\langle k_\parallel{}^2\rangle = \int_0^\pi k^2\cos^2\theta \sin\theta\, d\theta \Big/ \int_0^\pi \sin\theta\, d\theta = \tfrac{1}{3}k^2 \tag{3.276}$$

Then, $\langle k_\perp{}^2\rangle = (2/3)k^2$. Thus the average of Eq. 3.275 is

$$\frac{\partial}{\partial t}\ln S_1(\mathbf{k},t)\bigg|_{t=0} = -\left[\tfrac{1}{3}D_\parallel + \tfrac{2}{3}D_\perp + \tfrac{1}{18}D_r L^2\right]k^2 = -\left[D_G + \tfrac{1}{18}D_r L^2\right]k^2 \tag{3.277}$$

With $D_r = 9D_G/L^2$,

$$\frac{\partial}{\partial t}\ln S_1(\mathbf{k},t)\bigg|_{t=0} = -\tfrac{3}{2}D_G k^2 \tag{3.278}$$

Rotational motion makes the initial decay slightly faster at large $\mathbf{k}$.

Unlike the linear flexible chains, the initial decay rate at large $\mathbf{k}$ is proportional to $\mathbf{k}^2$ (Table 3.4). The difference is ascribed to the comparable diffusion coefficients (including $L^2D_r = 9D_G$) in the five modes of motion in the rodlike molecule. In the normal modes of a linear flexible chain, in contrast, higher-order modes have a significantly shorter relaxation time compared with the first mode.

3.5.4 Intrinsic Viscosity

In Section 3.3.3, we learned that the Mark-Houwink-Sakurada exponent greater than 1 indicates a stiffness in the chain conformation. Here, we consider the intrinsic viscosity of the rodlike molecule. However, calculation of the excess stress is tedious. We look at the result only. To the linear order of κ, the excess stress $\Delta\sigma_{\alpha\beta}$ is given as

$$\Delta\sigma_{\alpha\beta} = \frac{N_A c}{M}\frac{2}{15}\frac{k_B T}{D_r}(\kappa_{\alpha\beta} + \kappa_{\beta\alpha}) \tag{3.279}$$

In the shear flow given by Eq. 3.107,

$$\Delta\sigma_{xy} = \frac{N_A c}{M}\frac{2}{15}\frac{k_B T}{D_r}\kappa \tag{3.280}$$

Then with Eq. 3.109, the intrinsic viscosity calculated from the zero-shear viscosity is given as

$$[\eta] = \frac{N_A}{M}\frac{2}{15}\frac{k_B T}{D_r \eta_s} = \frac{2\pi}{45}\frac{N_A}{M}\frac{L^3}{\ln(L/b) - \gamma} \tag{3.281}$$

The molecular weight dependent factor in $[\eta]$ is $(L^3/M)(\ln(L/b) - \gamma)^{-1}$. The dependence is weaker than M^2 because of the ln M term in the denominator (Table 3.3).

3.5.5 Dynamics of Wormlike Chains

A wormlike chain is specified by the persistence length L_c and the contour length L_p. However, it does not have a thickness. We need to give it a diameter b for the chain to have a finite diffusion coefficient. The model is called a wormlike cylinder (Fig. 3.62). The expressions for the center-of-mass diffusion coefficient and the intrinsic viscosity were derived by Yamakawa et al.[42] in the rigid-rod asymptote and the flexible-chain asymptote in a series of b/L_c and L_c/L_p.

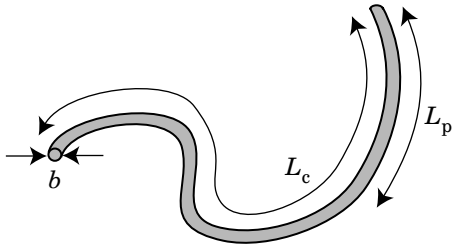

Figure 3.62. Wormlike cylinder has a finite thickness b in addition to the nature of the wormlike chain.

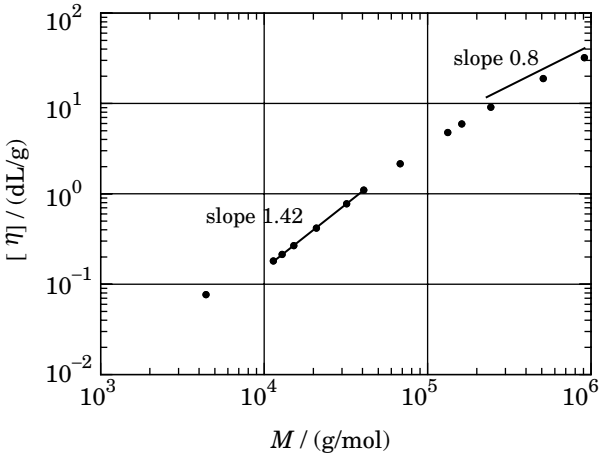

Figure 3.63. Intrinsic viscosity $[\eta]$ of a semirigid polymer, plotted as a function of the molecular weight M. The sample is poly(*n*-hexyl isocyanate) in toluene at 25°C. The molecular weight dependence of $[\eta]$ shows a cross-over from $\sim M^{1.42}$ to $\sim M^{0.8}$ with an increasing M. (From Ref. 43.)

Figure 3.63 shows the intrinsic viscosity of poly(*n*-hexyl isocyanate) in toluene at 25°C.[43] The polymer is semirigid with $L_p \cong 37$ nm and $b \cong 1.6$ nm. The slope of the tangent decreases from 1.4 to 0.8 with an increasing M. The locally rigid chain follows the viscosity law of the flexible chain when the molecular weight is sufficiently high.

3.5.6 PROBLEMS

Problem 3.29: Use the general formula, Eq. 3.55, to calculate the hydrodynamic radius of a rodlike molecule with length L and diameter b. The average between two beads at x and y on the rod measured from one of the ends is calculated only for $|x - y| > b$.

Solution 3.29:

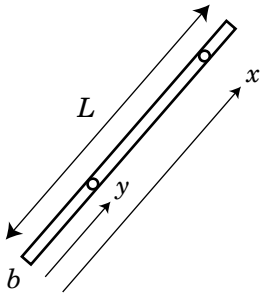

$$\frac{1}{R_{\rm H}} = \left\langle \frac{1}{|x-y|} \right\rangle = \frac{2}{(L-b)^2}\int_b^L \mathrm{d}x \int_0^{x-b} \mathrm{d}y \frac{1}{x-y}$$
$$= \frac{2}{(L-b)^2}\int_b^L \mathrm{d}x(\ln x - \ln b) = \frac{2}{(L-b)^2} L(\ln(L/b) - 1 + b/L)$$
$$\cong \frac{2}{L}[\ln(L/b) - 1 + (2b/L)\ln(L/b)]$$

This rough method gives the same result as Eq. 3.256 to the leading order.

Problem 3.30: The Legendre polynomial $P_l(z)$ satisfies the following differential equation:

$$(1-z^2)\frac{\mathrm{d}^2 P_l(z)}{\mathrm{d}z^2} - 2z\frac{\mathrm{d}P_l(z)}{\mathrm{d}z} + l(l+1)P_l(z) = 0$$

Prove Eq. 3.263.

Solution 3.30: Using the integral by parts leads to

$$\frac{\mathrm{d}\langle P_l(\cos\theta)\rangle}{\mathrm{d}t} = \frac{\mathrm{d}}{\mathrm{d}t}\int_0^\pi P_l(\cos\theta)\psi \sin\theta \,\mathrm{d}\theta = D_{\rm r}\int_0^\pi \mathrm{P}_l(\cos\theta)\frac{\partial}{\partial\theta}\sin\theta\frac{\partial\psi}{\partial\theta}\,\mathrm{d}\theta$$
$$= D_{\rm r}\int_0^\pi P_l'(\cos\theta)\sin^2\theta\frac{\partial\psi}{\partial\theta}\,\mathrm{d}\theta$$
$$= D_r\int_0^\pi [\sin^2\theta P_l''(\cos\theta) - 2\cos\theta P_l'(\cos\theta)]\psi\sin\theta\,\mathrm{d}\theta$$

where $P_l'(z)$ and $P_l''(z)$ denote the first- and second-order derivatives of $P_l(z)$. Use of the above differential equation converts this equation into

$$\frac{\mathrm{d}\langle P_l(\cos\theta)\rangle}{\mathrm{d}t} = -l(l+1)D_{\rm r}\int_0^\pi P_l(\cos\theta)\psi\sin\theta\,\mathrm{d}\theta = -l(l+1)D_{\rm r}\langle P_l(\cos\theta)\rangle$$

APPENDIX 3.A: EVALUATION OF $\langle \mathbf{q}_i^2 \rangle_{\rm eq}$

The amplitude of $\mathbf{q}_i$ at equilibrium can be directly evaluated from its definition by Eq. 3.118. Because it is an equilibrium property, it has nothing to do with the hydrodynamic interactions. It depends only on the chain statistics as shown below. Here, we use the integral form of Eq. 3.118, that is,

$$\mathbf{q}_i = \frac{1}{N}\int_0^N \mathrm{d}n\,\mathbf{r}_n \cos\frac{in\pi}{N} \tag{3.A.1}$$

to calculate $\langle \mathbf{q}_i{}^2 \rangle$:

$$\begin{aligned}\langle \mathbf{q}_i{}^2 \rangle &= \frac{1}{N^2}\int_0^N \mathrm{d}n \int_0^N \mathrm{d}m \langle \mathbf{r}_n \cdot \mathbf{r}_m \rangle \cos\frac{in\pi}{N}\cos\frac{im\pi}{N} \\ &= \frac{1}{(i\pi)^2}\int_0^N \mathrm{d}n \int_0^N \mathrm{d}m \frac{\partial^2}{\partial n \partial m}\langle \mathbf{r}_n \cdot \mathbf{r}_m \rangle \sin\frac{in\pi}{N}\sin\frac{im\pi}{N} \\ &= -\frac{1}{2(i\pi)^2}\int_0^N \mathrm{d}n \int_0^N \mathrm{d}m \frac{\partial^2}{\partial n \partial m}\langle (\mathbf{r}_n - \mathbf{r}_m)^2 \rangle \sin\frac{in\pi}{N}\sin\frac{im\pi}{N}\end{aligned} \tag{3.A.2}$$

where integration by parts was used, and the last equality is due to the identity: $(\partial^2/\partial n \partial m)\langle \mathbf{r}_n \cdot \mathbf{r}_m \rangle = -(1/2)(\partial^2/\partial n \partial m)\langle (\mathbf{r}_n - \mathbf{r}_m)^2 \rangle$. Now we use $\langle (\mathbf{r}_n - \mathbf{r}_m)^2 \rangle = b^2|n-m|^{2\nu}$. Then,

$$\begin{aligned}\langle \mathbf{q}_i{}^2 \rangle &= \nu(2\nu - 1)\frac{b^2}{(i\pi)^2}\int_0^N \mathrm{d}n \int_0^N \mathrm{d}m \, |n-m|^{2\nu-2} \sin\frac{in\pi}{N}\sin\frac{im\pi}{N} \\ &= \nu\Big(\nu - \tfrac{1}{2}\Big)\frac{b^2}{(i\pi)^2}\int_0^N \mathrm{d}n \int_0^N \mathrm{d}m \, |n-m|^{2\nu-2}\left[\cos\frac{i(n-m)\pi}{N} - \cos\frac{i(n+m)\pi}{N}\right]\end{aligned} \tag{3.A.3}$$

Here, we change the variables of integration from n and m to $u = n - m$ and $v = n + m$. Then,

$$\begin{aligned}\langle \mathbf{q}_i{}^2 \rangle &= \nu\Big(\nu - \tfrac{1}{2}\Big)\frac{b^2}{2(i\pi)^2}\left[\int_{-N}^0 \mathrm{d}u \int_{-u}^{2N+u} \mathrm{d}v (-u)^{2\nu-2}\left(\cos\frac{iu\pi}{N} - \cos\frac{iv\pi}{N}\right)\right. \\ &\quad \left. + \int_0^N \mathrm{d}u \int_u^{2N-u} \mathrm{d}v \, u^{2\nu-2}\left(\cos\frac{iu\pi}{N} - \cos\frac{iv\pi}{N}\right)\right] \\ &= \nu(2\nu-1)\frac{Nb^2}{(i\pi)^2}\left[\int_0^N \mathrm{d}u \, u^{2\nu-2}\cos\frac{iu\pi}{N} + \frac{2\nu}{i\pi}\int_0^N \mathrm{d}u \, u^{2\nu-2}\sin\frac{iu\pi}{N}\right]\end{aligned} \tag{3.A.4}$$

When $N \gg 1$, the upper limit of the integral can be replaced by ∞. Then, with Eqs. A3.2 and A3.4,

$$\begin{aligned}\langle \mathbf{q}_i{}^2 \rangle &= \nu(2\nu-1)\frac{Nb^2}{(i\pi)^2}\left[\int_0^\infty \mathrm{d}u \, u^{2\nu-2}\cos\frac{iu\pi}{N} + \frac{2\nu}{i\pi}\int_0^\infty \mathrm{d}u \, u^{2\nu-2}\sin\frac{iu\pi}{N}\right] \\ &= \nu(2\nu-1)\frac{Nb^2}{(i\pi)^2}\,\frac{\Gamma(2\nu-1)}{(i\pi/N)^{2\nu-1}}\left[\cos\frac{(2\nu-1)\pi}{2} + \frac{2\nu}{i\pi}\sin\frac{(2\nu-1)\pi}{2}\right] \\ &\cong \frac{b^2 N^{2\nu}}{i^{2\nu+1}}\end{aligned} \tag{3.A.5}$$

Because of the approximations we used, $\langle \mathbf{q}_i{}^2 \rangle$ vanishes when $\nu = 1/2$. The exponents are correct, however, in the final result.

APPENDIX 3.B: EVALUATION OF $\langle \exp[i\mathbf{k}\cdot(A\mathbf{q} - B\mathbf{p})]\rangle$

We obtain a formula for the statistical average of $\exp[i\mathbf{k}\cdot(A\mathbf{q} - B\mathbf{p})]$, where A and B are constants, and three-dimensional Gaussian random variables $\mathbf{p}$ and $\mathbf{q}$ are distributed with $f_P(\mathbf{p})$ and $f_Q(\mathbf{q};\mathbf{p})$, respectively:

$$f_P(\mathbf{p}) = (2\pi\sigma^2)^{-3/2}\exp(-\mathbf{p}^2/2\sigma^2) \tag{3.B.1}$$

$$f_Q(\mathbf{q};\mathbf{p}) = (2\pi{\sigma_Q}^2)^{-3/2}\exp[-(\mathbf{q} - \mathbf{p}\exp(-t/\tau))^2/2{\sigma_Q}^2] \tag{3.B.2}$$

with

$$\sigma^2 = \langle \mathbf{p}^2\rangle/3 \tag{3.B.3}$$

and

$${\sigma_Q}^2 \equiv \sigma^2(1 - \exp(-2t/\tau)) \tag{3.B.4}$$

At $t = 0, f_Q(\mathbf{q};\mathbf{p}) = \delta(\mathbf{q} - \mathbf{p})$. At $t \to \infty$, $\mathbf{q}$ becomes independent of $\mathbf{p}$.
The average is expressed as

$$\langle \exp[i\mathbf{k}\cdot(A\mathbf{q} - B\mathbf{p})]\rangle = \int f_P(\mathbf{p})\,d\mathbf{p}\int f_Q(\mathbf{q};\mathbf{p})\,d\mathbf{q}\exp[i\mathbf{k}\cdot(A\mathbf{q} - B\mathbf{p})] \tag{3.B.5}$$

First, the integration with respect to $\mathbf{q}$ is calculated as

$$\begin{aligned}
&\int d\mathbf{q}\, f_Q(\mathbf{q};\mathbf{p})\exp(iA\mathbf{k}\cdot\mathbf{q}) = (2\pi{\sigma_Q}^2)^{-3/2} \\
&\quad\times\int d\mathbf{q}\exp\Big[-(\mathbf{q} - \mathbf{p}\exp(-t/\tau) - i{\sigma_Q}^2A\mathbf{k})^2/2{\sigma_Q}^2 + iA\mathbf{k}\cdot\mathbf{p}\exp(-t/\tau) \\
&\quad - \tfrac{1}{2}{\sigma_Q}^2A^2\mathbf{k}^2\Big] \\
&= \exp\Big[iA\mathbf{k}\cdot\mathbf{p}\exp(-t/\tau) - \tfrac{1}{2}{\sigma_Q}^2A^2\mathbf{k}^2\Big]
\end{aligned} \tag{3.B.6}$$

Then, the overall average is given as

$$\begin{aligned}
\langle \exp[i\mathbf{k}\cdot(A\mathbf{q} - B\mathbf{p})]\rangle &= \exp\Big[-\tfrac{1}{2}{\sigma_Q}^2A^2\mathbf{k}^2\Big](2\pi\sigma^2)^{-3/2} \\
&\quad\times\int d\mathbf{p}\exp\Big[-[\mathbf{p} + i\mathbf{k}\sigma^2(B - A\exp(-t/\tau))]^2/2\sigma^2 \\
&\quad - \tfrac{1}{2}\sigma^2\mathbf{k}^2(B - A\exp(-t/\tau))^2\Big] \\
&= \exp\Big[-\tfrac{1}{2}\mathbf{k}^2\sigma^2(A^2 + B^2 - 2AB\exp(-t/\tau))\Big]
\end{aligned} \tag{3.B.7}$$

APPENDIX 3.C: INITIAL SLOPE OF $S_1(\mathbf{k}, t)$

We evaluate $A \equiv$ numerator in Eq. 3.210 for the ideal-chain conformation, $\langle \exp[i\mathbf{k}\cdot\mathbf{r}_{mn}(0)]\rangle_{mn} = \exp(-b^2\mathbf{k}^2|n-m|/6)$.

$$
\begin{aligned}
A &\equiv \sum_{m,n=1}^{N} \exp\left(-\frac{b^2\mathbf{k}^2}{6}|n-m|\right)\sum_{i=1}^{N}\frac{k_\mathrm{B}T}{\zeta_i}\cos\frac{in\pi}{N}\cos\frac{im\pi}{N} \\
&\cong \int_0^N \mathrm{d}n\int_0^N \mathrm{d}m\,\exp\left(-\frac{b^2\mathbf{k}^2}{6}|n-m|\right)\sum_{i=1}^{N}\frac{k_\mathrm{B}T}{\zeta_i}\cos\frac{in\pi}{N}\cos\frac{im\pi}{N} \\
&= \int_0^N \mathrm{d}n\,\exp(-b^2\mathbf{k}^2 n/6)\int_0^n \mathrm{d}m\,\exp(b^2\mathbf{k}^2 m/6)\sum_{i=1}^{N}\frac{k_\mathrm{B}T}{\zeta_i} \\
&\quad\times\left(\cos\frac{i(n-m)\pi}{N} + \cos\frac{i(n+m)\pi}{N}\right) \\
&= \mathrm{Re}\sum_{i=1}^{N}\frac{k_\mathrm{B}T}{\zeta_i}\int_0^N \mathrm{d}n\,\exp(-b^2\mathbf{k}^2 n/6)\int_0^n \mathrm{d}m\,\exp(b^2\mathbf{k}^2 m/6) \\
&\quad\times(\exp(\mathrm{i}i(n-m)\pi/N) + \exp(\mathrm{i}i(n+m)\pi/N)) \\
&= \mathrm{Re}\sum_{i=1}^{N}\frac{k_\mathrm{B}T}{\zeta_i}\int_0^N \mathrm{d}n\,\exp(-b^2\mathbf{k}^2 n/6 + \mathrm{i}in\pi/N)\int_0^n \mathrm{d}m \\
&\quad\times(\exp[(b^2\mathbf{k}^2/6 - \mathrm{i}i\pi/N)m] + \exp[(b^2\mathbf{k}^2/6 + \mathrm{i}i\pi/N)m]) \qquad (3.\mathrm{C}.1)
\end{aligned}
$$

After integration with respect to m,

$$
\begin{aligned}
A &= \mathrm{Re}\sum_{i=1}^{N}\frac{k_\mathrm{B}T}{\zeta_i}\int_0^N \mathrm{d}n\left[\frac{1-\exp[-(b^2\mathbf{k}^2/6 - \mathrm{i}i\pi/N)n]}{b^2\mathbf{k}^2/6 - \mathrm{i}i\pi/N}\right. \\
&\quad\left. + \frac{\exp(\mathrm{i}2in\pi/N) - \exp[-(b^2\mathbf{k}^2/6 - \mathrm{i}i\pi/N)n]}{b^2\mathbf{k}^2/6 + \mathrm{i}i\pi/N}\right] \\
&= \mathrm{Re}\sum_{i=1}^{N}\frac{k_\mathrm{B}T}{\zeta_i}\frac{1}{b^2\mathbf{k}^2/6 - \mathrm{i}i\pi/N}\left\{N - \frac{1-(-1)^i\exp(-Nb^2\mathbf{k}^2/6)}{b^2\mathbf{k}^2/6 - \mathrm{i}i\pi/N}\right. \qquad (3.\mathrm{C}.2) \\
&\quad\left. - \frac{1-(-1)^i\exp(-Nb^2\mathbf{k}^2/6)}{b^2\mathbf{k}^2/6 + \mathrm{i}i\pi/N}\right\} \\
&= \sum_{i=1}^{N}\frac{k_\mathrm{B}T}{\zeta_i}\frac{b^2\mathbf{k}^2/6}{(b^2\mathbf{k}^2/6)^2 + (i\pi/N)^2}\left[N - \frac{(b^2\mathbf{k}^2/3)[1-(-1)^i\exp(-Nb^2\mathbf{k}^2/6)]}{(b^2\mathbf{k}^2/6)^2 + (i\pi/N)^2}\right]
\end{aligned}
$$

The second term in the square bracket is negligible compared with N in both the small $\mathbf{k}$ and large $\mathbf{k}$ limits. Therefore,

$$A \cong N\sum_{i=1}^{N}\frac{k_{\mathrm{B}}T}{\zeta_i}\frac{b^2\mathbf{k}^2/6}{(b^2\mathbf{k}^2/6)^2 + (i\pi/N)^2} = N^2\sum_{i=1}^{N}\frac{k_{\mathrm{B}}T}{\zeta_i}\frac{k^2R_{\mathrm{g}}{}^2}{(k^2R_{\mathrm{g}}{}^2)^2 + (i\pi)^2} \quad (3.C.3)$$